The role of carbon dioxide in allophycocyanin biochemistry

ALEJANDRA GUILLEN-GARCIA

The role of carbon dioxide in allophycocyanin biochemistry

Alejandra Guillén García

Supervisor: Prof. Martin J. Cann

Department of Biosciences
Durham University

A thesis submitted for the degree of
Doctor of Philosophy
July 2021

I would like to dedicate this thesis to my loving parents ...

Declaration

I hereby declare that except where specific reference is made to the work of others, the contents of this dissertation are original and have not been submitted in whole or in part for consideration for any other degree or qualification in this, or any other university. This dissertation is my own work and contains nothing which is the outcome of work done in collaboration with others, except as specified in the text and Acknowledgements.

Alejandra Guillén García
July 2021

Acknowledgements

I want to thank the following people, without whom I would not have completed this research, and without whom I would not have made it through my PhD.

I wish to express my sincere appreciation to my supervisor, Professor Martin J. Cann. He convincingly guided and encouraged me to be professional and do the right thing even when the road got tough. Without his persistent help and everlasting optimism, the goal of this project would not have been realized. I would also like to thank Dr Lars-Olof Pålsson for patiently sharing his expertise with me and guiding me into the world of spectroscopy.

I am thankful to Conacyt-SENER; without their support and funding, this project could not have been possible.

It was great to work in the CG234 lab, but special thanks go to my beloved friend and mentor Vicki, for laying the groundwork for my PhD and supporting me in every aspect of my experience in Durham. Thanks also go to Harry for everyday encouragement and laughing at my jokes (or at me). Melissa, Meli, Yaz, Gem, and Kev, you guys made Durham feel like home; thank you for being awesome and for always being there.

To conclude, I cannot forget to thank my family, Martha, Hugo y Pao, for every video call across the Atlantic and all the unconditional support in this very intense academic experience. And special thanks go for Rodrigo, for all your help and patience through this years; you have made me laugh, watched me succeed and seen me fail. Thanks for keeping me strong all this time; getting to this point wouldn't have been the same without you. Gracias totales!

Abstract

Carbon dioxide (CO_2) plays an essential role in fundamental biological processes such as respiration and photosynthesis. The ability of cyanobacteria to use water as an electron source in photosynthesis contributes to the balance between CO_2 and O_2 in the atmosphere. However, the molecular mechanisms by which cyanobacteria directly detect environmental CO_2 are still unknown. Such knowledge could enhance opportunities for engineering cyanobacterial carbon responses in green biotechnology. CO_2 can react with neutral amines at physiological temperatures and pressures to form carbamates. This post-translational modification has been reported on RuBisCO and haemoglobin but is unexplored as a mechanism for CO_2 detection in cyanobacteria. This thesis identifies the carbamylation of the allophycocyanin alpha subunit (ApcA) in the photosynthetic cyanobacterium *Synechocystis* sp. PCC 6803. Allophycocyanin is a component of the cyanobacterial light-harvesting complex, the phycobilisome. This research presents work on the discovery of previously unknown allophycocyanin carbamate formation, as well as spectroscopic analysis of the CO_2-binding role in allophycocyanin energy transfer. Carbamate formation in ApcA Lys-6 was identified using ESI-MS/MS combined with ^{12}C and ^{13}C isotope addition. The proteomic screen was validated by the study of recombinant ApcA using ^{13}C NMR. CO_2-binding to the *Synechocystis* sp. PCC 6803 allophycocyanin alpha subunit of the light-harvesting complex proved to affect excitation energy transfer. Photoluminescence quantum yields of allophycocyanins increased in the presence of CO_2/HCO_3^- in isolated material and the whole organism. This thesis provides evidence of a novel area of research on the effects of CO_2 in the light-harvesting complex energy transfer.

Table of contents

List of figures

List of tables

Nomenclature

Roman Symbols

3-PGA 3-Phosphoglyceric acid

E. coli *Escherichia coli*

ACN Acetonitrile

Ap Ampicilin

APC Allophycocyanin

ATP Adenosine triphosphate

BCA Biocinchonic acid

BSA Bovine serum albumin

CA Carbonic anhydrase

$CaCl_2$ Calcium chloride

CCM Carbon concentrating mechanism

CD Circular dichroism

Chla Chlorophyll a

Ci Inorganic Carbon

Ci Inorganic carbon

Cm Chloramphenicol

CNBr Cyanogen bromide

CO_2 Carbon dioxide

CO_3^{2-} Carbonate ion

CRISPR Clustered regularly interspaced short palindromic repeats

Cyt Cytochrome

DAS Decay associated spectra

DCMU 3-(3,4-dichlorophenyl)-1,1-dimethylurea

DIC Dissolved Inorganic Carbon

DIC Dissolved inorganic carbon

DMSO Dimethyl sulfoxide

DNA Deoxyribonucleic acid

dNTP Deoxynucleotide triphosphate

DTT Dithiothreitol

EDTA Ethylenediaminetetraacetic acid

EET Excitation Energy Transfer

Fd Ferredoxin

Fe-S Iron-Sulfur

FRET Förster resoncance energy transfer

GEO Great Oxygation Event

H_2CO_3 Carbonic acid

H^+ Hydrogen ion

HCO_3^- Bicarbonate ion

IPTG isopropyl-β-D-1-thiogalactoside

KCl Potassium chloride

Km Kanamycin

LB Luria-Broth

LC-ESI-MSMS Liquid Chromatography Electro Spray Ionisation Tandem Mass

LC-MS/MS Liquid Chromatography with tandem mass spectrometry

LCM Core-membrane linker polypeptides

LRC Rod-core Linker polypeptides

MALDI Matrix-assisted laser desorption/ionization

$Mg_2{}^+$ Magnesium ion

MMTS methyl methanethiosulfonate

MW Molecular weight

NADH Reduced nicotinamide adenine dinucleotide

NADP Nicotinamide adenine dinucleotide phosphate

NADPH Reduced nicotinamide adenine dinucleotide phosphate

$NaHCO_3$ Sodium bicarbonate

NaOH Sodium Hydroxide

NMR Nuclear magnetic resonance

O_2 Oxygen

PAGE Polyacrylamide gel electrophoresis

PBP Phycobiliprotein

PBS Phosphate buffer saline

PBS Phycobilisome

PC Phycocyanin

PCB Phycocyanobilin

PCR Polymerase Chain Reaction

PE Phycoerythrin

PLQY Photoluminescence quantum yield

PQ Plastoquinone

PQH2 Plastoquinol

PSI Photosystem I

PSII Photosystem II

PTM Post Translational Modification

QA Primary quinone

QB Secondary quinone

RC Reaction centre

RNA Ribonucleic acid

ROS Reactive oxygen species

RubisCO Ribulose 1,5-bisphosphate carboxylase/oxygenase

SDH succinate dehydrogenase

SDS Sodium dodecyl sulfate

SEC Size exclusion chromatography

SOC Super Optimal broth with Catabolite repression

Sp Spectinomycin

TAE Tris-Acetate-EDTA

TB Terrific broth

TCEP (Tris(2-carboxyethyl)phosphine)

TCSPC Time-correlated single photon counting

TEAB Tetraethylammonium bromide

TEO Triethyloxonium tetrafluoroborate

TFA Trifluoroacetic acid

Tris-HCl Tris hydrochloride

UV Ultraviolet

WT Wild-type

Chapter 1

Introduction

1.1 Overview

This thesis provides evidence for the carbamylation of cyanobacterial proteins and the significance of carbamate formation on allophycocyanin energy transfer. Protein carbamylation is based on the formation of a carboxyl group at a neutral amine of a protein; this is a post-translational modification that converts the amine to an anionic group with possible functional consequences.

Despite the labile nature of carbamates, a method for identifying carbamate formation in the proteome of model organisms under comparable physiological conditions has been recently developed [48]. This method is a breakthrough in the field to uncover the importance and the involvement of carbon dioxide (CO_2) in physiology not only in photosynthetic organisms but in all living beings. Hence, this project aimed to use this method to discover new carbamates in a cyanobacterial proteome, which then enabled the investigation of the role of CO_2 carbamylation on a light-harvesting protein.

This chapter will begin by explaining the relevance of CO_2 to cyanobacterial metabolism. Additionally, a particular focus on cyanobacterial electron transfer will be described as relevant for the following experimental chapters.

1.2 Cyanobacteria: The green microbial factory

1.2.1 Introduction

The long evolutionary history of cyanobacteria on Earth has influenced our planet's geochemistry today. These organisms' ability to use water as an electron source in photosynthesis has mainly contributed to the balance between CO_2 and oxygen (O_2) in the atmosphere. Cyanobacterial predecessors appeared first around 2.7 billion years ago in stromatolites fossils. These bacterial communities depended predominantly on CO_2 fixation using H_2S as the hydrogen donor [15]. The accumulation of atmospheric O_2 levels, referred to as the Great Oxidation Event (GEO), is usually related to cyanobacteria as early as 2.45–2.32 Giga-annum (Ga) with the cyanobacterial fossil record starting at 1.8 Ga [35], and horizontal gene transfer analysis at 1.2-1.6 Ga [59]. Moreover, the relationship between the multicellularity of cyanobacteria and the rise of O_2 has been suggested to have played a key role in triggering cyanobacterial evolution around the GEO [81]. Nevertheless, as the major phototrophic lineages are considered not to be closely related to one another in bacterial phylogeny, the origins of their respective photosynthetic machinery (Fe–S type and Quinone type) remain unknown by time and sequence similarity; thus, the timing of oxygenic photosynthesis is still debated [22].

Cyanobacteria live in almost any environment, from seas to freshwater, soil to bare rocks, deserts to ice shelves, hot springs to Arctic and Antarctic lakes, and as endosymbionts in plants, lichens, and many protists. As a consequence of their ability to survive in various environments, cyanobacteria display a variety of secondary metabolites that are of interest as an excellent source of bioactive compounds, biofuel, biopolymers, colouring dyes, medicines, food supplements, and biofertilizers [44]. Additional to the many applications of cyanobacteria in biotechnology, these organisms have the potential to be a viable alternative bio-based system for the sustainable production of biofuel and other bioproducts. Therefore, further understanding of photosynthesis in cyanobacteria is of great importance.

1.2.2 Photosynthesis

Cyanobacteria are oxygenic photoautotrophs; they use light to synthesize organic compounds from CO_2 and water, producing O_2 as a waste product. Unlike plants, cyanobacteria photosynthesis and respiration require electron transport pathways catalyzed by protein complexes in lipidic membranes. These membranes, called thylakoids, separate the cytoplasm from the lumen.

The thylakoid membrane contains both photosynthetic and respiratory electron transport chains. These electron transport chains intersect and use part of the same membrane components. The photosynthetic machinery consists of a series of protein complexes that catalyze the light reactions (Fig. 1.1). The thylakoid membrane comprises four protein complexes: Photosystem II (PSII), Cytochrome b6f complex, Photosystem I (PSI), and ATP synthase. These complexes create the products ATP and NADPH [13]. The latter two species are mostly consumed to reduce CO_2 and subsequently turn it into chemical energy in sugars.

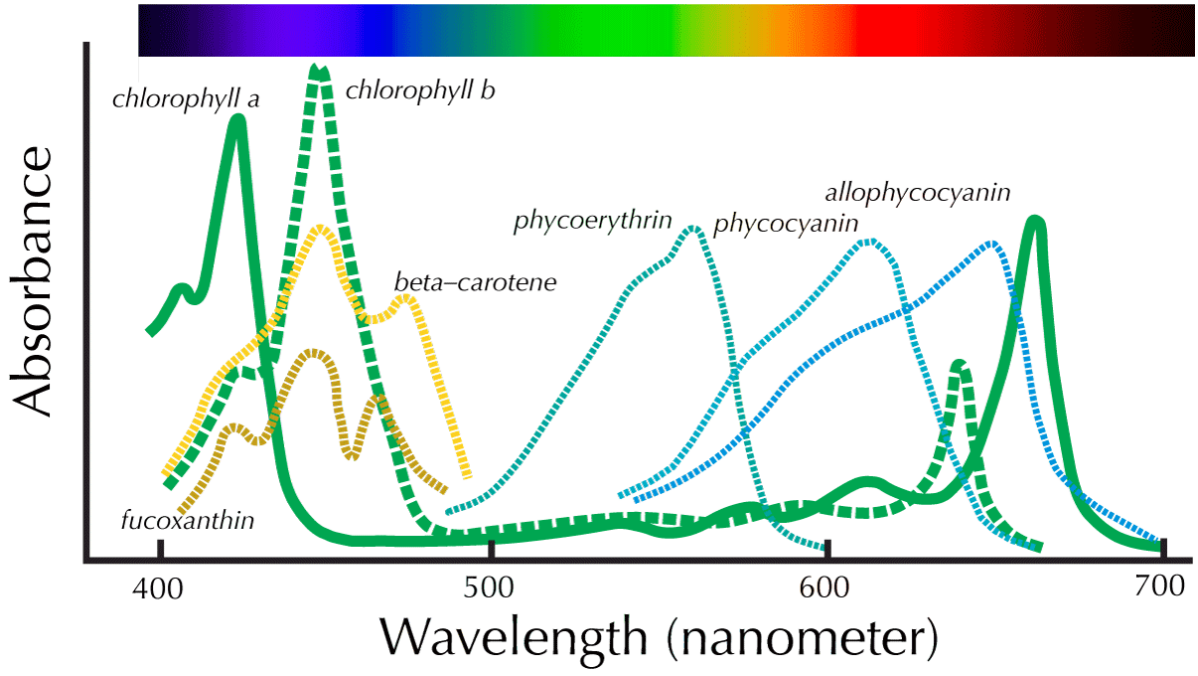

Fig. 1.1 Absorption spectra of photosynthetic pigments. Cyanobacteria can absorb energy from the blue to the red range of light (400-700 nm). Figure adapted from Goodwin and Mercer [30]

Energy transport flow

The electron transport chain in cyanobacteria starts with energy absorption from light through the phycobilisome (PBS). This complex is an integration of several antenna molecules: phycoerythrin (PE), which is absent in most cyanobacteria, phycocyanin (PC) and allophycocyanin (APC); which exhibit molecular masses in the range of 15-22 kDa. These pigments have different spectral properties; each has a specific absorption and fluorescence emission maximum in the visible range of light as represented in Fig. 1.2. The particular arrangement within the PBSs allows the absorption and unidirectional excitation energy transfer from light absorption to chlorophyll a (Chl a) of the photosystem II (PSII). The presence of linear tetrapyrroles (phycobilins) causes their strong absorbance in the visible spectrum, from 570 nm by PE in red algae, to 630 nm and 650 nm by PC and APC, respectively. These pigments are organized in a hierarchic structure so that the chromophore absorbing at higher energy (PC and PE) is located at the complex's periphery. And those absorbing at lower energy (APC) build up the PBS core (Fig. 1.2)[14][31]. Thereby, compared to algae and plants, the cells can take advantage of light's available wavelengths, not accessible to Chl a.

PBSs have a hemidiscoidal form, where the rod domain is built by six or eight cylindrical rods that emit to the core domain (Fig. 1.3). All these pigments contain their corresponding linker polypeptides which have only a structural function. The core domain is more commonly composed of three cylindrical sub-assemblies, although up to five cylinders have been found before in *Anabaena* sp. PCC 7120 [24]. Each core cylinder is made up of four disc-shaped phycobiliprotein (PBP) trimers, APC, allophycocyanin B (AP-B) and APC core membrane linker complex (AP-LCM) (Fig. 1.3A). The last protein core-membrane linkers distribute the remaining excitation energy between PS I and PS II [88].

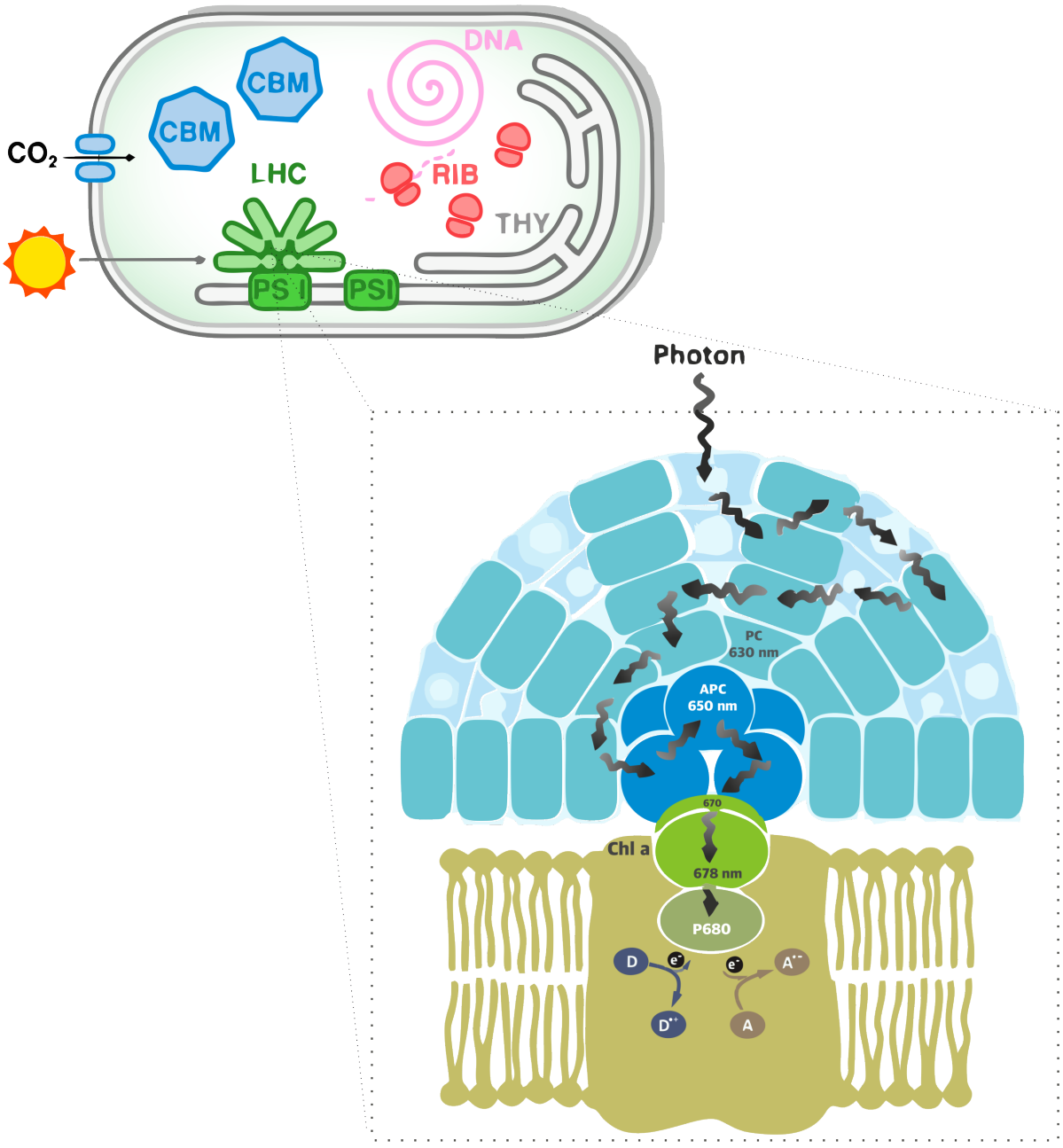

Fig. 1.2 Schematic representation of the arrangement of pigments and energy transfer pathways in PBS from *Synechocystis* PCC 6803. Photons from light are absorbed in the periphery by phycocyanins with a maximum absorption at 570 nm, then transferred to the allophycocyanin core complex absorbing at 650 nm and finally delivering energy to chlorophyll of PSII and/or PS I. Adapted from Govindjee [86].

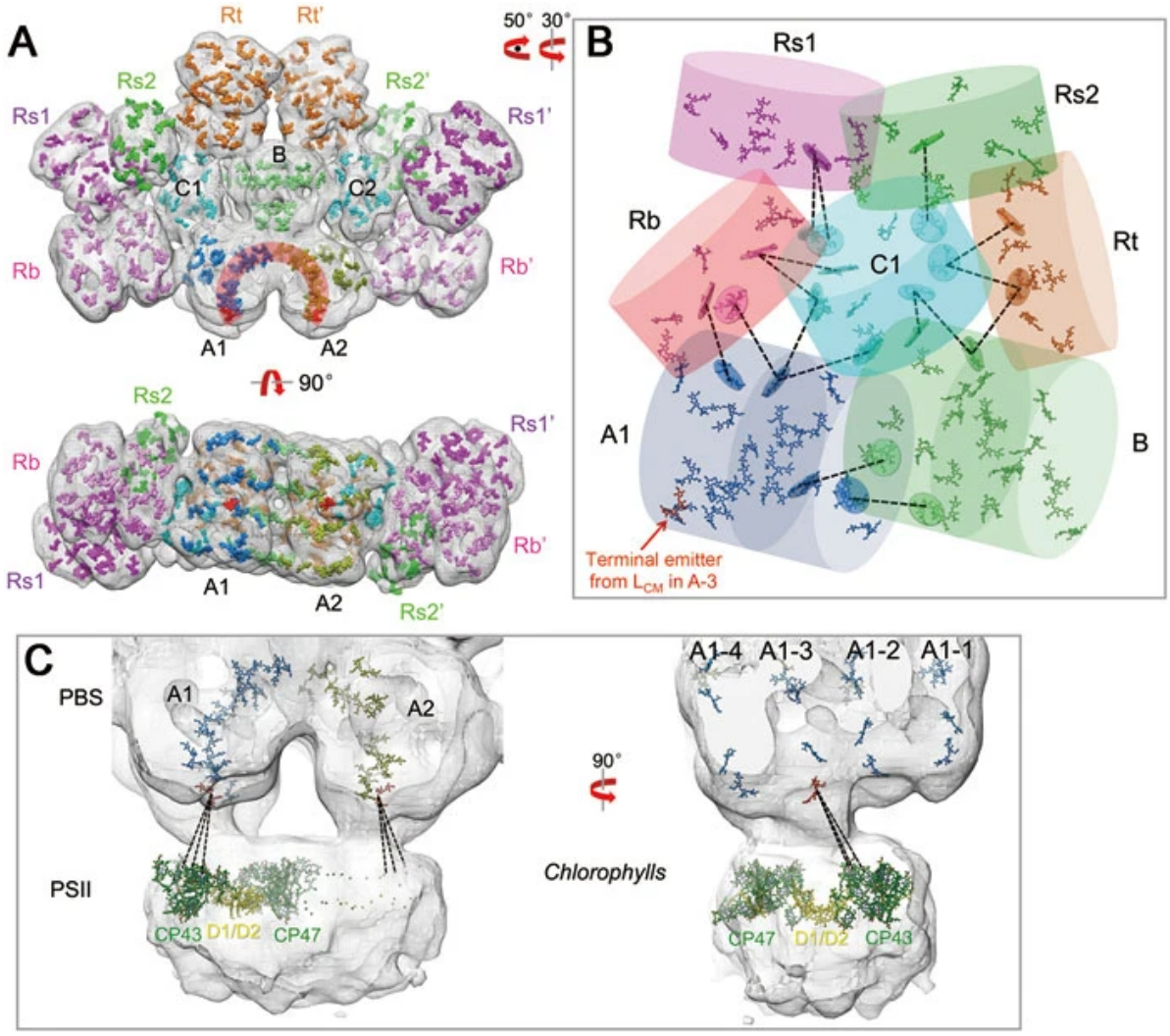

Fig. 1.3 Pigment arrangement and energy transfer pathways. **A.** Pigment arrangement in the intact PBS. Pigments from A1 and A2 (front view) form an inverted U shape (coloured dark orange), in which the terminal emitters from disc three are coloured red. **B.** Energy transfer from the rods to the core. All pigments in core cylinders A1, B, and C1 and the pigments from the core-connected PC trimers are shown. Dashed lines indicate the distances of one or two nearest pigment (from rods to the core). **C.** Energy transfer from PBS to PSII. The electron density map of the PBS-PSII complex is shown in mesh. Pigments from core cylinders A1 and A2 and chlorophylls from one PSII monomer (35 chlorophylls) are presented. Taken from Chang *et al.*[17]

Cyanobacteria can alter the transfer of excitation energy between PSI and PSII [42]. Illumination conditions that lead to excess excitation of PSII compared with PSI induce a transition to State 2, in which more absorbed excitation energy is diverted to PSI. When PSI is over-excited relative to PSII, this induces a transition to State 1, in which more energy is transferred to PSII. This process is called state transition. The physiological role of the state transition is still debated. Nevertheless, it was found that state transitions are physiologically important only at very low light intensities. In general, PBSs are considered an antenna delivering excitation to the reaction centres principally to PSII and a lesser extent to PSI [17]. This distribution will depend on changes in light conditions or metabolic demands. There is an association of the PBSs to PS I reaction centre, specifically under conditions that promote a high level of reduction of the inter-chain electron mediator plastoquinone, or strongly unbalanced excitation between the two photochemical centres [68]. It is considered that light-harvesting PBSs shuttle between both photosystems to balance this activity. Still, it has been shown that the rearrangement of the photosynthetic apparatus during dark-light transitions does not involve the photosystems. A small amount (13%) of the PBSs' total pool uncouples from PSI in the light [18].

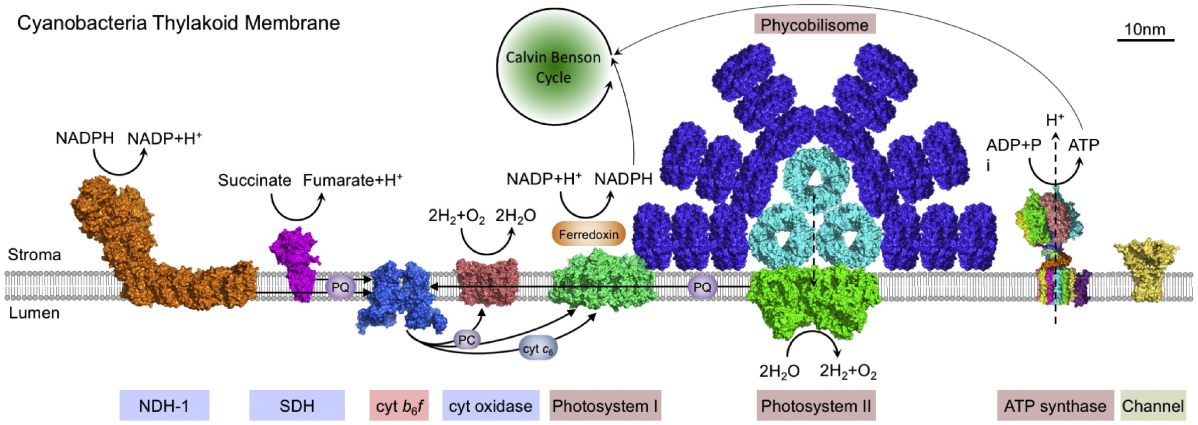

Fig. 1.4 Schematic representation of the intersecting photosynthetic and respiratory electron transport pathways in thylakoid membranes of the cyanobacterium *Synechocystis* sp. PCC 6803. The photosynthetic electron transport complexes in the thylakoid membrane include PBS, PSII, PSI, cyt b6f and ATP synthase. Also, small electron transport molecules, such as PQ, PC, and c6, function as electron carriers to shuttle electrons between each electron transport complex and functionally link all the complexes together. Adapted from Liu *et al.* [51].

After the photons pass through the antenna systems, they reach the reaction centre Chl a (P680) of the PSII complex priming linear electron transfer. In electron transfer (Fig. 1.4),

PSII uses light energy to split water, where the excited P680 donates its electron to an electron acceptor (lipophilic plastoquinone (PQ)). After acquiring two electrons and two protons, PQ becomes reduced to plastoquinol (PQH2) and diffuses into the PQ pool. From the PQ pool of the cytochrome (cyt) b6f complex electrons to the plastocyanin or cytochrome c 553. The last two acts as a one-electron carrier and can reduce the oxidised PS I reaction centre: chlorophyll $P700^{+}$. The oxidation of RC chlorophyll is done by a light-induced transfer of an electron from PSI to ferredoxin (Fd) and subsequently to NADP. NAPD is later reduced and used along with ATP for CO_2 fixation in the cytoplasm [45].

Respiratory electron transport

Cyanobacteria use respiration to maintain a transmembrane proton gradient that is required mainly for ATP production. Respiration occurs in the thylakoid membrane shared with the photosynthetic electron transport. Both share several components as PQ, cyt b6f and PC/cyt c6 (Fig. 1.4). Here a photosynthetic electron transfer promotes a proton gradient across the thylakoid membrane. The protons that are release come from water splitting in PSII and plastoquinol oxidation. And the proton gradient is finally used for ATP synthesis, which may be used for CO_2 fixation and other cell processes.

Cyanobacterial respiration is diverse, where different and alternative electron donors and oxidases exist; however, their contributions remain unclear. The principal components of the respiratory electron transfer process are NAD(P)H dehydrogenase (NDH-1), succinate dehydrogenase (SDH), Cytochrome b6f complex and Cytochrome c oxidase (COX), as well as other terminal oxidases. There have been several known respiratory terminal oxidases for cyanobacteria. Several terminal oxidases accept electrons directly from PQ. They include cytochrome bd-quinol oxidase (Cyd), the alternative respiratory terminal oxidase (ARTO) and plastid terminal oxidase (PTOX) [20].

Moreover, cytoplasmic membrane and alternative electron transport pathways have been proposed and studied. Many of these seem to function to protect cells under stress conditions. It is confirmed that many respiratory complexes play a crucial role in photoprotection, allowing cyanobacteria to respond to changes in light intensity and prevent over-reduction of the interlinked electron transport chain in thylakoid membranes with potentially damaging consequences [67].

1.2.3 Allophycocyanin. The core of the light-harvesting process

Allophycocyanins (APCs) are the PBPs with the longest wavelength absorbance and fluorescence among the PBSs. They assemble the PBS core by three types of linker polypeptides: the large core-membrane linker PBP (LCM); rod-core linker polypeptides (LRC); and small Lc linker polypeptides. APCs are observed in different cyanobacteria as bicylindrical, tricylindrical, and pentacylindrical cores. X-ray crystallography studies of different cyanobacteria species have shown the monomeric, trimeric and hexameric composition of APCs [61][11][50]. Allophycocyanin trimers have been determined with a C3-symmetry, constituted by three homo-monomers (Fig. 1.5). Each APC monomer contains two subunits (α and β), both subunits of allophycocyanin monomers show almost identical structures, even though the subunit homology is only about 38%. Each subunit contains one phycocyanobilin (PCB) pigment. The biliprotein chromophores are covalently attached to the apoproteins through thioether bonds to cysteine residues ($\alpha - 84$ and $\beta - 84$) represented in Fig. 1.5.

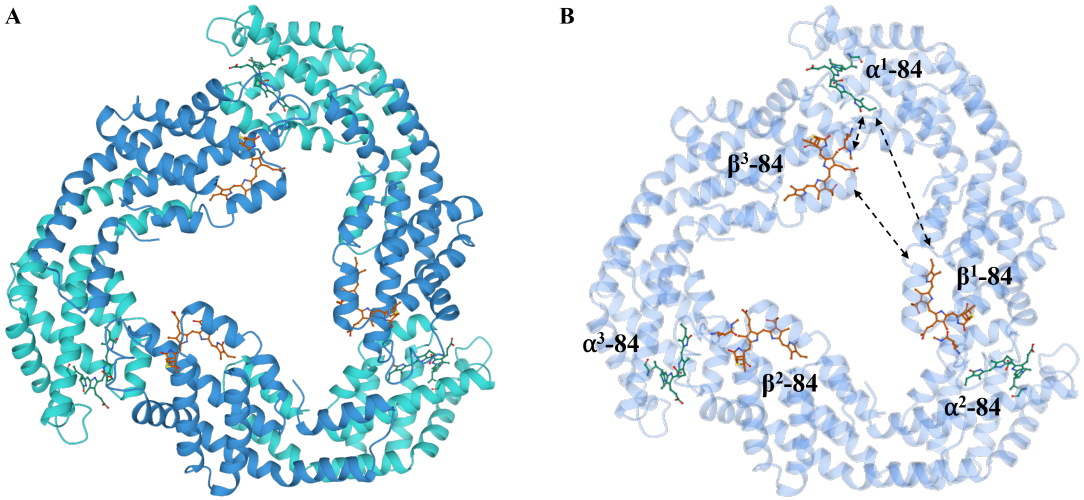

Fig. 1.5 Molecular structure of the PBP allophycocyanin adapted from Brejc *et al* [78]. Each $(\alpha\beta)_1$ monomer of the APC trimer binds two phycocyanobilin chromophores (shown in orange and green). **A.** 3D View produced from protein data bank structure 1ALL. **B.** Representative structure of chromophore located in each monomer, PCBs energy transfer shown with arrows. The strongest interaction between PCBs pairs occurs at the interface between the subunits.

The efficiency of APCs' entire energy transfer is one of the most successful in the photosynthetic world. It can be larger than 90% and occur in a very fast time frame: 100-200 ps or even less than 0.5 ps [84][78]. Several investigations have been reported to understand the energy transfer mechanism of this process. Experimental studies have shown a maximum absorption in the APC monomer at 615 nm, and maximum absorption of APC trimers at 650 nm with a notable shoulder at 620 nm [58]. Interestingly, the dissociation from trimers to monomers leads to the 650 nm absorption band. The maximum loss of the 660 nm is associated with a strong exciton coupling between the $\alpha 84$ and $\beta 84$ chromophores on adjacent monomers across the monomer-monomer interfaces [57]. Even though this suggests exciton coupling between chromophores, the excitation energy transfer (EET) has still been modelled invoking the Förster electronic energy transfer mechanism. A donor molecule being excited and by rapid vibrational relaxation goes to its first excited state's lowest vibrational level. The donor's and acceptor's spectra are not usually affected by this process. Hence they are considered independent entities, where the acceptor tends to be at lower energy than the donor. Förster resonance energy transfer occurs throughout photosynthesis and provides high efficiency over reasonable distances [28]. Within the framework of Förster's theory, computational studies of Ren *et al.* [78] calculated the shortest energy transfer time in the APC trimer of about 0.10 ps and about 170 ps in the APC monomer, which are similar with to the experimental finding of a very fast lifetime of 0.43–0.44 ps in APC trimers previously determined. Although, Ren *et al.* suggest these results are most likely attributed to the energy transfer of $\alpha^1 - 84$ and $\beta^3 - 84$ (0.23 ps), $\beta^1 - 84$ and $\alpha^2 - 84$ (0.11 ps) or $\beta^2 - 84$ and $\alpha^3 - 84$ (0.10 ps) (Fig. 1.5B).

Recent studies of Eisenberg *et al.* using *T. vulcanos* isolated APCs demonstrated the reorganizations of PCs reversing the energy flow differently depending on the environment [26]. The exposure of chromophores to the environment and their interactions with adjacent proteins are shown to tune the cyanobacterial light-harvesting system between two modes: an efficient funnelling toward RCs and an efficient quenching to the environment away from RCs. Their study showed that small changes in conformation can generate significant effects on the EET process's energetics that are still unknown.

1.3 CO_2: The biological role

1.3.1 CO_2 in bodies of water

CO_2 is a greenhouse gas of environmental concern and a key metabolite in living organisms. It plays an essential role in such fundamental biological processes as respiration, photosynthesis and cell signalling. CO_2 in water is 99% of the time present as the dissolved gas and less than 1% as carbonic acid, which then dissociates to hydrogen protons and bicarbonate anions (Fig. 1.6).

We can find dissolved inorganic carbon (DIC) in all natural waters. DIC concentration varies from less than 20 μM in soft acidic waters to more than 5000 μM in highly alkaline hard waters but ranges between 100 and 1000 μM in most systems. DIC consists of three main constituents (Fig. 1.6): free CO_2 (a gas), the bicarbonate ion (HCO_3^-), and the carbonate ion (CO_3^{2-}). Bicarbonate and carbonate are the major buffering system in most natural waters, whereas free CO_2 is the dominant acid in most natural waters. Thus, the ratio of CO_2 to HCO_3^- and CO_3^{2-} is the principal control of pH in most natural waters [19]. At the same time, CO_2 produced by cells during aerobic metabolism of glucose and fats provides the acid (H^+ and CO_2) and base (HCO_3^-) components for the bicarbonate buffering system. This buffering system maintains both intracellular and extracellular pH of living organisms [74].

1.3.2 The chemistry of CO_2 in aqueous solution

CO_2 is a soluble gas that reversibly reacts with water molecules to produce carbonic acid. And this carbonic acid can dissociate twice as observed in Fig. 1.6**A**. As shown in a Bjerrum plot (Fig. 1.7), when the solution is in equilibrium, the different inorganic carbon species' concentration will depend on pH. In seawater (pH about 8.1), of neutral or slightly alkaline water, the bicarbonate form predominates [63].

In biological systems, CO_2 is in equilibrium with its hydrated form H_2CO_3, followed by dissociation into H^+ and HCO_3^- in seconds via the enzyme carbonic anhydrase activity. Hence, biological systems are sensitive to pH. Cells actively transport H^- and HCO_3^- to regulate intracellular pH. Thus, levels of CO_2, HCO_3^- and H^+ are crucial to maintaining cellular homeostasis.

A

$$CO_2 + H_2O \rightleftharpoons H_2CO_3 \rightleftharpoons H^+ + HCO_3^-$$

B

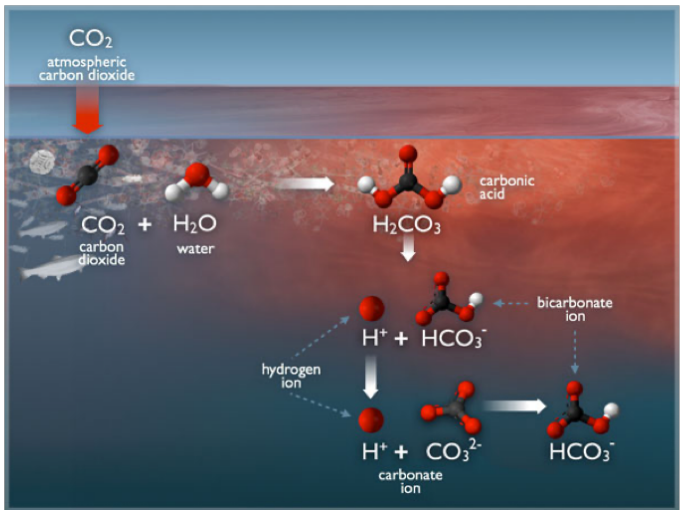

Fig. 1.6 Equilibrium of dissolved inorganic carbon in water. **A.** Equilibrium between CO_2 and HCO_3^- in solution; **B.** The ocean carbonate system from the Center for Environmental Visualization (2017)[16]

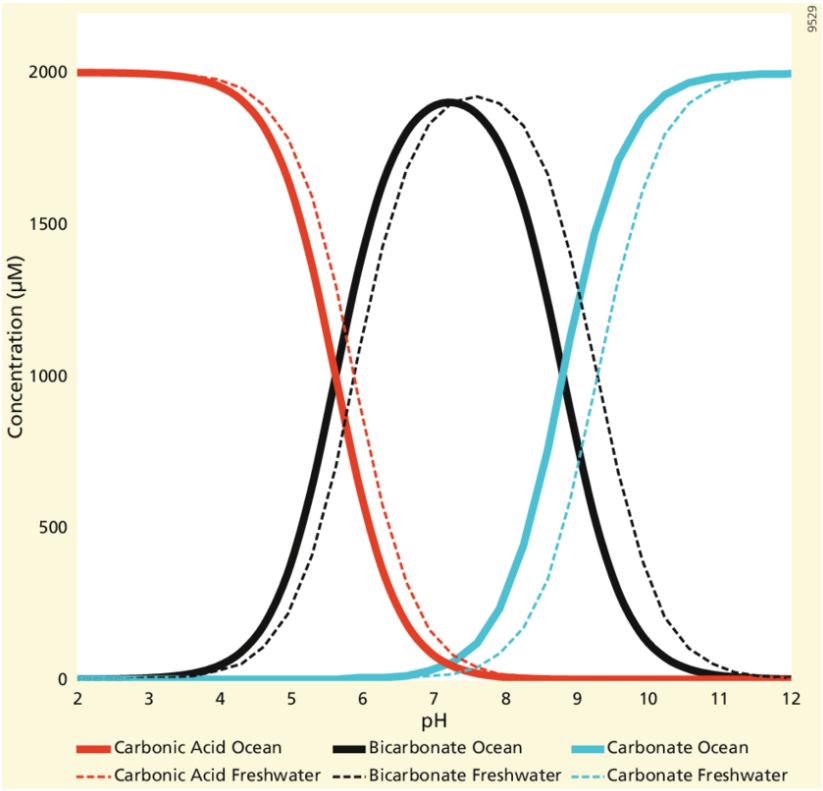

Fig. 1.7 Bjerrum plot showing the distribution of carbonic acid (red), bicarbonate (black) and carbonate (blue) ions as a function of pH in freshwater (dashed line) and seawater (solid lines). DIC = 2000 μM. Taken from Jack *et al.* [63].

1.3.3 Cyanobacteria inorganic carbon uptake

Cyanobacteria can be found in almost every habitat, from temporarily moist rock in deserts to oceans and even Antarctic rocks. Their resilience to every kind of climate conditions is based on their adaptation for inorganic carbon (Ci) uptake. Systems such as the Ci-Concentrating mechanisms are operational, and the intracellular Ci level is elevated to sustain high photosynthetic activity when photosynthetic microorganisms are grown under low CO_2 concentrations of air. The concentration of free CO_2 in cyanobacteria cells is expected to be between 0.2 to 3 mM from the extracellular Ci concentrations (0.9 to 6 mM) and intracellular pH. Internal Ci (CO_2/HCO_3^-) concentrations as high as 50 μM or higher have been reported in cyanobacteria grown in low CO_2 conditions. When the pH and the membrane potential across the cytoplasmic membrane are taken into account, it is clear that Ci accumulation occurs against its electrochemical potential gradient [40][6].

Carbon Concentrating Mechanisms

Cyanobacteria have evolved an advantageous single-cell CO_2 concentrating mechanism (CCM). This multi-component system is comprised of the carboxysome and a suite of Ci transporters, which have enabled cyanobacteria to proliferate under relatively low ambient atmospheric CO_2 and high O_2 levels.

Inorganic carbon enters the cells by diffusing over the plasma layer and accumulates in the cytoplasm via energy-dependent systems. To keep the loss of CO_2 from the cell and maintain an internal gradient of CO_2 over the cell envelope, cyanobacteria contain two $NADPH^-$ dependent systems that catalyze the hydration of CO_2 to HCO_3^-; NDH-I4 and NDH-I3 (Fig. 1.8). Regardless of whether HCO_3^-; or CO_2 is supplied, bicarbonate is the predominant species in the cytoplasm and the Ci species are not at chemical equilibrium there, being HCO_3^- less likely to escape through the cell membrane [73][5].

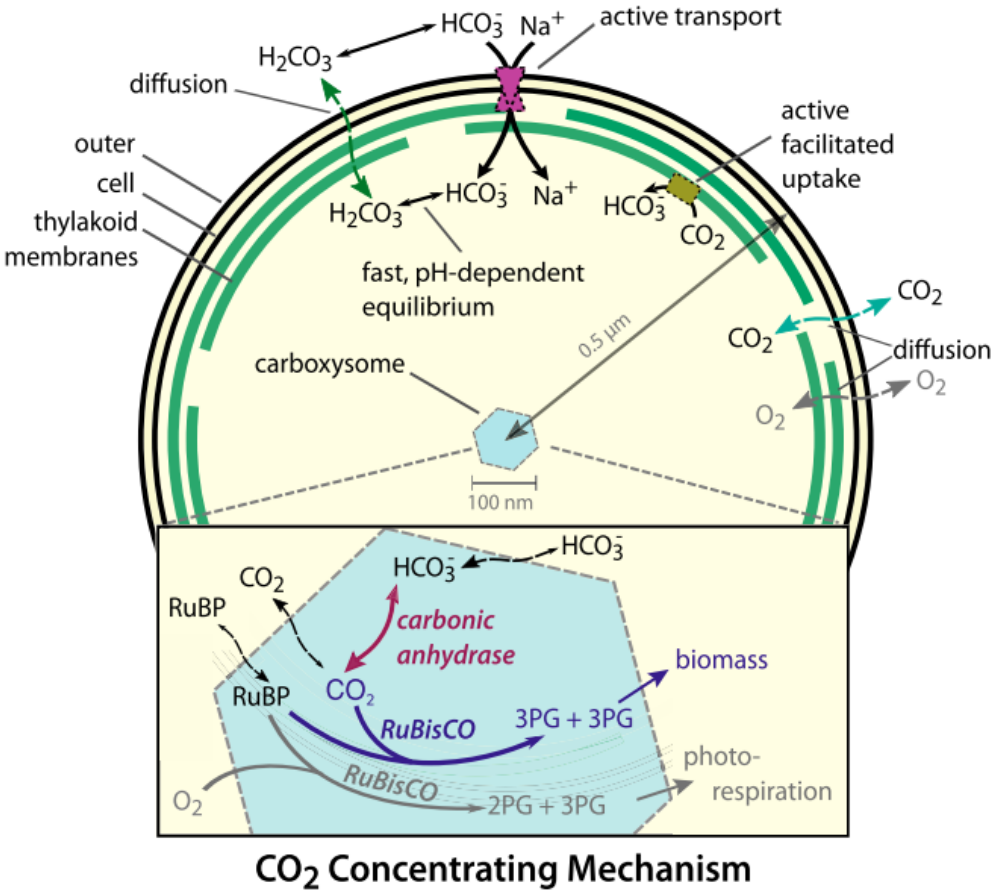

Fig. 1.8 Schematic representation of a model cyanobacterial CCM. Taken from Magnan *et al.* [60]

There are three active transport systems and CO_2 hydration components of the CCM that effectively generate a high concentration (up to 40 mM) of HCO_3^- within the cell. First, bicarbonate passes through the thylakoid region and enters the carboxysomes, where it is converted to CO_2 by carbonic anhydrase (CA). Second, some of the HCO_3^- is fixed at the adjacent carboxylation sites of ribulose biphosphate carboxylase-oxygenase (RubisCO) producing two molecules of 3-PGA. Finally, 3-PGA exits the carboxysome and is used by Calvin-Benson cycle enzymes (Fig. 1.8). Eventually, part of the CO_2 generated may leak from the carboxysomes to the cytoplasm. Here, the NADPH-dependent system converts it back to bicarbonate and minimises the waste leak of CO_2 from the cells [6] [88].

CO_2 has a noticeable role in cyanobacterial adaptation. Diverse experimental studies have found various changes when the culture is grown from a high CO_2 concentration (1-5%) to a low concentration (air concentration). Changes like: the modification of purine biosynthesis; a rapid increase in the ability to accumulate Ci within the cells (half-time of about one h), and hence a substantially higher apparent photosynthetic affinity for extracellular Ci; a change in the amount of RubisCO; an increase in the number of carboxysomes (about 4-fold) and a difference in their location from the cell-centre towards its periphery; an alteration in the thickness of some of the layers that comprise the cell envelope; and a change in the phosphorylation pattern of polypeptides [40].

Cyanobacteria adapt to rising CO_2 concentrations by enhancing photosynthesis. Quantitative proteomics technologies have allowed the screening of proteome-wide regulations by CO_2 of *Synechococcus elongatus*. Mehta and collaborators presented the response of *Synechoccosus* to different CO_2 conditions in the range of 0.04% to 10%. Interestingly, they found an up-regulation of photosynthetic machinery composition when cells were grown at high CO_2 concentrations, which could be due to the abundant inorganic substrate available for carbon fixing reactions. Contrarily, proteins involved in photoprotection and redox maintenance were found down-regulated [62].

Although the general function, structure and regulation of the cyanobacterial CCM have been studied in great detail during recent years, additional knowledge of Ci- depending adaptation processes- is not fully understood. Small regulatory RNAs and direct post-translational regulation of protein activities are potential candidates for cyanobacteria CO_2 acclimation.

1.3.4 The role of inorganic carbon in photosystems

The role of inorganic carbon (CO_2/HCO_3^-) is not restricted as a carbon source for storage of harvested energy from sunlight in the form of energy-rich carbohydrates. Additional evidence has demonstrated a connection between CO_2 fixation and availability to energy and electron transfer across several photosynthetic systems. For example, Mehta *et al.* found essential proteins like cytochromes, plastocyanin, reaction centres of PS-I and PS-II (photosystem-I and II) to be up-regulated as a response to high concentrations of CO_2. Specifically, allophycocyanin's alpha subunit was 3.6 folds up-regulated in 1% CO_2 condition, whereas the beta subunit showed a 0.17 folds down-regulation at 10% CO_2 [62].

It is important to emphasize that CO_2/HCO_3^- acts as a regulator of the photosynthetic electron transport in PSII in cyanobacteria, algae and plants. Bicarbonate's role in cyanobacteria energy systems has taken about 50 years to elucidate both in the acceptor side and the donor side reactions, also known as the bicarbonate effect of PSII. On the electron acceptor side, experimental data showed that HCO_3^- binds and plays a vital role in facilitating the reduction of QB and in protonation reactions near the QB-binding site [12]. On the donor side, Klimov and collaborators determined that HCO_3^- ions are required for the efficient photo-induced assembly of the Mn_4CaO_5 cluster capable of water splitting. Other groups indicated the requirement of HCO_3^- on the water-splitting side of PSII. Nonetheless, the binding site and the role of HCO_3^- ions in the water-splitting reaction of PSII needs further research. X-ray crystallography studies of PSII revealed single bound bicarbonate at the NHI in the cyanobacterial reaction centre (RC) [91]. Bicarbonate seems to have a unique role only in oxygenic photosynthesis that has not been found in anoxygenic phototrophs. HCO_3^- stabilizes the QA–NHI–QB structure of the PSII RC and allows efficient electron transport and protonation of QB via certain amino acids around QB.

Knowledge of carbon concentrating mechanisms and bicarbonate role in energy transfer clarifies how cyanobacteria cope with limiting or excessive CO_2/HCO_3^-, but there is still so much unknown of how CO_2/HCO_3^- availability is coupled to other mechanisms of energy transfer, metabolism, replication, and growth.

1.4 Carbamylation: CO_2 Post-Translational Modification

CO_2 carbamylation, or carboxylation, occurs when CO_2 reacts with protein uncharged amines to form carbamates. This post-translational modification (PTM) has been proposed as a biological regulatory mechanism where CO_2 converts these neutral amines into negatively charged groups. The introduction of a negative charge by CO_2 binding in this manner can alter protein function in its physiological environment.

1.4.1 Carbamate formation

Carbamylation is a post-translational modification with great biological importance. Carbamylation occurs by a nucleophilic attack of uncharged amines upon CO_2 (Fig. 1.9). In biological systems, carbamylation changes the functionality of side chain lysine or N-terminal residues from basic/neutral to acidic [56]. The formation of the carbamate bond is reversible. This reversibility allows the regulation of carbamate-dependent processes through the presence or absence of the reaction scheme's components, *i.e.* CO_2 or H^+ (Fig. 1.9).

$$\text{R-NH}_3^+ \overset{\pm\text{H}^-}{\rightleftharpoons} \text{R-NH}_2 + \text{CO}_2 \overset{\pm\text{H}^+}{\rightleftharpoons} \text{R-NH-COO}^-$$

Fig. 1.9 Carbamate formation equilibria

Specific conditions have been observed to encourage carbamate formation. The increase in pH promotes the amount of carbamate formed [89]. This suggests that the charge on the amine group is the controlling factor in carbamate formation. The pKa of an amine group on a lysine residue, for example, varies from 9 to 13 depending on the environment [1]. Therefore, under normal physiological conditions of pH 7.4, most lysine's amine groups are in a charged state. However, it is also proposed that the fold of a protein can create an environment favourable to carbamate formation. This has been observed on β-haemoglobin chains, where end terminal valines, with a pKa of 6.6, are contained within such an environment that facilitates carbamate formation [32].

Yet, carbamylation has not been thoroughly investigated; its labile PTM characteristic makes it difficult to identify as the carboxyl group is spontaneously released in acidic conditions. Hence mass spectrometry cannot detect lysine carboxylation. X-ray crystallography can identify carboxylated lysine residues, although it is not entirely reliable. Besides the challenges that protein crystallography entails, third-generation synchrotron radiation's most frequent damage its acidic residues' decarboxylation [76]. Nevertheless, some proteins have been discovered to interact with CO_2 via carbamylation on a privileged NH_2 group, which will be discussed in the following section. Where carbamate formation has been found to trigger conformational and physicochemical changes essential for the function of proteins.

1.4.2 Carbamylated proteins

Haemoglobin

As previously mentioned, carbamylation is one of the first PTM described in the early 1900s by Bohr and collaborators. Even though the molecular chemistry behind CO_2's effect was not explained, they demonstrated the decrease in O_2 affinity as the partial pressure increases. Roughton *et al.* studied the historical dimensions of the interaction of CO_2 with haemoglobin and its profound chemical contributions to our understanding of it [80]. He promoted the view over several years that the effect of CO_2 on the haemoglobin affinity of O_2 could be due to carbamate formation in the α-amino N-terminal groups. This view was unambiguously confirmed later by Kilmartin and Rossi-elegant Bernardi's experiments [79]. They demonstrated that blocking of N-terminal α-amino groups by haemoglobin tetramers carbamylation with cyanate, the expected effect of CO_2 on the O_2-affinity profile was abolished. Morrow *et al.* later demonstrated the physiological relevance of the CO_2 reaction with the α-amino group. The carbamylation at the Val1β site, linked to the β-chain O_2 haemoglobin binding site, stabilizes the protein's deoxygenated form [66].

RubisCO

Ribulose biphosphate carboxylase-oxygenase (RubisCO) catalyzes atmospheric CO_2 fixation in photoautotrophs using Mg^{2+} and inorganic carbon as co-factors. CO_2 functions as a RubisCO's carboxylase reaction substrate and a co-factor that binds to an alternative enzyme site via

carbamylation. When RubisCO was first purified in the 1970s from spinach leaf extracts, there was speculation that two versions of the enzyme existed due to the estimation of a low carboxylase activity(Km=200 μM) and no oxygenase activity. Chloroplasts, instead, had a native activity with a Km of 10 μM. Four years later, a possible explanation of these two apparent forms of the enzymes was found with the experimental addition of magnesium or manganese, showing to reduce Km of the purified enzyme equivalent to the native chloroplast. They demonstrated that the ensyme is only active as a result of the low-Km (CO_2) form produced by contact with Mg^{2+} and CO_2/HCO_3^- [3]. Later experiments using RubisCO's enzyme from *Rhodospirillum rubrum* in 1979 anticipated that the activator CO_2 is bound to the large (catalytic) subunit. In addition, carbon-13 studies of the NMR of *R. rubrum* provided evidence for carbamate formation for RubisCO activation [71].

Later studies tracking the $^{14}CO_2$ bound at the active site of RubisCO demonstrated that this bound CO_2 is not involved in the enzyme's carboxylase activity. RubisCO proved to be sensitive to CO_2 and pH as a critical component of a carbamate reaction. Since the carbamate reaction results in the reversible creation of H^+, decreased pH drives the equilibrium towards the formation of free CO_2 rather than carbamate bonds. This finding implies that a carbamate bond is involved in RubisCO activation. This observation was confirmed later when a peak characteristic of carbamate bond formation was observed in the ^{13}C-NMR spectra for RubisCO and CO_2. This observation demonstrated that CO_2 bound as a carbamate to the epsilon-amino group of a lysine residue on the catalytic subunit [56].

Bacterial carbamylated proteins

In addition to haemoglobin and RubisCO, stable carbamate modifications have been identified in various crystal structures and reported as functional, some of which are discussed here in more detail.

Ureases play essential roles in nitrogen metabolism. CO_2/HCO_3^- activates virulence factors associated with various human and animal pathogens. The catalytic sites containing Ni^{2+} ions are bridged to a carbamylated lysine residue (K217) required for appropriate enzymatic activity [94].

The structure of alanine racemase from *Bacillus stearothermophilus* provided evidence for the existence of a carbamate formed on the side-chain amino group of Lys129. This carbamate

is stabilized by interactions with Arg136 that interacts with the carboxylate group of propionate. Thus, Lys129 carbamylation influences both substrate binding and catalysis by positioning Arg136 and modulating its charge [64].

Transcarboxylase is a *Propionibacterium shermanii* multienzyme complex that couples two carboxylation reactions, transferring CO_2 from methylmalonyl-CoA to pyruvate to yield propionyl-CoA and oxaloacetate. The active site cobalt ion of transcarboxylase 5S is coordinated by its carbamylated LysC184 the same way as the oxaloacetate product's transferred carboxylate. The structure revealed a dimer of 88 barrels with an active site cobalt ion coordinated by a carbamylated lysine, except in the oxaloacetate complex where the product's carboxylate group serves as a ligand instead. Cys154 suggested functioning as Lys184 stabilizer when noncarbamylated in a conformation such that it does not interfere with the substrate or product binding. At the same time, Lys184 proved to be indispensable for 5S catalytic activity [33].

Class D OXA-10 β-Lactamases, the resistance enzymes for β-lactam antibiotics, depend critically on a carbamylated lysine as the basic residue for both the enzyme acylation and deacylation steps of catalysis. Golemi *et al.* structures showed that full carbamylation of B-lactamases dimers depends upon pH. Carbamylated Lys-70 is the basic residue that promotes the serine hydroxyl for the acylation step under physiological conditions. This carbamylated lysine is also suitable for activating the incoming hydrolytic water for the deacylation event. [29].

Phosphotriesterase is capable of detoxifying pesticides such as paraoxon and parathion and various inhibitors of mammalian acetylcholinesterase. In the phosphodiesterase binuclear metal cluster, crystal structures of phosphotriesterase isolated from *Pseudomonas diminuta* showed two bridging ligands to cadmium ions: a water molecule and a carbamylated lysine residue (Lys169). Therefore, it is proposed that the enzyme uses a carbamylated lysine rather than a glutamate residue, so it is possible to delocalize the pair of electrons on the nitrogen, enabling negative charges to be carried by both O_2 ligands [8].

Carbamylation has also been found to predominate in the algae world. Yokota *et al.* examined the form of inorganic carbon accumulated in *Euglena gracilis* using ^{13}C-NMR carbamate resonance where carbamate formation was observed to be dependent on photosynthesis. The complex of *Euglena* protein - ^{14} CO_2 extracted from photosynthesizing was estimated to be about 1 nmol/mg protein when the cells accumulated 1 mM of Ci. In contrast, complex protein-

CO_2 was suppressed by darkening the cells or adding DCMU, an inhibitor of the photosynthetic electron transport chain. They proposed that protein carbamate constitutes about 50% of the intracellular Ci, where protein is likely to be contributing to the temporal accumulation of Ci in the cells [96].

1.4.3 Bioinformatics carbamate identification

CO_2 binding has also been studied using quantum mechanics and molecular modelling. Cundari *et al.* concluded that acid/base interactions are the dominant chemical force by which proteins bind CO_2. Beta-sheets were observed to be more susceptible to CO_2 binding between both classes of standard structural secondary elements than alpha-helices, and the amino acids most commonly found in CO_2 protein binding sites were arginine (pI-10.8), lysine (pI-9.5,) and histidine (pI-7.6). However, according to their molecular modelling, His is somewhat more common in CO_2 binding sites, despite Lys' greater basicity. Furthermore, the difference in electronegativity between carbon and oxygen yields a polarity of the $C\delta^+$=Oδ^- bond that can be used to bind CO_2. Thus, while serine (pI-5.7) and threonine (pI-5.9) are much less basic than Arg, His, and Lys, they have relatively high CO_2 affinities. Contrarily, negatively charged Asp and Glu exhibit very low binding tendencies, suggesting that CO_2 binding typically does not occur through the $C\delta^+$ [21].

Recent computational lysine carboxylation predictor estimated that carbamylation at a lysine residue can occur around 1.3% of protein structures with more than 200 amino acids [38]. This finding implies a threefold rise over those already identified.

1.5 Project Rationale

CO_2 is thoroughly involved in cyanobacteria metabolism. The biotechnological interest to use these microorganisms to produce metabolites of commercial interest in cyanobacteria is emerging. Cyanobacteria has attracted many scientists to use it as a green factory to develop biofuels, food ingredients, pharmaceuticals and cosmetic products. Efforts in optimizing CO_2 synthesis in cyanobacteria have been developed [4], although little has been done to identify how CO_2 interacts with proteins beyond its use as a substrate.

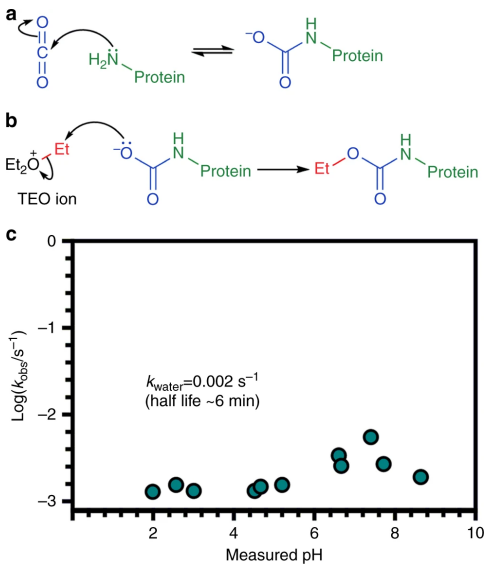

Fig. 1.10 Protein carbamate formation and trapping with TEO taken from Linthwaite *et al.*[48]. **a.** Carbamates form through the reversible reaction between CO_2 and neutral amine groups. **b.** Proposed trapping mechanism of a protein carbamate with TEO. TEO transfers an ethyl group (red) to the anionic carbamate derived from CO_2 (blue) and protein primary amine (green). **c.** Observed pseudo-first-order rate constants, k_{obs}, for the hydrolysis of TEO plotted as a function of pH (where $k_{obs} = k_{water} + [k_{hydroxide} K_W / 10^{-pH}]$)

The recent development of a technology to identify carbamylation in living organisms [48] has led us to investigate the impact of CO_2-mediated post-translational modification in cyanobacteria. Linthwaite *et al.* have tackled the labile limitation to identify protein carbamylation at physiological conditions. They developed a technology to trap the carbamates formed in complex proteomes. In this method, Triethyloxonium (TEO) is used to alkylate carbamates in CO_2-containing solutions at physiological pH (7.4-8.5). TEO transfers an ethyl group to the negatively charged carbamate formed by CO_2 in a privileged environment

(Fig. 1.10). Carbamate formation was confirmed in small peptides by the presence of a peak at 164 ppm by ^{13}C NMR spectroscopy and TEO trapping by LC-ESI-MS. Linthwaite *et al.* successfully identified eight carbamylation sites in *A. thaliana* proteome by the CO_2-trapping. In their work, AtPRX34, a Class III peroxidase PRX34, showed carbamate formation on Lys262 and Lys268 which are involved in the enzyme's specific activities at atmospheric CO_2 concentrations.

The importance and emergence of the role of CO_2 in physiological processes are evident. Because cyanobacteria can accumulate high concentrations of CO_2 intracellularly, carbamylation may be the only mechanism through which CO_2 can interact with proteins or by which inorganic carbon is detected. However, it is a post-translational modification in photosynthetic organisms that has not yet been explored.

1.6 Hypothesis and Objectives

We hypothesize that CO_2 interacts with a high number of proteins in cyanobacteria. Addressing this hypothesis will elucidate how cyanobacterial metabolism respond to changes in environmental CO_2 levels.

The overall aim of this project is to investigate carbamylation in cyanobacteria response to environmental CO_2 levels. We have employed TEO to identify CO_2-binding proteins in the cyanobacterial PBSs to determine the mechanistic basis for coupling CO_2 availability to electronic energy transfer (EET).

This investigation is divided into three main objectives. First, to identify and confirm carbamylation in cyanobacteria proteome under physiological conditions. Second, to find CO_2 role in APC photosynthetic activity. And third, to determine the *in vivo* role of APC Lys 6 carbamate formation.

This thesis will demonstrate that a light-harvesting protein (allophycocyanin) Lys 6 is carboxylated. First, ^{13}C-NMR and LC-MS/MS were used to demonstrate carbamate formation (Chapter 3). To elucidate the specific response to CO_2, spectrophotometric analysis of recombinant proteins was performed, examining how CO_2 modulates the PBPs' parameters (Chapter 4). Finally, *in vivo* assays were combined with genetic analyses to explore the role of the identified CO_2 binding site in the intact organism's physiology (Chapter 5).

Chapter 2

Materials and Methods

2.1 Materials and Equipment

All materials were purchased from Sigma-Aldrich unless otherwise stated. ESI Mass spectra were obtained on a Waters Ltd Orbitrap or Thermo LTQ XL QToF. Samples were lyophilised on an Eppendorf vacuum concentrator. pH measurements were carried out on a Fisherbrand™ accumet™ AB150 pH Benchtop Meter. The probe was calibrated using Thermo Fisher standards at pH 4, 7 and 10.

2.1.1 Cell lines

NEB® 5-alpha competent *E. coli* DH5 α (no antibiotic resistance, NCBI:txid668369) cells were obtained from New England BioLabs Inc. and used for cloning. *E. coli* strain BL21 (DE3) (NCBI:txid469008) cell lines, with no antibiotic resistance, were obtained from New England BioLabs Inc. and used for protein expression.

Synechocystis sp. PCC 6803 (NCBI:txid1111708) cells were donated by Professor Nigel Robinson from Durham University, United Kingdom. Which were used for CRISPR cloning and *in vivo* experiments.

2.2 Carbamate Trapping method

All protein (4 mg) CO_2 trapping experiments were carried out in phosphate buffer (4 mL, 50 mM, pH 7.4). First, this solution was transferred to a TIM856 Titration Manager (Radiometer Analytical) and incubated at 25°C with stirring. Next, Triethyloxonium tetrafluoroborate (Et_3OBF_4; various amounts in 1 mL phosphate buffer; details in Chapter 3) was added stepwise with a constant pH being maintained (pH 7.4) through the slow addition of 1 M NaOH solution via the automatic burette. Finally, the reaction mixture was stirred, and the pH maintained, for 1 h after the final Et_3OBF_4 addition to ensure that all TEO was hydrolysed.

2.2.1 Protein Digest

After trapping, samples were dialysed into 1 L Milli-Q water at 4°C overnight and the supernatant was removed using an Eppendorf®centrifugal vacuum concentrator Complete Model 5301. Samples were vacufuged at a fixed speed of 1400 rpm at 30 °C. The resulting protein pellet was digested using either the FASP or S-Trap method described below. Peptides were analysed by Liquid Chromatography Electro Spray Ionisation Tandem Mass Spectrometry (LC-ESI-MSMS).

FASP Method

Dried protein sample was resuspended and incubated in Formic Acid (500 μL) and CNBr (50 μL) overnight. The CNBr solution was removed by vacuum centrifugation at 1400 rpm at 30 °C. The resulting pellet was washed twice with ammonium bicarbonate buffer (500 μL of 50 mM). Next, pellets were resuspended in 8% SDS (115 μL) and 8 M Urea (115 μL) and sonicated in a water bath sonicator for 10 minutes. To reduce samples, 0.5 M TCEP (2.3 μL) was added and incubated at room temperature for 10 minutes. After reduction, FASP Protein Digestion Kit and usage guidelines from Expedeon were used for reduction, alkylation and trypsin digestion of protein material. The digest was carried out at 37°C overnight. The resulting peptides were eluted as stated in the kit protocol and later dried in a vacuum concentrator.

S-Trap^{TM} Method

S-Trap™columns and protocols from Protifi were used for protein digest [98]. Protein pellets were resuspended with 11.5 μL of lysis and solubilization buffer (5% v/v SDS, 50 mM TEAB pH 8.5). Suspensions were vortexed. Reduction and alkylation were performed by adding 1 μL of 120 mM TCEP solution and incubated for 15 minutes at 55°C. Disulfide bonds were further alkylated by adding 1 μL of 500 mM MMTS in isopropanol. Samples were acidified with 2.5 μL of 27.5% phosphoric acid (v/v) and further diluted with 165 μL of binding buffer (100 mM TEAB in 90% methanol). Protein samples were loaded on the S-Trap™micro columns and centrifuged at 10,000 g for 30 sec to trap proteins. The column was washed with 150 μL of binding buffer was used; centrifuged at 10,000 g for 30 sec and repeated three times. A 1:10 weight to weight ratio of Trypsin Gold MS grade, from Promega, was added to the amount of protein trapped on the column. The final volume of digestion buffer containing enzyme added to each column was 20 μL. Columns were further incubated for 4 hours at 37°C using a water bath. The digested peptides were eluted with 40 μL of elution buffer (50 mM TEAB), 40 μL of Elution buffer 2 (0.2% aqueous formic acid), and 40 μL of Elution buffer 3 (50% acetonitrile in water) applied and centrifuged independently at 10,000 rcf for 1 min. Pooled eluted peptides were dried down for further LC-MS/MS analysis.

2.2.2 Sample cleaning

C18 tips (Thermo Fisher) were used to clean trapped samples after protease digest. Columns were equilibrated with 0.1% TFA (20μL) in water before the peptides were bound and then washed to remove salt by aspirating 0.1% TFA in 5% ACN (20μL). Peptides were eluted in 50% ACN 0.1% TFA (100μL).

2.2.3 LC-ESI-MS

Dry residues from digests were re-suspended in 0.1% TFA and acidified to pH 3 with more TFA if necessary. Samples were next centrifuged at 20,000g for 5 minutes and supernatant was transfered to an injection vial. These samples were run with a gradient of acetonitrile from 2-80% containing 0.1% formic acid.

LC-MS analysis of peptides was performed on a SCIEX TripleTOF 6600 mass spectrometer linked to an Eksigent nanoLC 425 chromatography system via a 50-micron ESI electrode in a DuoSpray source (SCIEX). Sample injection and peptide separation used a trap and elute method flowing at 5 ml/min. Peptides were loaded and washed on a YMC TriArt C18 guard column (1/32", 5 mm, 5 ´ 0.5 mm) and online chromatographic separation performed over 90 min on a YMC TriArt C18 column (1/32", 12 nm, S-3 mm,150 × 0.3 mm). Peptide elution used sequential linear gradients of 3–30% acetonitrile, 0.1% formic acid over 60 min and 30–40% acetonitrile, 0.1% formic acid over 17 min; followed by a shift to 80% acetonitrile, 0.1% formic acid over 2 min, a column wash for 3 min before return to 3% acetonitrile, 0.1% formic acid over to 2 min and re-equilibration for 6 minutes (Table 2.1). Data-dependent LC-MS-MS acquisition was for 85 minutes from the gradient start. Each MS cycle consisted of a 250 msec precursor-ion scan from 400 to 1,600 m/z followed by fragmentation of up to 30 selected ions for 30 msec each to generate MS/MS spectra of 100 to 1,500 m/z (cycle time 1.2 sec). Switch criteria applied were +2 to +5 ions, of intensity >500 cps, with a rolling exclusion time of 15 sec. Buffer A and Buffer B used for LC-MSMS gradient consisted of water plus 0.1% formic acid and ACN plus 0.1% formic acid, respectively.

Table 2.1 Buffer concentrations of LC-MSMS gradient used for CO_2-trapping experiments

Time (min)	0	60	77	79	82	84	90
%A	97	70	60	20	20	97	97
%B	3	30	40	80	80	3	3

For $^{13}CO_2$-trapping experiment, LC-MS analysis was performed as above, but with next differences:MS1 precursor scan 250 msec 400-1600 m/z, switch criteria applied were +2 to +5 ions, of intensity >400 cps, with a rolling exclusion time of 12 sec, MS2 = top 10, for 100 msec each to generate spectra 100- 1600 m/z, MS acquisition time, 35 minutes from gradient start, cycle time = 1.3 sec. Buffer gradient used for^{13}C-trapping LC-MSMS was as follows:

Table 2.2 Buffer concentrations of LC-MSMS gradient for $^{13}CO_2$-trapped protein

Time (min)	0	18	23	25	29	31	40
%A	97	75	65	20	20	97	97
%B	3	25	35	80	80	3	3

2.2.4 LC-ESI-MS Data analysis by *de novo* sequencing

The PEAKS Studio 10.5 (Bioinformatics Solutions, Waterloo, Ontario, Canada) software was used to analyse MS/MS spectra. Raw data (.raw and .wiff) were converted to *.mgf peak lists using MSconvert [36]. Data refinement of the *Synechocystis* sp. PCC 6803 or *Synechococcus* sp. PCC 7002 FASTA file was performed before *de novo* sequencing by correcting precursor scans according to mass and charge states (minimum and maximum charge states = 2 and 8, respectively). PEAKS *de novo* sequencing was performed with precursor and fragment error tolerance values of 15 ppm and 0.01 Da, respectively. Trypsin was used as a protease allowing three maximum missed cleavage. Carbamidomethylation was set as fixed modification; carboxyethylation and ethylation were set as variable modifications. A maximum of three variable modifications per peptide was allowed. Subsequently, PEAKS DB, which is a database search module in PEAKS Studio 10.5, was used in the second step to identify peptide spectrum matches (PSMs) from existing protein databases [39]. The *Synechocystis* sp. PCC 6803 (Proteome ID UP000001425) or *Synechococcus* sp. PCC 7002 (Proteome ID UP000194437) protein database retrieved from the Uniprot website was used as a reference database. To determine a confidence threshold for PSMs, the PEAKS-embedded target-decoy approach, "decoy fusion", was used to estimate the FDR of the PEAKS DB result.

To detect single amino acid substitutions, the LC-MS/MS dataset was searched using the SPIDER software, integrated with the PEAKS software, against the *Synechocystis* sp. PCC 6803 reference database. The PSMs reported by SPIDER were filtered to 1%. The *de novo* only score was set to 80%, and post-translational modifications (PTMs) scores were set to $\geq$20. In addition, scores for all identified proteins using the PEAKS/SPIDER algorithm were given as a —10log p—value, with a minimum score of 30 and at least a single and significant peptide per protein group. PTMs and single amino acid substitution (SAS) was only considered significant if the following criteria were met: a) spectra with well-defined "b" or "y" series at the position of the substituted amino acid; b) mutation ion intensity of at least 1%. Therefore, all peptide matches from both PEAKS DB and SPIDER search modules were manually verified to ensure quality before being included as valid PTM or SASs in the final peptide list.

2.3 Molecular Biology

2.3.1 *Synechocystis* sp. PCC 6803 cultivation conditions

The cyanobacterium *Synechocystis* sp. PCC 6803 wild type and its K6A ApcA and K6E ApcA mutant, were grown for 4–8 days at 30°C with constant shaking in standard liquid BG-11 medium under continuous Philips cool-white fluorescent light of 30-40 μmol photons per m^2 s^{-1}. BG11 medium was prepared using Cyanobacteria BG-11 Freshwater 50X Solution (SKU C3061-500 mL) from Sigma Aldrich.

Before the assay procedures, cells were harvested by centrifugation at 3000 rpm for 10 minutes and washed in fresh BG11 media, pH 8.0.

2.3.2 *Synechocystis* sp. PCC 6803 growth curve measurements

The culture growth was characterized at 30°C. The light intensities used for the growth curves characterization were 30 μmol(photons) m^{-2} s^{-1} of white light. Starting OD_{680} of all the batch experiments was 0.005. Each batch experiment (with a set pH of 8.0) lasted up to 312 h, and samples were taken at 8-h and 24-h intervals. For sampling, we withdrew 2 mL of liquid using a syringe inserted through a tube that reached midway into the culture. Optical density (OD) was measured immediately by a spectrometer at 730 nm (Synergy H4 Plate Reader or Cary 5000 UV-Vis-NIR).

2.3.3 *Synechocystis* sp. PCC 6803 protein extraction

The cyanobacterium *Synechocystis* sp. PCC 6803 was cultivated in BG-11 liquid medium (250 mL) as in 2.3.1 with a pH of 8.0 at 28°C. The light was provided by 18W Philips fluorescence above flasks on an orbital shaker. 100 mL of cells were harvested at OD_{730nm} mid-exponential phase, centrifuged (15 min) at 3745 g. The pellet was resuspended with 5 mL phosphate-buffered saline (PBS) pH 7.4 and sonicated three times for 2 minutes at a frequency of 250 W (20 kHz). The protein solution was centrifuged for 10 min at 3745 g, and the remaining pellet was resuspended in PBS.

2.3.4 PBSs isolation

The PBSs were isolated according to the method of Ducret *et. al* 1996 with small modifications [23]. *Synechocystis* cells were harvested by gentle centrifugation at 4000 rpm for 25 min (Beckman JA-25 ROTOR, 18°C). Cells were suspended in isolation buffer (0.9M Potassium phosphate, 2 mM EDTA, 1 mM sodium azide, pH 7.0) and passed four times through French press CF1 Cell Disrupter from Constant Systems Limited at 40 000 psi. A final concentration of 1 mM Pefabloc and 2% v/v Triton X was added to release the PBSs complex from the thylakoid membrane. After one hour of incubation (20°C) with gentle rolling, the unbroken cells and debris were removed by centrifugation at 20 000 rpm for 25 min (4°C, JA 25.50 Beckman Rotor). The supernatant was loaded onto a linear (0.5-2 M) sucrose density gradient in 0.75 M Potassium-phosphate buffer (pH 7.6) for ultracentrifugation at 21 000 rpm for 18h at 20°C (SW41Ti Beckman Rotor). The material was collected from the 1.2 M sucrose zone using a thin needle.

2.3.5 DNA quantification

For estimation of DNA and protein concentration, 2μL of the sample was used and read at 260 nm and 280 nm, respectively, using a NanoDrop^{TM} 2000/2000c Spectrophotometer and the inbuilt software to automatically estimate the concentration of double-stranded DNA or using an extinction coefficient of respective protein for estimation of protein concentration.

2.3.6 *Synechocystis* sp. PCC 6803 DNA extraction

10 mL of *Synechocystis* cells were harvested during the late-exponential growth phase (day 7 to day 14 of growth) and pelleted at 12 000 g for 2 min and resuspended in 500 μL of Milli-Q water. The suspension was incubated at 98°C for 10 min and then pelleted at 16 000 g for 10 min to yield a crude preparation of genomic DNA in the supernatant.

2.3.7 Genotyping of *Synechocystis* sp. PCC 6803

Allophycocyanin (*apcA*) sequence of different *Synechocystis* sp. cell lines were examined by Polymerase Chain Reaction (PCR) to confirm nucleotide substitution from CRISPR-cpf1 editing (Subsection 2.3.20). 50 μL PCR reactions consisting of: 1X Q5 Reaction Buffer (New England Biolabs, Ipswich, MA), 100 ng DNA template, 0.5 μM primers, 200 μM dNTPs (Thermo Scientific), and 1 unit of Q5 High-Fidelity DNA Polymerase(New England Biolabs, Ipswich, MA). *apcA* was amplified with primers MJC 1039 (5' CGGAGGAATCCATCCATGAG 7') and MJC 1040 (5' ATACAAGCCGCATAGCGAC 7'). The primers used were designed based on conserved nucleotide sequences of *apcA* available in the UniProt database (Accession number B1XQM2).
The amplification program was set with 35 cycles of 1 min denaturation step (98°C), 1 min annealing step (62°C), and 1 min elongation step (72°C) using Mastercycler® nexus X2. The 35 cycles were appended with initial denaturation step at 98°C of 5 min and a final extension step at 72°C for 10 min.
The 0.5 kb PCR product was purified following Monarch® PCR & DNA Cleanup Kit guidelines and the final elution was performed with ultrapure water. At least 150 ng of purified DNA product was sent to the Department of Biosciences Genomics Facility to sequence with primer MJC 1040. DNA sequencing data was analysed using SnapGene software (from Insightful Science; available at snapgene.com). *Synechocystis* sp. *apcA* sequence was obtained from Uniprot (Accession number B1XQM2). Targeted data were aligned to the *apcA* sequence (Accession number B1XQM2, https://www.uniprot.org/uniprot/B1XQM2).

2.3.8 Polymerase Chain Reaction

Reactions using Phusion or Q5 DNA Polymerase were set up on ice following the manufacturer's protocol. Reactions typically contained 20 mM Tris-HCl pH 8.8, 10 mM KCl, 10 mM $(NH_4)_2SO_4$, 2 mM $MgSO_4$, 1% (v/v) Triton X-100, 0.1 mg mL^{-1} BSA, 25 pmoles of each primer, 200μM dNTPs, 250 ng DNA template and 1 unit of Phusion or Q5 DNA polymerase. Reactions were typically analysed by agarose gel electrophoresis.

2.3.9 Agarose gel electrophoresis

1%, 1.5 % or 2% (w/v) agarose gels in TAE buffer (40 mM Tris-acetate, 1 mM EDTA pH 8.0) were run at 12 V cm-1. A DNA sample was mixed 6:1 (sample:buffer) with Thermo Fisher DNA Gel loading dye (10 mM Tris-HCl (pH 7.6) 0.03% bromophenol blue, 0.03% xylene cyanol FF, 60 % glycerol 60 mM EDTA.)before loading, DNA sizes were estimated relative to a 1 kilobase DNA marker ladder. Visualisation of DNA was attained through the in gel presence of ethidium bromide (0.5 μg mL^{-1}) and a UV transilluminator.

2.3.10 Extraction of DNA from agarose gels

The DNA band was excised from an agarose gel and purified following Monarch DNA Gel Extraction Kit guidelines. Column centrifugations were performed at 12,000g for 2 min and DNA elution from the column by adding deionized water. Sample containing DNA was stored at -20°C until further use.

2.3.11 Purification of plasmid DNA

A 5 mL overnight culture of *E. coli* was centrifuged (5,000 g, 10 min) and the pellet was processed using a commercial Thermo Fisher plasmid miniprep kit according to the manufacturer's protocol.

2.3.12 Restriction digestions

40 μL restriction digests were set up on ice, contained 200 ng of plasmid DNA, and were incubated for either one hour or overnight at 37°C with restriction enzymes (SacI, BamHI, XhoI, and BgII from Thermo Fisher Scientific) or 15 minutes when using High Fidelity restriction enzymes (EcoRI and AaI from New England Biolabs). Digests contained two different restriction endonucleases; the reaction buffer used and relative amounts of enzyme used were determined following guidelines on the manufacturer's website (Monarch or Thermo Fisher) for double digests. DNA vectors were also digested in the presence of 2 U of Calf alkaline intestinal phosphatase for dephospohorylation of 5' and 3' ends of DNA. Digests were

analysed by agarose gel electrophoresis and correct DNA fragments were purified for further use.

2.3.13 DNA ligations

10 μL DNA ligation reactions were set up on ice and contained 40 mM Tris-HCl pH 7.8, 10 mM $MgCl_2$, 10 mM DTT, 5 mM ATP, 3 Units T4 DNA Ligase, and a 3:1 molar ratio of purified DNA insert:vector. Ligations were incubated at room temperature for 1 hour before a 2 μL aliquot was transformed into competent cells.

2.3.14 Preparation of chemically competent *E. coli*

25 mL LB medium was inoculated with 250 μL of an overnight LB starter culture and grown with shaking (180 rpm) at 30°C were transferred to ice for 15 minutes, centrifuged (2700 g, 10 min, 4°C resuspended in 30 mL ice-cold wash solution (80 mM $MgCl_2$ and 20 mM $CaCl_2$. Cells were centrifuged again (2700 g, 10 min, 4°C), resuspended in 1 mL ice-cold 100 mM $CaCl_2$, split into 50 μL aliquots in chilled micro-centrifuge tubes, and stored at -80°C.

2.3.15 Transformation of chemically competent *E. coli*

Frozen 50 μL aliquots of chemically competent *E. coli* were thawed quickly in the hand and transferred immediately onto ice. 25 ng of plasmid DNA or 2 μL of a DNA ligation mixture was added, gently mixed, and left on ice for 30 minutes. Cells were heat-shocked for 45 seconds in a 42°C water bath and immediately placed back on ice for 2 minutes. 950 μL of 37°C SOC medium (2% (w/v) tryptone, 0.5% (w/v) yeast extract, 8.5 mM NaCl, 10 mM $MgCl_2$ and 20 mM glucose) was added to the cells and then cultured at 37°C for 2 hours before plating onto LB agar plates containing required selection agents. Plates were grown at 37°C overnight.

2.3.16 One-step site-directed mutagenesis

Single-site mutations of recombinant allophycocyanin protein were performed following Liu *et al.* protocol [49]. The primer pairs MJC985/MJC986 and MJC1029/ MJC1030 (Table 2.3) were used in one single-site mutagenesis reactions to substitute residues Lys6 by Ala or Lys6 by Glu.

Primers were designed using SnapGene software (from Insightful Science; available at snapgene.com) and synthesized by Eurofins Genomics. Each primer pair contained non-overlapping sequences at their 3' end and primer-primer complementary (overlapping) sequences at the 5' end. The mutation sites were placed in the complementary region. Mutagenesis PCR reactions were performed as in 2.3.8. The PCR products were treated with 5 units of DpnI at 37°C for 2 hours, and then 10 μl of each PCR reaction were analyzed by agarose gel electrophoresis as in 2.3.9. An aliquot of 2 μl of full-length plasmid DNA product was transformed into *E. coli* DH5α competent cells by heat-shock.

Table 2.3 Primers used for mutagenesis

Primer	Direction	Sequence 5' to 3'
MJC985	Sense	ATGAGTATTGTCACGGCATCCATCGTGAATGCCGAC
MJC986	Antisense	GTCGGCATTCACGATGGATGCCGTGACAATACTCAT
MJC1029	Sense	GTCACGGAATCCATCGTGAATGCCGACGCTG
MJC1030	Antisense	GATGGATTCCGTGACAATACTCATGGTGAAGGGATG

Table 2.4 Plasmids used in this study. [1]*Synechococcus sp.* PCC 7002, [2]*Synechocystis* sp. PCC 6803

Plasmid	Recombinant protein(s) produced	Parent Vector	Reference
pApcAB	[1]ApcA and [1]ApcB	pET100	Biswas *et al.* (2010)
pCpcBA	[2]CpcB and [2]CpcA	pCDF Duet	Biswas *et al.* (2010)
pPcyA	[2]Ho1 and [1]PcyA	pACYC Duet	Biswas *et al.* (2010)
pCpcUS	[1]CpcU and [1]CpcS	pCOLA Duet	Biswas *et al.* (2010)
pK6AapcA	Lys6Ala mutated [1]ApcA	pET100	This study
pK6EapcA	Lys6Glu mutated [1]ApcA	pET100	This study
pK6AapcAB	Lys6Ala mutated [1]ApcA and [1]ApcB	pET100	This study
pK6EapcAB	Lys6Glu mutated [1]ApcA and [1]ApcB	pET100	This study

2.3.17 Expression and purification of recombinant PBPs in *E. coli*

Plasmids used in this project are listed in Table 2.4. Some of the expression vectors used in this project were previously described and kindly provided by Schlutchter's group from the University of New Orleans [9][52]. All expression constructs newly produced for this study were sequenced at the Molecular Genetics Laboratory of Durham University to confirm that no mutations had been introduced during PCR amplification and cloning.

Protein expression and purification were performed according to Biswas *et al* [9]. Expression plasmids were cotransformed into E. coli BL21(DE3) cells and colonies were selected on Luria-Bertani (LB) medium plates in the presence of appropriate combinations of antibiotics (Table 3.1 and Table 3.2) at the following concentrations: ampicillin (Ap), 100 μg ml^{-}1; chloramphenicol (Cm), 34 μg ml^{-}1; kanamycin (Km), 50 μg ml^{-}1; and spectinomycin (Sp), 100 μg ml^{-}1.

For *Synechococcus sp.* 7002 allophycocyainin alpha subunit expression, plasmids: pApcAB, pK6AapcAB and pK6EapcAB (Table 3.2), were digested with 10 units of AanI from Thermo Fisher and 60 units of EcoRI from New England Biolabs. Samples were incubated overnight at 37°C, ran in agarose gel as mentioned in 2.2.5 and the released band of $\approx$ 1460 bp was gel-purified as in 2.2.6. Samples were blunted with 1μL Thermo Fisher DNA blunting enzyme incubating at 70°C for 8 minutes. Blunted DNA was cleaned with Monarch® PCR & DNA

Cleanup Kit and ligated at RT for three hours. The remaining vector was transformed into BL21 cells as stated in 2.2.13.

Small scale protein expression

Recombinant PBPs were produced for *in vitro* spectrophotometric analysis. A 300 mL overnight starter culture was added to 6 litres of LB medium (50 mL per litre) with the appropriate combination of antibiotics. The culture was incubated with shaking at 37°C for 4 hours until OD_{600} = 0.6. Protein translation was induced with a final concentration of 0.1 mM isopropyl-β-D-1-thiogalactoside (IPTG) and cooled to 28°C to reduce inclusion bodies. The cultures were further incubated for 16 h in the dark. The next day, the cells were harvested by centrifugation and washed with equilibration buffer (20 mM sodium phosphate, 500 mM NaCl and 20 mM imidazole pH 7.4 buffer).
Pellets were sonicated six times at 250 W (20 kHz)for 10 seconds each time with 10 seconds on ice intervals. After centrifugation, the lysates were loaded onto a pre-equilibrated 5 mL HisPur™ Ni-NTA Resin (Thermo Fisher Scientific) chelating affinity columns. The column was then washed with washing buffer (20 mM sodium phosphate, 500 mM sodium chloride and 50 mM imidazole, pH 7.4), to remove weakly bound host proteins. Finally, the recombinant proteins were then eluted with elution buffer (20 mM sodium phosphate, 500 mM sodium chloride and 335 mM imidazole, pH 7.4) and then dialyzed overnight with 50 mM PBS pH 8.0. Eluate was concentrated to 2 mL with a Vivaspin 20 (Sartorius) centrifugal concentrator as per the manufacturer's guidelines. PBPs were then dialysed overnight with 1 litre of phosphate-buffered saline (PBS: 10 mM phosphate buffer, 2.7 mM KCl, 137 mM NaCl, pH 7.4), following with a second dialysis of 1 hour with fresh PBS and then stored at 4°C until needed.

Large scale protein expression

For NMR experiments (see subsection 2.4.1) large quantities (>10 mg) of PBPs were needed. We therefore, expressed a large scale (20 L) of recombinant PBPs in *E. coli*.

Large scale expressions were set up in an Epiphyte3's LEX ("Large-scale EXpression") bioreactor allowing better aeration and temperature control. 250 mL of Terrific Broth (TB) with appropriate antibiotics was inoculated with BL21(DE3) *E. coli* previously transformed with the appropriate plasmid (section 2.3.16). 200 mL of starting culture were used to inoculate

20 L of TB with antibiotics (10 mL per 1 L of media), and incubated at 37°C until an OD_{600} of 1-1.2 was reached. Cells were induced at this growth stage with 1 mM final concentration of IPTG and incubated overnight at 18°C. The following day cells were pelleted by centrifugation, washed with equilibration buffer and continued purification with Ni^{2+} chelating affinity and size exclusion chromatography as in subsections 2.3.17 and 2.3.18.

2.3.18 Size Exclusion Chromatography

Size exclusion chromatography was performed at 4°C and used to separate expressed phycobiliproteins based on size/shape. The purified protein (section 2.3.17) was dialysed into PBS and applied to a HiLoad®16/600 Superdex®200 pg column pre-equilibrated with PBS buffer. The column was run at 1 ml $min^{-}1$. Fractions were analysed for protein content by UV spectrophotometry at 280 nm, and peak fractions were analysed via SDS-PAGE gel electrophoresis (section 2.3.19). Selected fractions were pooled and concentrated with a vivaspin 20 centrifugal concentrator (Sartorius Biolab) as per the manufacturer's guidelines and stored at 4°C.

2.3.19 SDS-PAGE

Protein molecular weights were assessed using sodium dodecyl sulphate- polyacrylamide gel electrophoresis (SDS-PAGE) gel. Protein samples (10-20 μg) were made up 5:1 in loading buffer (200 mM Tris-HCl pH 6.8, 10 mM dithiothreitol, 10% (w/v) SDS, 0.5% (w/v) bromophenol blue, 20% (v/v) glycerol) and were incubated for 5 min at 95 °C to enable protein denaturation. The samples were run on resolving gels in the range 12 – 15% (w/v) with 5% stacking gel. A protein ladder (Pageruler^{TM} pre-stained) was used to estimate protein size. The gels were run in running buffer (25 mM Tris-HCl pH 7.5, 200 mM glycine, 0.1% (w/v) SDS) at 180 V for 1 h. The gel was incubated with InstantBlue® Protein Stain with rocking for 15 minutes.

2.3.20 Construction of markerless Knock-ins in *Synechocystis* sp. PCC 6803

Synechocystis sp. PCC 6803 was mutated for *in vivo* analysis of allophycocyanin Lys 6. Point mutations in the gene slr2067 were created via CRISPR-cpf1.

The plasmid pSL2680 containing *cpf1*, the native *Francisella novicida* CRISPR array and *lacZ* amplified from the pCrispomyces-2, was obtained as a kind gift from Himadri Pakrasi (Addgene plasmid # 85581 ; http://n2t.net/addgene:85581).Construction of knock-ins was performed following Pakrasi *et al.* methods [92]. pSL2680 served as the base plasmid for construction of editing plasmids. Expression of full-length pre-crRNA in pSL2680 was constructed by cloning annealed oligos into the AarI sites. The MJC1006/MJC1007 annealed oligos (Table 2.5) were ligated into the AarI sites on pSL2680 to yield pSL2680-apcAgRNA.

PCR was used to synthesize the homology regions which were then cloned into the KpnI site on the plasmids containing the matching crRNA. First, the point mutation homology region was constructed in two piece using primers MJC997/MJC999 and MJC998/MJC1000 or MJC997/1045 and MJC998/MJC1046 (Table 2.5). The homology template was then assembled, linearized with KpnI and using two-step PCR to generate pSL2680-K6AapcA and pSL2680-K6EapcA.

Table 2.5 Primers for APC Knock-in of *Synechocystis* sp. PCC 6803

Primer	Direction	Sequence 5' to 3'	Vector
MJC1006	Sense	AGAT ATTTCGTGACGATACTCATGG	pSL2680
MJC1007	Antisense	AGAC CCATGAGTATCGTCACGAAAT	pSL2680
MJC997	Sense	CATTTTTTTGTCTAGCTTTAATGCGGTAGTTGGTACCCTTTAATAAGCTTGGGTACACAGAC	pSL2680-apcAgRNA
MJC998	Antisense	GCCCGGATTACAGATCCTCTAGAGTCGACGGTACCGGCTCACCTGTGATGCCATTG	pSL2680-apcAgRNA
MJC999	Sense	GCTTCTGCATCAGCATTCACGATCG ATGCCGTGACGATACTCATGG	pSL2680-apcAgRNA
MJC1000	AntiSense	CCATGAGTATCGTCACGGCATCGATCGTGAATGCTGATGCAGAAGC	pSL2680-apcAgRNA
MJC1045	Sense	GCTTCTGCATCAGCATTCACGATCGATTCCGTGACGATACTCATGG	pSL2680-apcAgRNA
MJC1046	AntiSense	CCATGAGTATCGTCACGGAATCGATCGTGAATGCTGATGCAGAAGC	pSL2680-apcAgRNA

2.3.21 *Synechocystis* natural transformation

25 ml liquid BG11 medium was inoculated with *Synechocystis* sp. PCC 6803 and grown to an OD_{750} of 0.5-0.8 under continuous illumination at a light intensity of 20 μmol/m^2/s at 28°C and permanent agitation (150 rpm). 10 ml of the cell culture was centrifuged (5 min, 20°C, 2000 x g), and the cell pellet was resuspended in 5 ml BG11 medium and equally distributed between five sterile 15 ml-reaction tubes. DNA (3 to 5 μg of circular plasmid DNA) was added, and cells were gently mixed by tapping and incubated in darkness at 28°C overnight. Following dark incubation, 200 μl of cells were plated on BG11 agar plates lacking antibiotics and incubated in continuous light at a light intensity of 20 μmol/m^2/s at 28°C. After 2 days of incubation under constant light, the agar plates were supplied with kanamycin at a 15 μg/ml concentration to the bottom of the petri dish. Plates were sealed with parafilm and further incubated under continuous illumination as before. Colonies appeared after 2 to 3 weeks. To achieve complete segregation, single colonies were picked and streaked on BG11 plates containing the appropriate antibiotics. When cells were grown (about one to two weeks), cells were streaked again on new BG11 plates containing the appropriate antibiotics. This successive streak purification was repeated for at least four rounds (in total) to ensure segregation. Positive clones were maintained on BG11 agar plates containing appropriate antibiotics under continuous illumination (20 μmol/m^2/s) and were re-streaked at 2-week intervals.

2.3.22 *Synechocystis* conjugal transformation

E. coli was employed to transfer circular plasmids to *Synechocystis* sp. PCC 6803 by conjugal transformation. *Synechocystis* sp. was cultivated as in 2.3.1. *E. coli* with cargo plasmid pSL2680 and *E. coli* with conjugal plasmid pRL443 were grown overnight at 37°C.

E. coli cultures were pelleted (10 ml cargo and 10 ml helper) at 3000 rpm for 10 mins and washed in 10 ml LB media without antibiotics. Cargo and helper cultures were combined, rewashed and resuspended in 200 μl. Cyanobacterial cultures (50 ml at late exponential phase) were centrifuged at 3000 rpm for 10 min at room temperature, resuspended in 5 mL of BG11 media. Further cell dilutions(1:1, 1:50 and 1:100) were prepared in a final volume of 1 ml.
To set up conjugational cultures, 200 μl of *E. coli* cargo/helper culture were mixed with 100 μl of a given dilution of cyanobacterial culture in an Eppendorf tube and incubated for 30 min to

5 h at 30°C before plating. Next, 300 μl of the *E. coli* and cyanobacteria mix were poured into BG11 agar plates without antibiotics and incubated for 2 days at 30°C with light. Finally, the antibiotic was added under the plate as in 2.3.21 and incubated at 30°C with light for 10 days until colonies appeared.

2.3.23 Cryopreservation of cyanobacteria

Freezing

10 mL of *Synechocystis* sp. PCC 6803 liquid culture from the late exponential phase were harvested by centrifugation at 2000 rpm for 30 minutes. Sterile Dimethyl sulfoxide (DMSO) was used as a cryoprotectant. This cryoprotectant was added to the BG11 liquid sterile medium to a final concentration of 50% BG11 and 5% DMSO. Cyanobacteria pellets were resuspended by pipetting in the dark in BG11-DMSO sterile solution (3 mL). Aliquots (1.5 mL) of the resulting suspensions were dispensed into 2-mL cryogenic vials (Corning Inc, USA), and held for 45 min in an ice bath. Vials were set in a styrofoam container and cooled to -20°C in a freezer for 4 h, transferred to -80°C freezer o/n and subsequently stored kept at -150°C in chest freezer.

Thawing

Cyanobacteria cultures to be revived were removed from -150°C chest freezer storage and warmed rapidly to room temperature by immersing the vials in a 35°C water bath. Cells were immediately pelleted by minimum RCF centrifugation of the cryovial, and the supernatant was discarded. Next, one ml of fresh BG11 growth medium was placed into the vial to suspend the pellet carefully. The cryovial lid was slightly loosened to allow gas exchange, and the contents of the vial were kept in complete darkness for 1-2 days. The culture was then incubated in liquid growth media under normal growth conditions. Viable cells began normal growth within 1 - 2 days.

2.3.24 Protein Quantification

Bradford assay

Standards were prepared with bovine serum albumin (BSA). Bradford reagent was added (1 mL to 20 μL sample) and the samples incubated for 15 min at RT. The absorbance was measured at 595 nm and the values plotted to generate a standard curve. This curve could then be used to measure unknown sample protein concentrations within this range.

Bicinchoninic acid (BCA) assay

Standards were prepared with bovine serum albumin (BSA). Samples (25 μL) were then incubated with a BCA working reagent (Pierce^{TM}) (200 μL) for 30 min at 37°C and then the absorbance measured at 562 nm. The blank measurement was subtracted from the other readings and the measurements plotted as a standard curve. This curve could then be used to measure unknown sample protein concentrations within this range.

2.4 Spectroscopy Analysis

2.4.1 Nuclear Magnetic Resonance (NMR)

Unless stated otherwise, recombinant allophycocyanin alpha subunit and K6A mutant samples consisted of ApcA ($\approx$ 0.55 mM) prepared in phosphate saline buffer (700μl), pH 7.4, 25 or 50 mM $NaH^{13}CO_3$ with 20-50% D_2O. Samples were prepared using 5 mm tubes fitted with a J. Young cap to shield the sample from the variations in atmospheric pressure that could affect the hydrogen carbonate dissolved in the sample.

NMR experiments were acquired with a Varian 600 MHz MHz spectrometers equipped with Agilent OneNMR Probe able to deliver a maximum pulsed-field gradient strength of 62 G cm^{-1}.

To check the presence of small molecule impurities that could interfere with the process under study, a ^1H spectrum was acquired. The strong interfering water signal was eliminated using the Robust-5 pulse sequence [2]. Thirty-two scans were collected each comprising 65 536 complex data points and a spectral width of 10 kHz. The repetition time was 6.3 s, of which 3.3 comprised the acquisition time. The W5 inter-pulse delay was set to 240 µs. In all cases rectangular 1 ms pulsed-field gradients were used with a strength of G1 = 28.3 G cm^{-1} (first pair) and G2 = 4.9 G cm^{-1} (second pair). The gradient stabilization delay was 0.5 ms. The first pair of lock pre-focusing field gradients were separated by a 1.5 ms delay from the first radio-frequency pulse.

^1H experiments were recorded in 12h collecting 131072 complex points. The repetition time was 6.7 s, of which 1.7s comprised the acquisition time. The excitation pulse angle was set to 45 degrees.

2.4.2 Optical Spectroscopy Measurements

Absorption spectra and fluorescence spectra were obtained using a Synergy H4 Plate Reader, Cary 5000 UV-Vis-NIR or Fluorolog®-3 with FluorEssence - HORIBA.
The absorption spectra were recorded from 500 nm to 700 nm at room temperature, with a bandwidth of 1 nm, and a scan speed of 240 nm/min. The fluorescence emission spectra were

recorded with excitation at 590 nm or 610 nm. The emission slit widths were set at 3 nm, and the scan speed was 240 nm/min. Sample concentrations were adjusted to an absorbance between 0.05 – 0.1 at the absorption maximum of each protein. Spectral responses were analysed with and without the presence of $NaHCO_3$ or NaCl. Spectral ranges used for the different experiments are summarized in Table 2.6.

2.4.3 Photoluminescence Quantum Yields

The photoluminescence quantum yields (PLQY) were recorded with a Fluorolog®-3 spectrofluorometer (HORIBA Scientific) and a Quanta-φ F-3029 Integrated Sphere at room temperature in 1 cm x 1cm quartz cuvettes. The sample is placed in the integrating sphere, and excited with appropriate wavelength of light. The quantum yield, φ , is, by definition, photons emitted to photons absorbed:

$$\varphi = \frac{E_{\mathrm{c}} - E_{\mathrm{a}}}{L_a - L_c}$$

where E_c is the integrated luminescence of the sample caused by direct excitation, and E_a is the integrated luminescence form an empty integrating sphere (only a blank). The term L_c is the integrated excitation profile when the sample is directly excited by the incident beam. L_a is the integrated excitation profile from an empty integrating sphere (without the sample, only a blank). Measurements were determined in phosphate saline buffer and sample concentrations were adjusted to an absorbance of $\approx$0.1 at the maximum fluorescence. PLQY (φ) resulted in an average of four scans. The spectral ranges used in this study to record the fluorescence spectra are listed in Table 2.6.

2.4.4 Time-resolved Fluorescence Lifetimes

To measure the time-resolved fluorescence from *Synechocystis* cells a 3.5 mL Suprasill quartz material (QS) 10 x 10 mm path length cuvette (Hellma) was employed. The cuvette was placed inside the sample chamber of a HORIBA Scientific DeltaFlex fluorescence lifetime spectrometer.

Table 2.6 Spectral wavelength ranges (nm) used for characterization or testing of Allophycocyanin properties

Assay	Absorbance range	Fluorescence range		PLQY	
		EX	EM	EX	EM
PBSs	500-700	500-675	500-700	570	610-750
				610	620-750
Recombinant PBPs	500-700	500-685	600-720	615	620-750
Synechocystis sp. PCC 6803	400-800		600-800	580	590-750

The experiment was performed by placing 2 mL of *Synechocystis* sp. PCC 6803 culture from exponential phase diluted to 10 μg/mL of Chl a in the quartz cuvette. A final concentration of 1 mM NaCl or $NaHCO_3$ was added and, fluorescence decays measured. The cyanobacterial culture was previously exposed to light for 20 minutes to induce inorganic carbon (Ci) starvation. The time required for starvation was estimated using a Clark type electrode, the liquid culture was withdrawn when the rate of oxygen evolution reached 0 nmol/min.

The DeltaFlex was operated in Kinetic TCSPC mode and allowed for the collection of up to 10 000 sequential fluorescence counts, from data-acquisition times ranging from 1 ms to 1 min.

A data-collection time of 10 ns was used, and 10 000 decays were collected, along with the instrumental response to analyze the data using reconvolution analysis. Data analysis was performed in a batch mode using DAS6 analysis software (HORIBA Scientific). The excitation source was a DeltaDiode-425L operating at a repetition rate of 100 MHz. Detection was at 600 and 690 nm using a PPD-650 detection module. The instrument response was measured using the same cell, but with 1 mL of Ludox® used as a scattering solution.

2.4.5 Circular dichroism

Circular dichroism spectra were recorded on a Jasco J-1500 spectropolarimeter equipped with a mini-circulation bath and Peltier stage, using a 1 mm quartz cuvette.
Circular Dichroism spectra for secondary structure determination of allophycocyanin alpha subunit and K6A mutant was measured from 190 nm to 240 nm with 200 μl of protein in phosphate saline buffer, pH 7.4, at a concentration of 0.3 mg/mL.
For the chromophore interaction experiment, 300 μl of respective protein with a final concen-

tration of 1 mM of NaCl or $NaHCO_3$ was added to the quartz cuvette, and CD spectra were detected from 500 to 700 nm.

2.4.6 Steady-state oxygen evolution measurements

The PSII-mediated activity of the whole linear electron transport chain was evaluated according to the measurements of the light-dependent oxygen evolution by the cell suspension in culture medium (chlorophyll concentration was between 5-10 μg per mL) by a Clark-type oxygen electrode (Oxygraph, Hansatech Instruments) in a 3 ml stirred cuvette maintained at 25 °C. The high power 100 W lamp with a Hama 55mm Variable Neutral Density Filter were used for the illumination (range of light from 0 to 700 μmol m^{-2} s^{-1}).

2.5 Statistical analysis

All error bars represent the 95% confidential intervals (CI). All statistics and graphical analysis were performed using GraphPad Prism 8 (GraphPad Software, inc.). All data shown are representative of at least three independent experiments (unless otherwise stated).

Chapter 3

Cyanobacterial carbamate discovery

3.1 Overview

As previously mentioned in Chapter 1, CO_2 reacts rapidly with neutral amines to form carbamates at physiological temperatures and pressures. Carbamylation PTM has been shown to be implicated to a broader extent as a biological regulatory system. In plants, the identification of carbamates in the *A. thaliana* proteome has been reported [48]. In algae, protein carbamate has been shown to constitute about 50% of the intracellular CO_2/HCO_3^- in *E. gracilis* [96]. However, which proteins interact with CO_2 in algae or cyanobacteria, have not yet been identified. There is little knowledge of carbamylation as a PTM in these organisms.

This Chapter reveals the discovery and validation of a photosynthetic cyanobacterial carbamate. This investigation followed the trapping technology described by Linthwaite *et al.* using triethyloxonimum tetrafluoroborate (TEO) to identify carbamates within a cyanobacterial proteome. We hypothesized that cyanobacteria have significant CO_2-binding sites as carbamates in their proteome that can be identified by mass spectrometry proteomics analysis. This Chapter includes previous work on the identification of a CO_2-binding site in cyanobacterial protein lysate. The carbamate search in cyanobacterial protein lysate involved attempts to minimize the probability of a false positive occurring. Regardless, confirmation that the carbamate is forming on an isolated and purified protein was used to validate data from mass spectrometry. To validate the site of carbamate formation, a mutant protein was expressed in *E. coli* featuring a substituted lysine residue to alanine as a negative control. Mass spectrometry carbamate

formation data was confirmed by ^{13}C-NMR-spectroscopy, where Lys carbamate specificity was corroborated with the removal of ^{13}C-NMR carbamate peak in the protein of our interest.

3.2 Previous Work

The presence of CO_2-binding sites in a plant proteome was shown by a prior study of $^{14}CO_2$ trapped via TEO on *Arabidopsis thaliana* whole protein lysate. Thus, Cann and Linthwaite hypothesized that cyanobacteria would also have CO_2-binding sites as carbamates PTMs in their respective proteome. For this study, *Synechocystis sp.* PCC 6803 (*Synechocystis*) was used as a cyanobacterial model organism. It was chosen for CO_2 carbamate screening as it is likely to identify proteins crucial for CO_2 interactions.

Triethyloxonimum tetrafluoroborate (TEO) was used as the ethylating reagent for carbamate trapping following Linthwaite *et al.* previous work [47]. TEO has a half-life of 7.4 min [41]. When using this reagent, the solution's pH is reduced caused by the formation of H^+ ions. To maintain pH within a 7.4-7.6 range, we, therefore, used a pH-stat, which allowed the slow addition of 1 M sodium hydroxide (NaOH) during the reaction to keep pH close to physiological conditions.

For the initial cyanobacterial carbamate screening, a protein lysate from *Synechocystis* was incubated with 20 mM $NaH^{14}CO_3$ and trapped with TEO. Likewise, a small amount of $^{14}CO_2$ was introduced into the protein extracts without TEO. In the absence of TEO, the inability to detect protein-bound $^{14}CO_2$ is likely due to the ready reversibility of carbamylation that results in the sample being degassed during preparation for analysis. The protein lysate trapped with TEO contained significant $^{14}CO_2$ (Fig. 3.1**A**). We concluded that *Synechocystis* protein extract contains carbamylated CO_2-interacting proteins exchangeable with the environment at labile sites. Therefore, we proceeded to identify carbamate sites with LC-MS/MS to determine proteins that could associate CO_2 sensing with photosynthesis.

For *Synechocystis* carbamate identification, soluble protein lysate was equilibrated with CO_2/HCO_3^- at pH 7.4, and TEO was applied to trap carbamylated proteins within the proteome. Trypsin was used to digest the trapping reaction mixture, and samples were analyzed by ESI-MS/MS. Data for variable post-translation modifications on lysine with a mass of 72.0211 Da (trapped carbamate) and 28.0313Da (O-ethylation on glutamate and aspartate side chains) by this stage of the project were examined using Tandem software.

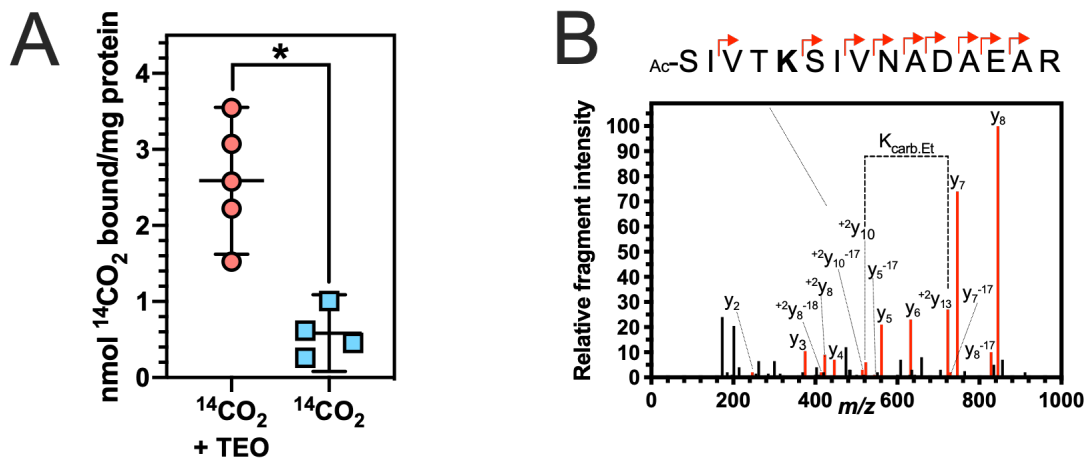

Fig. 3.1 CO_2 binds ApcA. **A.** Identification of exchangeable CO_2-binding sites on *Synechocystis* protein lysate. $^{14}CO_2$ trapped onto protein lysate of *Synechocystis sp.* PCC 6803 (*p=0.002, two-tailed t-test, n = 4-5 independent replicates, t = 4.794, df = 7, ±95% C.I.).**B.** Identification of exchangeable CO_2-binding sites on ApcA by MS-MS. Plots of relative fragment intensity versus mass/charge ratio (m/z) for fragmentation data from MS-MS identifying ethyl-trapped carbamate on whole *Synechocystis sp.* PCC 6803

The open reading frame Slr2067 was identified with a lysine carbamylation site (MSMS peptide amino acids 2-16 SIVT**K**SIVNADAEAR, suggested carbamylation on K6) (Fig. 3.1**B**). The K6 carbamate modifications were identified on the peptide's internal lysine residue, a so-called missed cleavage. Carbamylation destroys the positive charge of trypsin on the lysine necessary for determining the cleavage site. The lysine's missed cleavage adds confidence to discovering carbamates on Slr2067 K6, as a missed cleavage is rare for trypsin.

The gene slr2067 encodes the allophycocyanin-alpha subunit (ApcA). ApcA represents the α-subunit of the allophycocyanin $(\alpha\beta)_3$ trimer and has a critical function in electronic energy transfer (EET) from the PBS antennal proteins terminal pigment to the photosystem. Once Lys 6 was identified as a potential carbamate site under comparable physiological conditions, we aimed to confirm carbamylation in isolated PBSs material.

3.3 PBSs carbamate trapping

3.3.1 Isolation of PBSs

Proteomic analysis of a protein lysate from *Synechocystis* identified a carbamate PTM on Lys 6 of the phycobilisomes (PBSs) component protein, ApcA. I first sought to confirm this finding by investigating the ApcA K6 carbamate PTM in purified PBS samples. For this aim, *Synechocystis* cells were disrupted, and PBSs were isolated by ultracentrifugation (Fig. 3.2**A**), followed by sucrose density centrifugation (Fig. 3.2**B**). PBSs were collected from the 1.2 M sucrose concentration zone using a thin needle and dialyzed with PBS buffer (pH 7.4) after extraction. PBS complexes were visualized over the purification through their characteristic blue colour (Fig. 3.2).

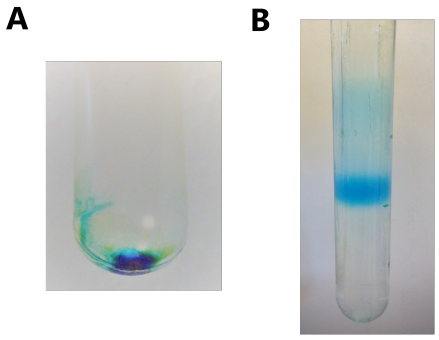

Fig. 3.2 Isolation of phycobilisomes from *Synechocystis* sp. PCC 6803 **A.** Pellet obtained after unbroken cells and debris removal by ultracentrifugation. **B.** Tube containing PBSs in a sucrose density gradient.

The PBS complex component proteins were assessed by SDS-PAGE electrophoresis on a 15% resolved polyacrylamide gel. The polypeptides identified by SDS-PAGE (Fig. 3.3) were consistent with those previously described for *Synechocystis* [97]: ApcE (100 kDa), FNR (48 kDa), rod linkers, CpcC1 and CpcC2 (35 and 33 kDa), CpcG1 rod-core linker (27 kDa),

α and β sub-units of PC (19.8 and 17.6 kDa, correspondingly), the ApcA (17.2 kDa) and ApcB subunit (16.2 kDa),the small rod-distal(CpcD, 9.3 kDa),and core-distal(ApcC, 7.7 kDa) linker polypeptides. Therefore, we conclude that the PBS complex has been purified and is appropriate for use in CO_2-trapping experiments.

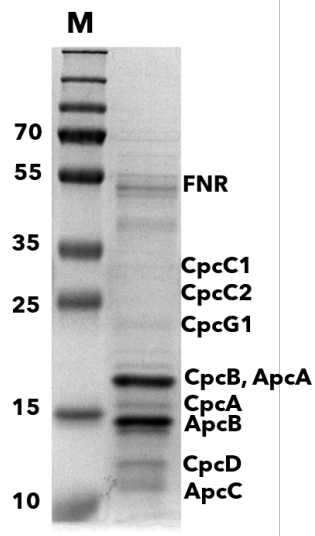

Fig. 3.3 Polypeptide composition of the PBS from *Synechocystis* analysed by SDS-PAGE. Molecular mass markers (M) are indicated in kDa. FNR (48 kDa), rod linkers, CpcC1 and CpcC2 (35 and 33 kDa), CpcG1 rod-core linker (27 kDa), α and β sub-units of PC (19.8 and 17.6 kDa, correspondingly), the ApcA (17.2 kDa) and ApcB subunit (16.2 kDa), the small rod-distal(CpcD,9.3 kDa), and core-distal(ApcC,7.7 kDa) linker polypeptides bands are indicated.

3.3.2 PBS TEO carbamate trapping

To confirm *Synechocystis* potential carbamate site, isolated PBSs (5 mg) in PBS pH 7.4 were trapped with TEO in the presence of 1 mM $NaHCO_3$. Trypsin was used to digest the trapping reaction following the FASP method (Section 2.2.1). Protein peptides were fragmented by Electrospray ionization (ESI) and identified by tandem mass spectrometry (MSMS).

The extensive complex protein MSMS data obtained from LC-ESI-MSMS was analyzed using PEAKS Studio 8 Software (Bioinformatics Solutions Inc., Waterloo, Ontario, Canada). Data were searched against the NCBI *Synechocystis sp.* PCC 6803 protein database. Carbamates hits were searched for in PEAKS by searching for a carbamate mass with the addition of an ethyl group (carboxyethyl PTM with a mass shift of 72.0211 Da, Section 2.2.4). In addition to PTM software's assignment, a manual validation was performed to ensure correct peptide identification.

PEAKS analysis under a peptide False Discovery Rate (FRD) of $\geq 4.7\%$ detected twelve proteins from the PBS trypsin digest with a $\geq 40\%$ peptide coverage. Each peptide identification software's core is a scoring function that evaluates the matching quality between a peptide and an MS/MS spectrum. For every MS/MS spectrum in the data, the software searches the protein database to find a peptide that maximizes the peptide-spectrum matching score. The match between the spectrum and the highest-scoring peptide is usually referred to as a peptide-spectrum match (PSM). To control the resulting quality, the PSMs are sorted by their scores. By choosing a proper score threshold, the quality of the PSMs above the threshold can be satisfied. The false discovery rate, or FDR, is defined as the ratio between the false PSMs and the total number of PSMs above the score threshold. [90].

Within the proteins identified, two proteins were found to have a lysine carboxyethyl PTM (mass shift of 72.02 Da): Allophycocyanin alpha chain (Accession Q01951, -10lgP=294.69) and C-phycocyanin alpha chain (Accession Q54715, -10lgP=395.04).

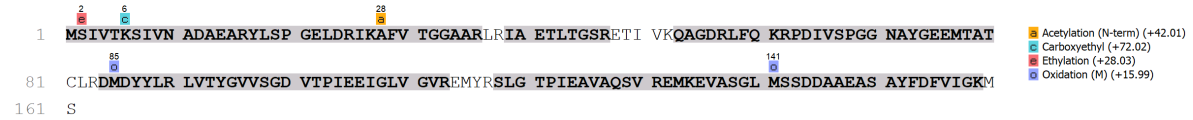

Fig. 3.4 Coverage of the native ApcA from isolated PBS tryptic digests identified using PEAKS Studio 8 software. The sequence corresponding to ApcA is shown in black coloured font. The coverage of tryptic peptides identified are highlighted; these are representative of a total of 37 peptides identified in CpcA. PEAKS confident PTM sites are shown (Ascore≥200).

Allophycocyanin α-chain (ApcA) was identified with a 90% peptide coverage (Fig. 3.4). Lysine carboxyethylation was found at the first peptide of the protein. Carboxyethyl Lys 6 missed cleaved peptide MSIVTK(+72.02)SIVNADAEAR(+28.03) had a confident modification site Ascore=1000 and peptide score -10lgP=16.73 (Fig. 3.5). PEAKS determines PTM sites by the presence of site-determining fragment ions. One can determine confident modification sites by selecting a threshold of the modification Ascore, which calculates an ambiguity score as -10 × log10 P. The p-value indicates the likelihood that the peptide is matched by chance. Therefore the higher Ascore, the better [34][7].

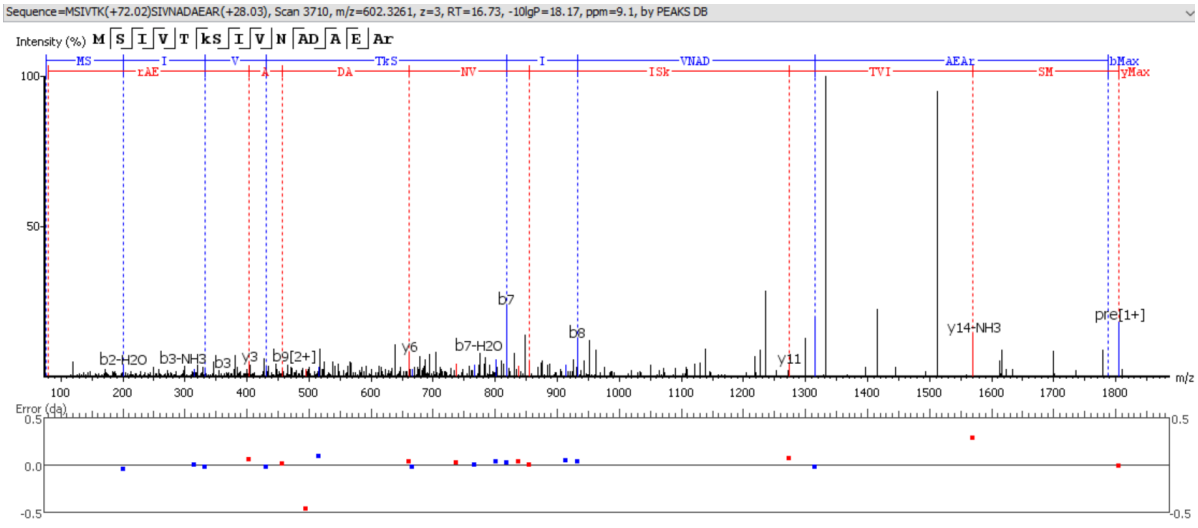

Fig. 3.5 MS/MS spectra of ApcA peptide with missed cleaved carboxyethylated lysine. Series of y- and b-ions are highlighted in blue and red, respectively. Lowercase k represent the carboxyethylated lysine residue, Lowercase r represent an ethylated arginine residue.

In addition to ApcA Lys 6 carboxyethyl modification, CO_2 mediated PTM was found at the Lys 2 residue of the C-phycocyanin alpha chain in *Synechocystis* PBSs. The protein coverage

was of 83% (-10lgP = 434.74) with 73 unique peptides (Fig. 3.6). A carboxyethyl modification was found at the peptide sequence MK(=72.02)TPLTEAVSTADSQGR (-10lgP=74.45) shown in Fig. 3.7.

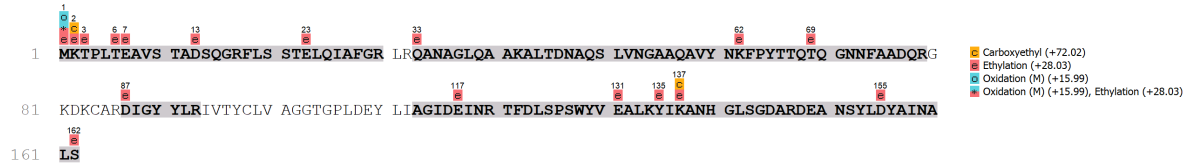

Fig. 3.6 Coverage of the native CpcA from isolated PBSs tryptic digests identified using PEAKS Studio 8 software. The sequence corresponding to CpcA is shown in black coloured font. The coverage of tryptic peptides identified are highlighted; these are representative of a total of 37 peptides identified in ApcA. PEAKS confident PTM sites are shown (Ascore≥200).

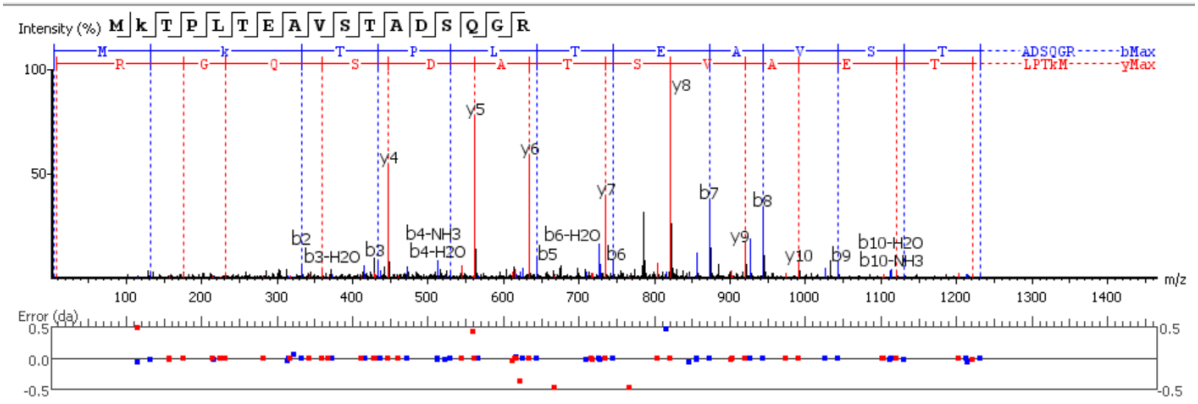

Fig. 3.7 MS/MS spectra of CpcA peptide with missed cleaved carboxyethylated lysine. Series of y- and b-ions are highlighted in blue and red, respectively. Lowercase k represents the carboxyethylated lysine residue.

Potential carbamate formation was identified in lysines of ApcA and CpcA from *Synechocystis* purified PBS with CO_2 trapping. We chose ApcA's modification site for further investigation as we had previously identified ApcA Lys 6 carbamate site in *Synechocystis* lysate.

3.4 Recombinant Allophycocyanin carbamate trapping

The identification of ApcA Lys 6 from the PBSs sample supported cyanobacterial water soluble protein lysate carbamate site identification. However, challenges across the protein digest and peptide purification methods led to a reduced ion coverage of the peptide modification. Initial protein concentrations may have been a limitation for this matter. Thus, we sought to produce recombinant APC protein to increase the concentration of digested carbamates from trapping. In addition, to validate the carbamate formation in Lys 6 with ^{13}C-NMR, ApcA Lys 6 was mutated to alanine, which is not capable of forming a carbamate. This section, will present the expression and purification of recombinant WT and mutant APC, as well as the carbamate trapping and validation of carbamate formation in recombinant APC protein.

3.4.1 Production of a mutant APC protein

Hypothesized carbamylation site Lys 6 of ApcAB was mutated to Ala and Glu for the expression of recombinant proteins. First, one site-directed mutagenesis was performed as mentioned in section 2.3.16, to obtain a mutated construct. Next, PCR was conducted to amplify the complete pApcAB plasmid (Table 2.4) using primers MJC985/MJC986 that yielded plasmid pK6AapcAB; and primer pair MJC1029/MJC30 (Table 2.3) that produced pK6EapcAB. The correct size of the resulting construct was verified by running 10 μl of amplicon in a 2% agarose gel (data not shown). Finally, the mutated plasmids were sequenced and aligned to pApcAB construct to confirm a correct single-site mutation of Lys 6 to Ala or Glu.

Plasmids pK6AapcAB and pK6EapcAB were co-transformed with plasmids pCpcUS and pPcyA into *E. coli* BL21 (DE3) cells (Table 3.2) and; grown on a large scale under the conditions developed for the wild-type ApcAB to produce ApcAB^{K6A} and ApcAB^{K6E} (Subsection 2.3.17). Proteins were purified (Subsection 2.3.17) and used for CO_2 trapping and *in vitro* experiments.

3.4.2 Co-transformation of *E. coli*

To further investigate ApcA carbamate Lys 6 site by trapping CO_2 with TEO, the trimeric $(\alpha\beta)_3$, monomeric $(\alpha\beta)$ and α-subunit of allophycocyanin were expressed in *E. coli*.

Allophycocyanin exists in the core of the PBSs in a trimeric form. ApcA and ApcB forms each monomer of the trimer. For the recombinant expression of allophycocyanin trimeric and monomeric form, three plasmids were co-transformed into BL21 (DE3) cells (Section 2.3.15) using 100 ng of total DNA. For this, plasmid pPcyA was first transformed into BL21 cells and made chemically competent. BL21 with pPcyA was then co-transformed with 50 ng of each plasmid described in Table 3.1 and Table 3.2.

Table 3.1 Plasmids for PBPs expression of *Synechococcus* sp. PCC 7002 and *Synechocystis* sp. PCC 6803. APC: Allophycocyanin, PC: Phycocyanin.

PBP	Plasmids co-transformed	Antibiotic	Reference
[1]APC (α and β)	pApcAB pPcyA pCpcUS	Ap Cm Km	Biswas *et al.* (2010)
[2]PC (α and β)	pCpcBA pPcyA pCpcUS	Sp Cm Km	
α APC	pApcA pPcyA pCpcUS	Sp Cm Km	This study Biswas *et al.* (2010)

Table 3.2 Plasmids for Lys 6 mutated PBPs of *Synechococcus* sp. PCC 7002. PBP: Phycobiliprotein, PC: Phycocyanin, APC: Allophycocyanin.

Mutation	PCB	Plasmids co-transformed
Lys 6 by Ala	α_{APC}	pK6AapcA pCpcUS pPcyA
	$\alpha\beta^{APC}$	pK6AapcAB pCpcUS pPcyA
Lys 6 by Glu	α_{APC}	pK6EapcA pCpcUS pPcyA
	$\alpha\beta^{APC}$	pK6EapcAB pCpcUS pPcyA

3.4.3 Recombinant Allophycocyanin expression in *E. coli*

BL21 (DE3) cells were used to express Allophycocyanin monomers. APC trimers $(\alpha\beta)_3$ are self-assembled by three monomers $(\alpha\beta)$ initiated with the junction process of α and β subunits; trimers were formed *in vitro* at high concentrations of monomers. Chromophorylation of AP and PC subunits were assessed by the CpcS-I/CpcU bilin lyase by attaching chromophores to the Cys-81 positions of ApcA and ApcB [85].

The plasmids used to express recombinant allophycocyanin and phycocyanin were donated from Biswas *et al.*. Their study showed that the heterologous CpcS-I/CpcU-type bilin lyase was required for maximal and correct PCB addition to ApcA. Also, the heterologous *in vivo* expression system using PcyA from *Synechococcus* sp. strain PCC 7002 and Ho1 from *Synechocystis* sp. strain PCC 6803 was very efficient for PCB biosynthesis, which generates large amounts of PCB in *E. coli* [9].

For this study, a three-plasmid system was used to reconstitute recombinant APC. All plasmids were maintained in cells by continuous selection with Ap, Km and Sp. The use of three plasmids in the same cell allowed the expression of genes *apcA*, *apcB*, *cpcS*, *cpcU*, *ho1* and *pcyA*. The *apcAB* operon was attached to a His-tag near the N-terminus to allow metal affinity purification. Previous studies have shown that the His-tag did not significantly interfere with trimer assembly [46]. After induction with IPTG, an intense green culture was observed as chromophorylated subunits were formed. Blue cell pellets (Fig. 3.8**A**) were harvested by centrifugation and resuspended in 50 mM sodium phosphate, as previously mentioned in Chapter 2 (Section 2.3.17).

3.4.4 Purification of APC trimers

APC (ApcAB) trimers and monomers were purified in several chromatographic steps, including metal affinity, Sephadex G-25, and Superdex 200 size-exclusion chromatography. The subunits' aggregation state was determined by the distinctive difference in the absorption and fluorescence emission spectra of APC monomers and trimers (Section 1.2.3).

To verify the molecular weight of recombinant proteins, SDS-PAGE analysis was performed (Fig. 3.8). Two distinctive Coomassie blue-stained bands were observed in the co-transformed strain lysates after IPTG induction and purified solutions. These two bands corresponded to a

calculated molecular mass of 21.4 kDa for ApcA and a molecular mass of 17.2 kDa for ApcB (Fig. 3.8).

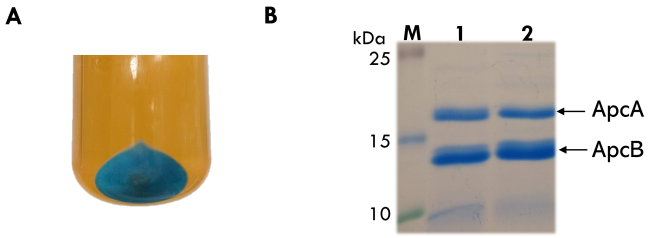

Fig. 3.8 *Synechococcus sp.* PCC 7002 Allophycocyanin recombinant expression in *E. coli*. **A.** Pellet from protein expression strain. **B.** SDS PAGE analysis of proteins purified by size-exclusion chromatography. Lane 1: APC^{WT}, Lane 2: APC^{K6A}, both purified by Superdex 200 size-exclusion chromatography. M: molecular mass standard.

The absorption maximum of the APC affinity-purified protein solution was 615 nm, and the fluorescence emission maximum was 647 nm, both of which are typical of APC monomers. After buffer exchange by dialysis, the absence of imidazole resulted in trimeric APC development, which has a maximum absorption at 620 nm with another peak at 650 nm. A high concentration of imidazole has been reported to act as a monomer-promoting solution, inhibiting APC subunit association [52].

Freshly purified ApcAB was analyzed by analytical size exclusion chromatography in PBS (pH 7.4), using a Superdex 75 column. $ApcAB^{WT}$ and $ApcAB^{K6A}$ elution profiles were compared to standard protein profiles: BSA (66.5 kDa), Aprotinin (30 kDa), Cytochrome c (12 kDa) and Carbonic anhydrase (6.5 kDa). Fractions from a retention volume from 60 to 70 mL were mainly composed of monomers ($\sim$39 kDa) according to standard protein profiles (Fig. 3.9). Fractions from Superdex 75 from a retention volume from 45 to 60 mL suggested were mainly composed of trimers and aggregates ($>$66 kDa), similar to the molecular weight of native APC (105 kDa). $ApcAB^{WT}$ and $ApcAB^{K6A}$ presented similar elution profiles.

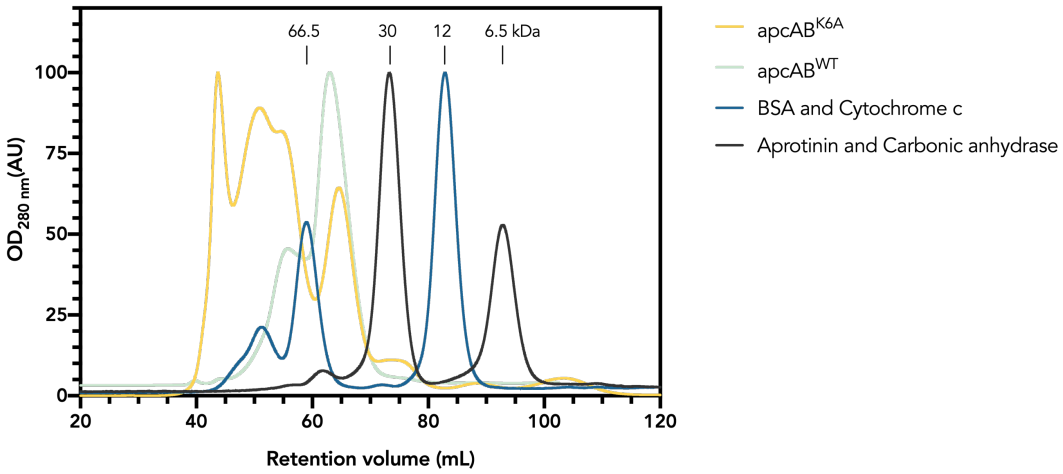

Fig. 3.9 Recombinant Allophycocyanin elution profile on Superdex 75. Inset: plot of the standard proteins. Size exclusion chromatography markers (Sigma Aldrich): BSA (66.5 kDa) and Cytochrome c (12 kDa), Carbonic anhydrase (30 kDa), and Aprotinin (6.5 kDa).

Predominant purified elutions from size exclusion chromatography exhibited a prominent peak at 620 nm, suggesting that the trimeric APC was not fully formed. Native Allophycocyanin trimers have a red-shifted maximum at 650 nm and a shoulder near 620 nm. The SEC fractions expected to be composed mainly by trimers was found to have a 650/620 ratio from 1.1-1.5. All fractions with ratios greater than one were pooled and used for trapping experiments.

3.4.5 Production of mutant Allophycocyanin α subunit

For the validation of carbamylation occurring in Lys 6 of the APC alpha chain by ^{13}C-NMR and APC subunit CO_2 trapping assays, a K6A recombinant alpha subunit mutant was expressed. For this purpose, pET100 plasmids expressing ApcAB^{WT} and ApcAB^{K6A} mutant were digested with restriction enzymes (Section 2.3.17). *apcB* was removed from *apcAB* operon present in plasmids pApcAB, pK6AapcAB and pK6EapcAB (parent vector pET100) by digest with AanI and EcoRI restriction enzymes. The remaining vectors were pApcA, pK6AapcA and pK6EapcA (Table 3.2).

3.4.6 Expression and purification of ApcA^{WT} and ApcA^{K6A}

ApcA, heme oxygenase 1 (*ho1*) and 3z-phycocyanobilin ferredoxin oxidoreductase (*pcyA*) were co-expressed in BL21 (DE3) cells to produce ApcA^{WT} and ApcA^{K6A}. ApcA subunits were expressed on a large scale of 24 L for each batch of protein. ApcA^{K6A} was expressed following the same conditions as established for ApcA^{WT}.

Purification of ApcA^{WT} and ApcA^{K6A} was similar to ApcAB (Subsection 3.4.4). Proteins were affinity-purified using Ni-columns and subsequently purified by Superdex 200 size-exclusion chromatography. A single band of 21.4 kDa was observed at SDS PAGE analysis from freshly purified ApcA^{WT} and ApcA^{K6A}(Fig. 3.10).

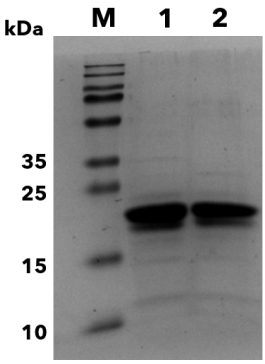

Fig. 3.10 SDS PAGE analysis of ApcA^{WT} and ApcA^{K6A} purified by Superdex 200 size-exclusion chromatography. M, molecular mass standard. Lane 1, ApcA^{WT}. Lane 2, purified ApcA^{K6A} mutant.

Elutions from a single peak of SEC were pooled and concentrated using Vivaspin® 20 centrifugal concentrators to a minimum concentration of 8 mg/mL for CO_2 trapping and ^{13}C-NMR experiments.

3.4.7 Allophycocyanin Carbamate trapping

A previously unkown carbamate was successfully trapped on a complex protein system: the *Synechocystis* lysate and isolated PBS antennae. The next aim was to improve the y and b-ion coverage of the carbamate trapped peptide. Increasing the initial amount of carbamylated protein would increase the concentration of trapped digested peptides to be detected by ESI-MSMS. First, the ApcA subunit was buffered with a $NaHCO_3$ solution to provide CO_2. After that, the buffered solution was replaced with $NaH^{13}CO_3$ to confirm that carboxyethyl modification is due to experimental performance.

$^{12}CO_2$ ApcA trapping

The recombinant $ApcA^{WT}$ carbamate was trapped with TEO in the presence of 200 mM $NaH^{12}CO_3$ in PBS pH 7.4. Trypsin digested peptides from ApcA trap were analyzed by LC/ESI-MS/MS, and proteomic data were analysed with PEAKS Studio 8 software searching against the NCBI *Synechococcus sp.* PCC 7002 protein database. This file was slightly modified by adding the pET100 His-tag and Xpress tag (AA1 to AA37) to potentially identify all digested peptide sequences, mainly the first peptide including the Lys 6.

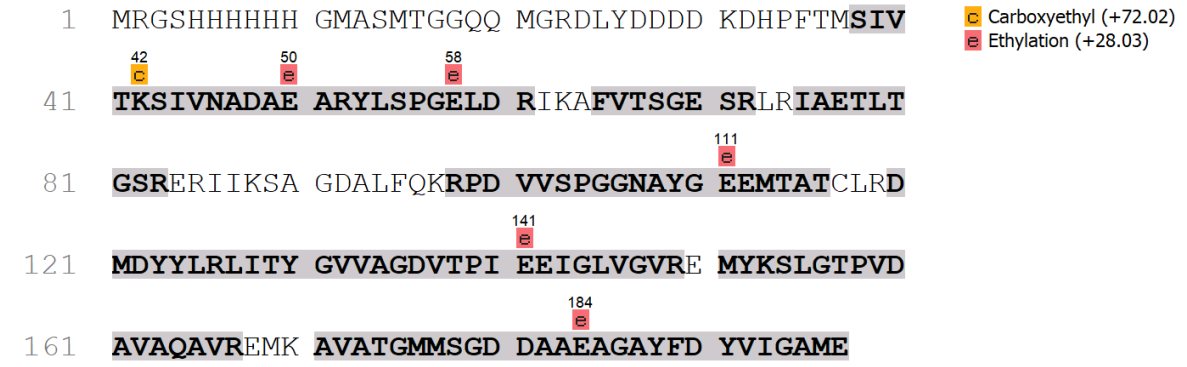

Fig. 3.11 Coverage of the $ApcA^{WT}$ tryptic digests from CO_2 trapping identified using PEAKS Studio 8 software. The sequence corresponding to ApcA is shown in black coloured font. The coverage of tryptic peptides identified is highlighted; these represent 31 unique peptides identified in ApcA. PEAKS confident PTM sites are shown on top of the amino acid (Ascore≥200).

PEAKS DB analysis with an FDR of 1% yielded an ApcA peptide coverage of 68% with 31 unique peptides (Fig. 3.11). The trapped carbamate was confirmed at the Lys 6 of the ApcA protein by the observed carboxyethyl modification with a mass shift of 72.0211 Da (Lys 42 in tag added FASTA file, Fig. 3.12). The peptide SIVTK(+72.02)SIVNADAEAR containing the carboxyethyl modification on Lys 6 had a confident modification site AScore=1000 and a peptide score of -10lgP=39.06. We observed increased ion intensity of y-ions covering the missed cleaved carboxyethylated lysine. Ion intensity covering Lys 6 carboxyethyl (y10 and y11) was 95%. Therefore, increased concentration of protein carbamates at the trapping allowed to obtain sufficient material after peptide digest and sample purification for enhanced detection.

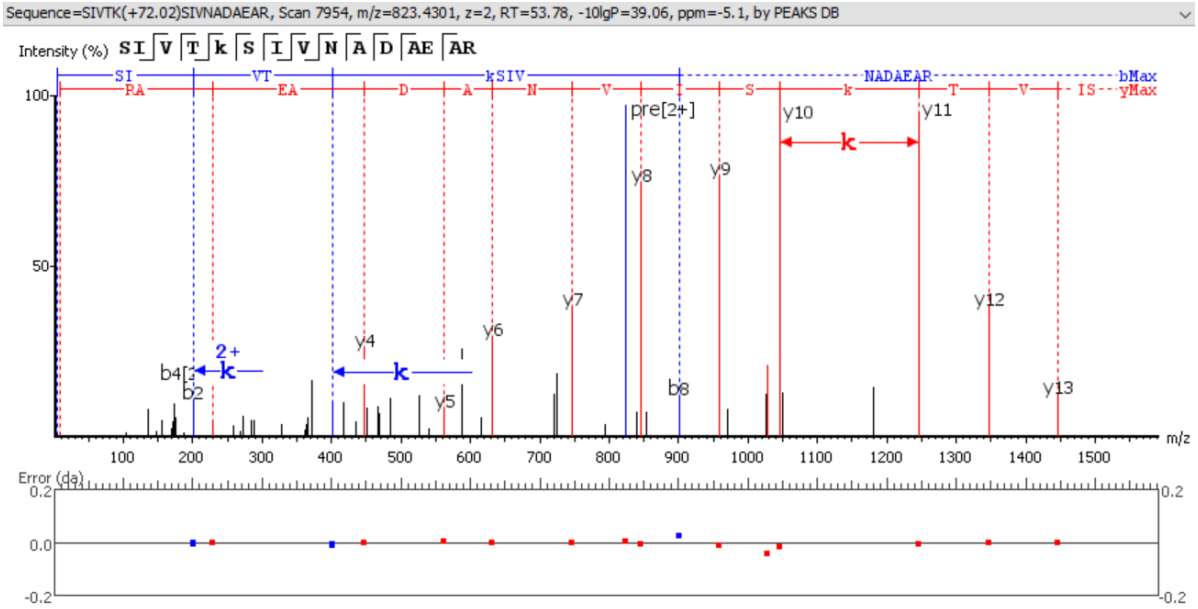

Fig. 3.12 MS/MS spectra of ApcA peptide with missed cleaved carboxyethylated lysine. Series of y- and b-ions are highlighted in blue and red, respectively. k: carboxyethylated lysine residue.

$^{13}CO_2$ ApcAB trapping

An isotope trapping experiment using $NaH^{13}CO_3$ was performed to confirm that the carbamate formation and trapping were due to the experimental method. $NaH^{13}CO_3$ has been previously used to investigate Hb carbamate binding [65]. In our experiment, the presence of the same peak

of carboxyethyl modification with an additional 1 Da mass change would validate carbamate formation when analyzed with MS/MS.

Recombinant ApcAB protein solution, composed of APC ($\alpha\beta$) monomers and $(\alpha\beta)_3$ trimers, was trapped with TEO in the presence of 50 mM $NaH^{13}CO_3$. Collected data from ESI-MSMS was analyzed with PEAKS Studio 8 software under an FDR of 1%. Allophycocyanin was identified by the software with a peptide coverage of 56% for ApcA (Fig. 3.13) and 40% for ApcB.

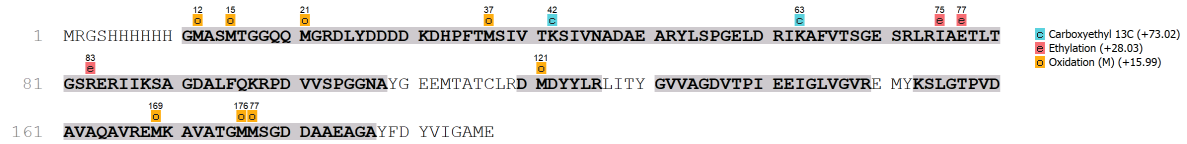

Fig. 3.13 Coverage of the $ApcA^{WT}$ tryptic digests from $^{13}CO_2$ trapping identified using PEAKS Studio 8 software. The sequence corresponding to ApcA is shown in black coloured font. The coverage of tryptic peptides identified are highlighted; these represent a total of 60 unique peptides identified in ApcA (-10lgP=320.67). PEAKS confident PTM sites are shown on top of the amino acid (Ascore≥200).

^{13}C carboxyethyl modification was found in miss-cleaved Lys 6 of ApcA as expected with the additional 1 Da mass change (Fig. 3.14). The 73.02 Da shift mass was found on peptide Scan F2: 10683.
Sequence of peptide was SIVTK(+73.02)SIVNADAEAR with a score of -10lgP=36.46 and a PTM confident Ascore=1000. Similarly to the trapping performed with $NaH^{12}CO_3$, we observed higher intensity of y-ions covering Lys modification compared to MSMS spectra previously obtained from PBS and lysate trapping.

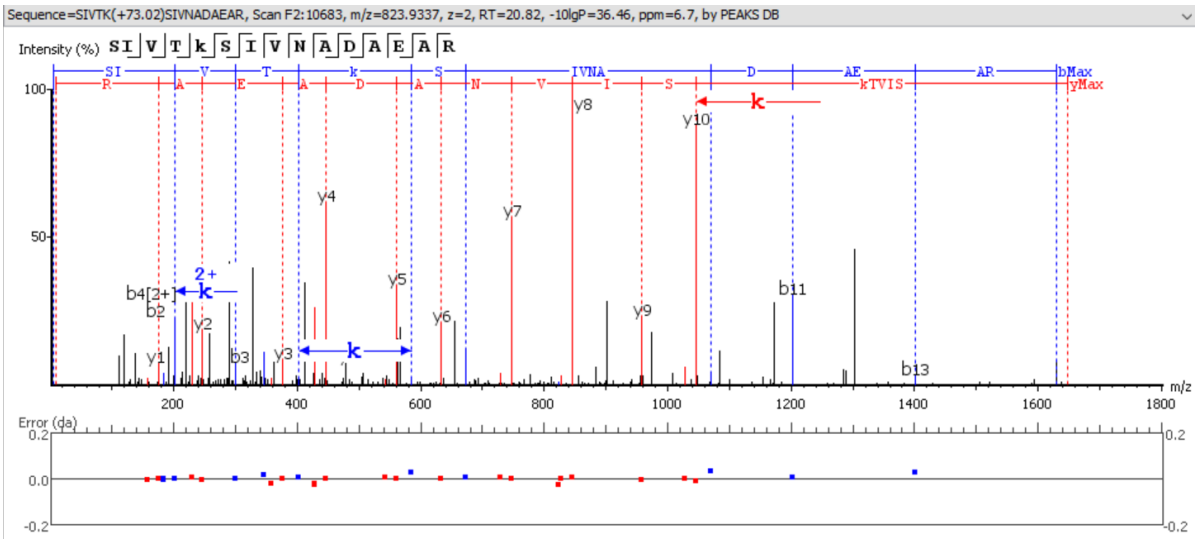

Fig. 3.14 MS/MS spectra of ApcA peptide with missed cleaved Lys 6 ^{13}C carboxyethylated. Series of y- and b-ions are highlighted in blue and red, respectively. Lowercase k represents a carboxyethylated lysine residue with a 1 Da mass change. Scan F2: 10683, m/z=823.9337, -10lgP=36.46.

From this experiment, an additional lysine was found to have a ^{13}C carboxyethylated modification. PEAKS identified Lys 27 (Lys 63 including recombinant Xpress tag) from ApcAB with a +73.02 mass shift located in peptide sequence IK(+73.02)AFVTSGESR with a -10lgP=42.76 and PTM Ascore=1000. Ions covering K27 +73.02 modification were b_2-NH_3 and y_9 (Fig. 3.15), which also included isoleucine. This identification had not appeared in previous ^{12}C trapping experiments with PBS nor recombinant ApcAB, even at very high CO_2/HCO_3^- concentration (200 mM). Thus, further trapping repeats are needed to confirm Lys 27 hypothesized carbamate site.

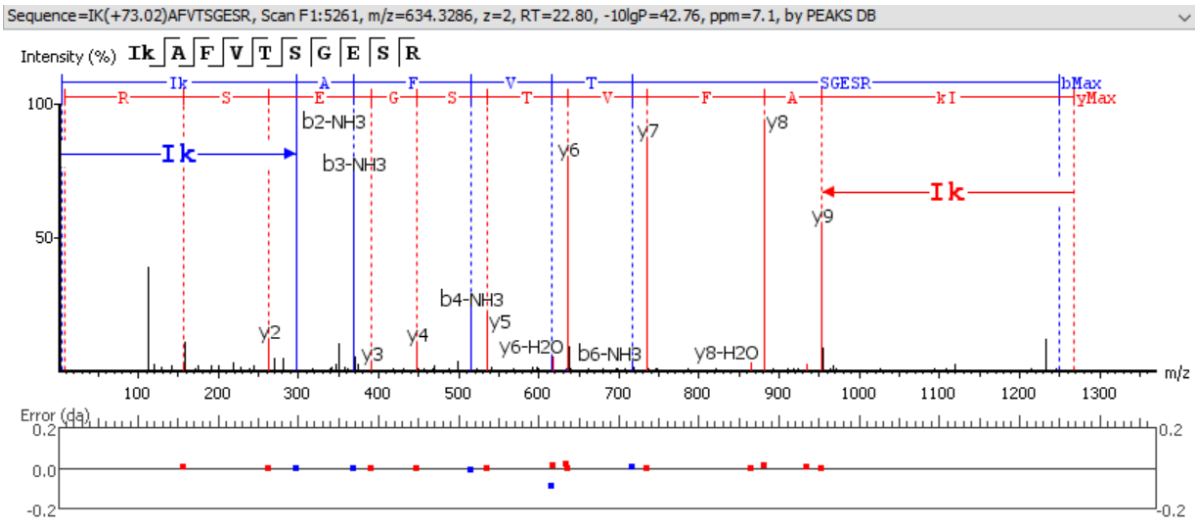

Fig. 3.15 MS/MS spectra of ApcA peptide with missed cleaved Lys27 ^{13}C carboxyethylated. Series of y- and b-ions are highlighted in blue and red, respectively. k: ^{13}C carboxyethylated lysine residue. Scan F1: 5261, m/z=634.3286, -10lgP=42.76.

Recombinant APC carbamate trapping was performed on recombinant ApcA and ApcAB. The formation of the carbamate in Lys 6 was confirmed, the ^{13}C labelled carbamate trapping supported the hypothesis that carboxyethyl modification is due to reaction conditions.

3.5 Validation of ApcA Lys 6 carbamylation by ^{13}C NMR

Nuclear Magnetic Resonance spectroscopy (NMR) has been used before to analyze the presence of carbamates in different proteins. A peak between 163.5 and 167 ppm has been identified as characteristic of a carbamate [53] [96] [66]. To validate the carbamate formation on the amino group of ApcA lysine, carbamylated protein was ^{13}C-labelled and identified by Carbon NMR spectroscopy.

We first incubated ApcA (10 mg) recombinant protein with 50 mM Na$H^{13}CO_3$ in pH 9.0, favouring carbamate formation with high pH. We used BSA as a negative control, as there is no evidence for carbamate formation in this protein. BSA (8 mg) was incubated under the same conditions as ApcA^{WT}. From the results of this experiment, we observed a peak at 163.5 ppm on ApcA^{WT} ^{13}C-NMR, which was absent in BSA (Fig. 3.16**A**).

We then sought to investigate carbamate formation under physiologically relevant conditions of pH. Recombinant ApcA (10 mg) was incubated with 25 mM $Na^{13}CO_3$ in PBS at pH 7.4. Lysozyme (8 mg), used as a negative control, was incubated in the same conditions. Carbamylation formation under comparable physiological conditions was confirmed by observing a signal at 163.6 ppm, which matched literature values of a carbamate peak (Fig. 3.16**B**).

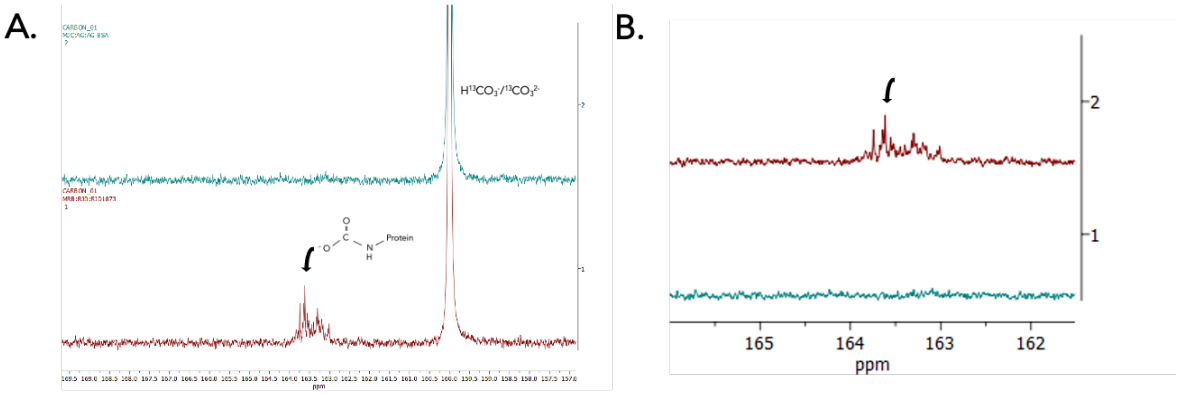

Fig. 3.16 ^{13}C NMR comparison of ApcA and BSA in the presence of Na$H^{13}CO_3$. **A.** ^{13}C NMR spectrum of proteins incubated with 50 mM $^{13}CO_2/H^{13}CO_3^-$. Showing the presence of carbamate peak at 163.6 ppm. Cyan: BSA; Red: ApcA^{WT}.**B.** ^{13}C NMR spectrum of proteins incubated with 25 mM $^{13}CO_2/H^{13}CO_3^-$. Cyan: Lysozyme; Red: ApcA^{WT}

Carbamylation site specificity to Lys 6 was tested with the use of the ApcA^{K6A} mutant. The spectroscopic profile of the expressed ApcA^{K6A} mutant was identical to ApcA^{WT}. The amino acid mutation performed on ApcA did not alter the secondary structure of the protein, judged by the identical circular dichroism spectra on both proteins. In the same way, ApcA^{K6A} protein presented similar fluorescence and absorbance activity to ApcA^{WT} that was analysed before NMR experiments.

Recombinant proteins (10 mg), ApcA^{WT} and ApcA^{K6A}, were incubated in PBS with 50% D_2O and 25 mM $Na^{13}CO_3$ (pH 7.4). The carbamate peak at 163.6 ppm was detected only in the ApcA^{WT} protein (Red spectrum at Fig. 3.16). High signals were also obtained at 160 ppm and 124 ppm (Fig. 3.17), which correspond to the equilibrium between bicarbonate and carbonate ions, and to free carbon dioxide, respectively.

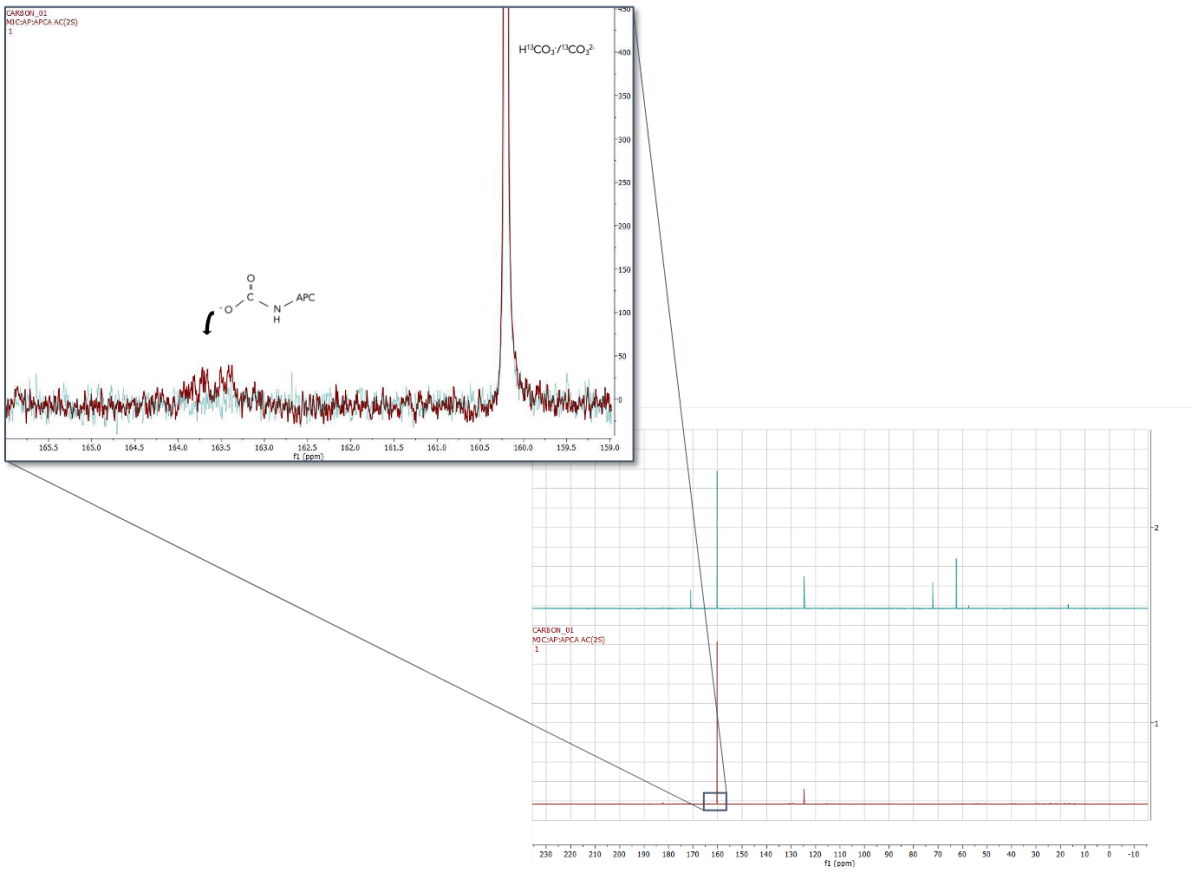

Fig. 3.17 Superimposed ^{13}C-NMR spectrum demonstrating demonstrating carbamate formation on ApcA Lys 6 by the appearance of a peak at 163.6 ppm only in ApcA^{WT}. **Red**: ApcA^{WT}; **Cyan**:ApcA^{K6A}

Based on ^{13}C NMR of $ApcA^{WT}$, it was demonstrated that carbamate formation occurs in ApcA Lys 6 under relevant physiological $CO_2/H^{13}CO_3^-$ concentrations for cyanobacteria. The ApcA spectrum (Fig. 3.15) shows key signals that corroborate the findings from LC-ESI-MSMS.

3.6 Conclusions

This Chapter presented the first efforts to identify carbamates in cyanobacteria proteome using TEO as an ethylated reagent to trap CO_2 mediated protein PTM. This method enabled cyanobacterial carbamate identification by locking the reversible nature of this PTM.

The results discussed in this Chapter showed the identification of carbamate formation in ApcA Lys 6, a protein previously unknown to bind CO_2. The carbamate identification in repeated trapping experiments of PBS and recombinant protein indicates that true carbamate formation occurs in ApcA and not by lysate or isolated PBS interactions. The trapping of low concentrations of CO_2/HCO_3^- demonstrated the occurring PTM at comparable physiological concentrations of CO_2, representing a more accurate cellular environment.

Unfortunately, more cyanobacterial proteins were not identified in this study. Experimental limitations and the complexity of a lysate limit the number of peptides identified in the last step of sample preparation for LC-MS/MS. For example, the abundance of a group of proteins in the lysate sample like the phycobilisomes that account for up to 60% of the total protein mass in cyanobacteria might decrease the protein coverage of the resulting analysis. Optimization in the workflow for sample preparation, such as MS fractionation of the sample to increase the protein coverage of the resulting analysis, could address this matter in question. However, this research aimed to elucidate CO_2 binding effect in APC alternatively. Thus, ApcA carbamylation was later validated with isotope labelling. When using ^{13}C-NMR to monitor protein carbamylation, care must be taken as carbamylation of residues other than lysine, like the N-terminus, can occur. Nevertheless, the identified carbamate peak in $ApcA^{WT}$ and its absence in $ApcA^{K6A}$ presented in this Chapter supports lysine-specific binding to CO_2. Here is proved that^{13}C-NMR spectroscopy combined with genetic tools is a feasible approach to study lysine-carbamylation.

Chapter 4

CO_2 involvement in Allophycocyanin Energy Transfer

4.1 Overview

In the last chapter, we described the identification of a novel carbamylation site in cyanobacteria. Allophycocyanin Lys 6 interacts with CO_2 to form a carbamate. The carbamylation of a PBP and its impact on energy transfer has never been described before. Here, we present the study of the ApcA Lys 6 modification on photosynthetic energy transfer.

We hypothesised that CO_2 plays an important role in energy transfer in the PBS antenna that has not been elucidated before. To investigate this role, we first analysed the fluorescence properties of the antenna in the presence of CO_2/HCO_3^-. Once we identified the CO_2 effect in the PBSs complex, we asked whether Lys 6 carbamylation promotes a more efficient energy transfer in the system. Therefore, we replaced the ApcA Lys 6 amino acid with Ala or Glu to represent unmodified Lys and a negative charged Lys. And the fluorescence performance of the mutated recombinant proteins was evaluated in the presence of CO_2/HCO_3^-. Measurements of photoluminescence quantum yields (QYs) of PBSs and ApcAB $(\alpha\beta)_3$ trimers were shown to be enhanced by CO_2/HCO_3^- compared to NaCl, suggesting to be dependent on carbamylation of ApcA Lys 6.

4.2 Representation of ApcA Lys 6 across cyanobacterial species

4.2.1 Introduction to Allophycocyanin energy transfer

Allophycocyanin (ApcAB) is a biliprotein located in the core of the photosynthetic antenna in charge of final energy transfer to cyanobacteria photosystems. L^{CM}, β^{16}, and α^{B} are three other core proteins with chromophores. Allophycocyanin provides energy to the L^{CM} and α^{B} biliproteins, transferring that energy to chlorophyll in the thylakoid membrane.

As previously mentioned in Chapter 1, allophycocyanin is native as a trimer, with each monomer being an $\alpha\beta$ structure. ApcAB monomers have α and β subunits in a 1:1 molar ratio. Each subunit, α and β, has one phycocyanobilin chromophore (Fig. 1.5). Biliprotein chromophores are covalently attached to apoproteins through thioether bonds to cysteine residues.

The X-ray crystal structure of allophycocyanin trimers from *Arthrospira platensis* has previously been obtained [11]. It can be observed that ApcA Lys 6 is located in a privileged pocket formed by the monomer arrangement of α and β APC subunits. The Lys 6 residue is placed close to amino acids sited on an ApcB α-helix that connects to the chromophore-binding pocket, where it forms a salt bridge with D99 (Fig. 4.1). The distance between Lys 6 and the closest chromophores is in the range of 26-28 Å.

Allophycocyanin monomers have an absorption maxima at around 615 nm. ApcAB trimers have a red-shifted maximum at 650 nm, and a shoulder near 620 nm. This red-shift modification of absorption from monomeric to the trimeric state, can be explained due to PCB conformational changes [70] and a strongly coupled dimer, which causes a redshift of the absorption indicative of exciton splitting [57]. From the first proposal, sugar showed to cause enhancement of the 650 nm band without altering the molecular size of ApcAB. According to Murakami *et al.*, a specific local protein environment produced chromophores shift to 650-nm. Then energy should be transferred from the 620-nm band to the 650-nm band via Föster resonance energy transfer. From the second proposal, there is strong exciton coupling between two chromophores of the trimer near each other through the monomer-monomer interface. The strong contact causes exciton splitting and a red shift in absorption.

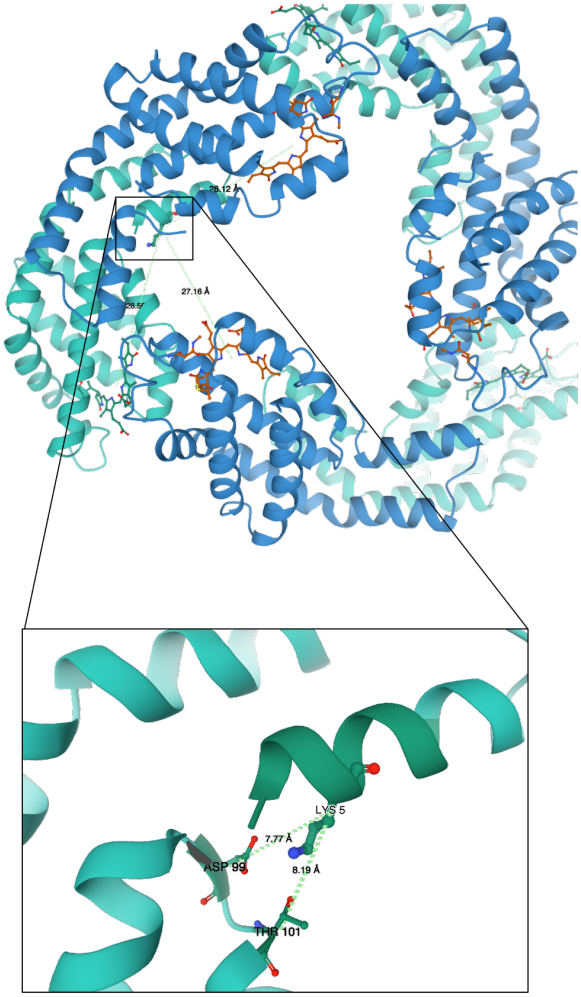

Fig. 4.1 Allophycocyainin trimeric model based on crystal structure with close-up to Lys 5 residue of 1ALL crystal structure. PDB accession number 1ALL showing the residues surrounding the K5 putative carbamate site. K5 is located close to Asp 99(7.77Å) and Thr 101(8.19 Å).

I, therefore, asked whether Lys 6 is represented across cyanobacteria species and carbamylation of Lys 6 modifies the local environment of ApcAB energetic interface.

4.2.2 pLogo analysis of Lys 6

A multiple sequence alignment was run to analyse the importance and representation of Lys 6 in cyanobacteria allophycocyanin. I investigated the frequency of conserved regions based on the alignment of ApcA sequence window centred around the target Lys residue across fifteen species.

I generated a type of sequence logo (pLogo) which computes the likelihood of amino acids being over or underrepresented at the positions surrounding the carbamylation site (Fig. 4.2). The plogo consists of stacks of symbols, one stack for each position in the sequence. The overall height of the stack indicates the sequence conservation at that position. In contrast, the height of symbols within the stack indicates the relative frequency of each amino at that position. The sequence plot was generated with the pLogo-tool (http://plogo.uconn.edu; [72]) using the sequences bordering the identified lysine-carbamylated site.

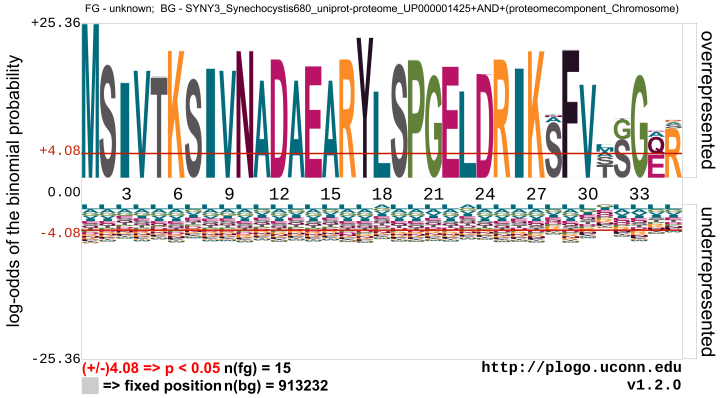

Fig. 4.2 Sequence logo of the lysine-carbamylated amino acid motif which residue heights are scaled relative to their statistical significance. The pLogo depicts under- and over-represented amino acids, which are scaled to their log10-odds of the binomial probability — as a direct measure of a residue's likelihood of being statistically significantly over-or underrepresented. The horizontal red line indicates the threshold of the Bonferroni corrected p-value of $p < 0.05$.

Significant conservation of Lys 6 and surrounding amino acids across different cyanobacterial species was identified. In addition, we observed an environment over-represented by hydrophobic and uncharged amino acids. We concluded that the representation of Lys 6 across different cyanobacteria species could indicate an important, yet to be discovered, role for lysine carbamylation in electronic energy transfer.

4.3 CO_2 effect in PBS Energy Transfer

The identification of a carbamylation site in the PBS was described in Chapter 3, but the role of CO_2 PTM in ApcAB was still unclear. Therefore, the spectroscopic properties of ApcAB were analysed to gain insight into the effect of CO_2 in PBSs energy transfer.

PBS from *Synechocystis* sp. PCC 6803 were isolated by sucrose gradient ultracentrifugation and analysed by measuring fluorescence intensity in the presence of CO_2/HCO_3^-. Cyanobacteria can store up to 1000X the extracellular concentrations of inorganic carbon. Different concentrations of inorganic carbon were first explored to investigate the hypothesized effect of CO_2/HCO_3^- in PBSs fluorescence.

CO_2 was introduced to the system using sodium bicarbonate ($NaHCO_3$). Upon dissociation in solution, sodium bicarbonate forms sodium and bicarbonate ions which then forms carbonic acid (**1**), which is next dissociated to give CO_2 (**2**)(Scheme 4.1). To prevent any effect from Na cations, NaCl was used as a control.

$$Na^+ HCO_3^- + H_2O \rightleftharpoons Na^+ H_2CO_3 + OH^- \quad (1)$$
$$H_2CO_3 \rightleftharpoons CO_{2(aq)} + H_2O \quad (2)$$

Scheme 4.1 Dissociation of sodium bicarbonate to carbonic acid which then produces CO_2

In this study, we decided to use $NaHCO_3$ to introduce CO_2 under representative physiological pH (7.4-8). Under these conditions, the carbonate system of 1 mM and 10 mM $NaHCO_3$ would dissociate into 100 µM of dissolved CO_2 and 700 µM, respectively.

4.3.1 Measuring fluorescence with a Synergy H4 plate reader

To test the effect of CO_2, the fluorescence of PBSs in phosphate saline buffer (pH 7.4) was first analysed with a Synergy H4 plate reader. PBSs were treated either with a final concentration of 1 and 10 mM of $NaHCO_3$ (CO_2/HCO_3^-) or 1 and 10 mM NaCl. PBSs were excited at 615 nm, and fluorescence emission was measured from 600 to 680 nm with a 1 nm increment.

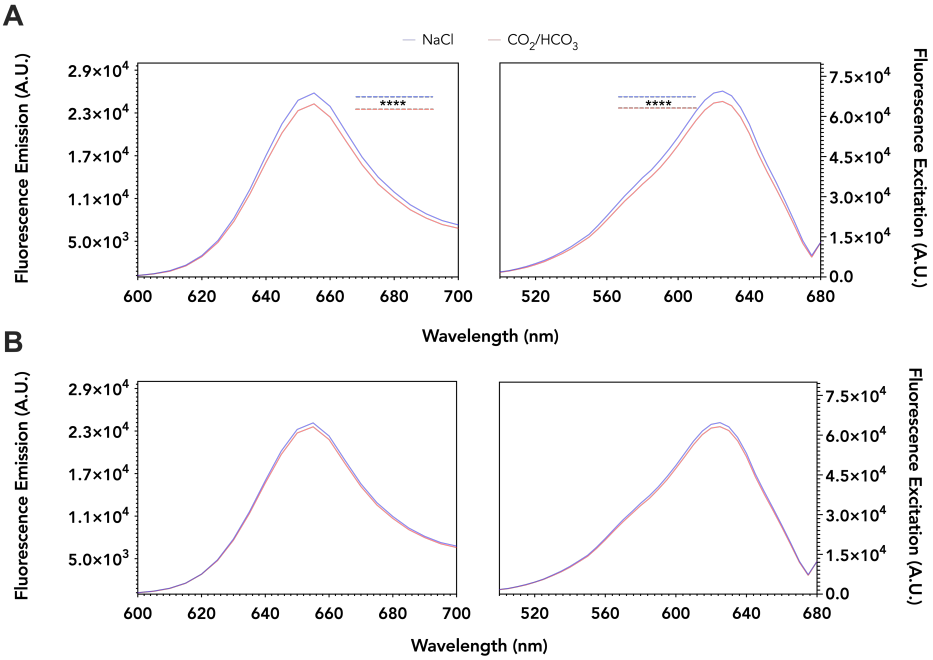

Fig. 4.3 PBSs from *Synechocystis* sp. fluoresce more with CO_2/HCO_3^- (Blue) compared to a control system (Red). Fluorescence emission and excitation of PBS with **(A)** 1 mM CO_2 and **(B)** 10 mM CO_2. Proteins were excited at 580 nm. (Ordinary one-way ANOVA, ****p<0.0001, n=12 t=4.393, df=44)

PBSs with different concentrations of CO_2 and NaCl showed a similar maximum emission peak at 655 nm and an excitation peak at 625 nm (Fig. 4.3**A**). Similar to previously reported in literature, indicating that PBS isolation was performed accurately. An increment in fluorescence emission was observed in the presence of CO_2/HCO_3^- compared to NaCl. This difference was not observed when adding a higher concentration of both additives (10 mM) (Fig. 4.3**B**).

The analysis of PBSs fluorescence using a plate reader indicated a possible effect of CO_2 in the energetic antenna pathway. Even though care was taken to normalise initial concentrations

of PBS complex, absolute absorption of molecules in the solution was not considered in this experiment. We, therefore, used a different approach to investigate deeper the absolute fluorescence efficiency in the presence of CO_2.

Measuring photoluminescence quantum yield (PLQY) would consider the absolute effect of CO_2 in samples, minimizing the error of protein concentrations of the sample being tested. Thus, to measure overall energy transfer efficiency, *i.e.* total photon emission from photons absorbed, we used an integrating sphere coupled to a Fluorolog 3 fluorimeter.

4.3.2 Measuring QYs with Fluorolog 3 fluorimeter

The integrating sphere method is a direct method of measuring PLQY. The PLQY of an ensemble of molecules is defined as the number of photons emitted as a fraction of the number of photons absorbed. With this method, radiation from the excited sample strikes the reflective walls of the sphere. It then is reflected at the sphere walls until capture and detected by the fluorimeter.

Measurements are taken from the fluorescence emission (E_c) and the scatter (L_c) of the sample, as well as the emission and scatter of a blank (E_a and L_a). From these two spectral measurements (sample and blank), the PLQY can be calculated from the equation in 4.1.

$$\phi_f = \frac{E_c(1-A)\cdot E_b}{L_a \cdot A} = \frac{E_c - E_a}{L_a - Lc} \tag{4.1}$$

E_b is the integrated luminescence from the sample caused by indirect luminescence from the sphere and A is the absorbance of the sample at the excitation wavelength. A simple calculator that incorporates the two traces and with appropriate spectral correction factors are used to give the PLQY and associated error analysis.

For this experiment, PBSs samples were set to 0.1 of its maximum absorption and introduced into the integrating sphere (Quanta-φ) fibre-coupled to the fluorimeter with direct excitation to the solution. PBSs were excited at two different wavelengths, 570 and 610 nm, to compare energy transfer within the antenna in the presence of CO_2.

Quantum yields were calculated from two spectral measurements: absorption and emission. Absorption was detected from 600 to 620 nm and emission from 620 to 750 nm (Fig. 4.4). QYs were calculated with the FluorEssence^{TM} software as described above.

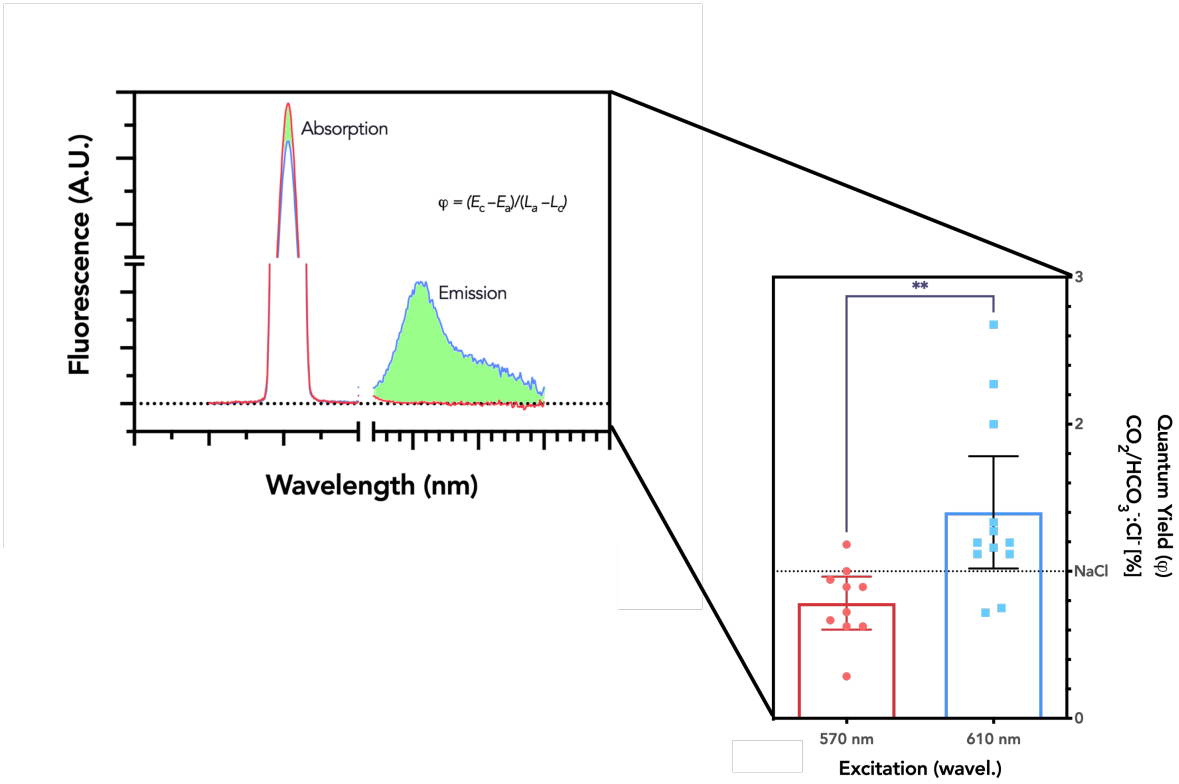

Fig. 4.4 PBSs PLQY are enhanced with CO_2/HCO_3^-. Ratio of the measured quantum yield with 1 mM $NaHCO_3$ (red and blue bars) and NaCl (Normalised to 1) for isolated PBSs excited at two different wavelengths. Image at the back represents the spectrum from where QY is calculated. (**p = 0.006, two-tailed t-test, n > 9 independent replicates, ±95% C.I.).

QYs of PBSs from the addition of 1 mM CO_2/HCO_3^- were normalised to PBSs QYs with NaCl. QYs with CO_2/HCO_3^- suggested an increase of almost 25% of energy transfer efficiency compared to NaCl (normalised to 1.0) when exciting PBSs at 610 nm (Fig. 4.4). Contrarily, a small decrease on the ratio of the measured QY excited at 570 nm was observed. This results indicate a more efficient energy transfer from lower energy to the final emitting species in PBS. We concluded that the system was altered when adding inorganic carbon. We, therefore, decided to get an insight with solely ApcAB.

4.4 ApcAB fluorescence emission response to CO_2

4.4.1 Testing CO_2 concentrations

PBSs experiment demonstrated an increase in fluorescence quantum yield when inorganic carbon was present. Similar to the approach taken for PBSs analysis, we sought first to analyze inorganic carbon concentrations to observe a difference in ApcAB activity. For these assays, recombinant PBPs were expressed in *E. coli* and purified by size exclusion chromatography, referred to in sections 2.3.17 and 3.4.4.

To investigate concentrations to which CO_2 affect ApcAB, APC monomeric response to CO_2 was tested. The purified protein was treated with either $NaHCO_3$ (to incorporate CO_2) or NaCl. Samples were excited at 610 nm, and fluorescence emission was detected in a Synergy H4 plate reader from 600 to 750 nm. Concentrations of 1 and 10 mM of $NaHCO_3$ and NaCl were tested.

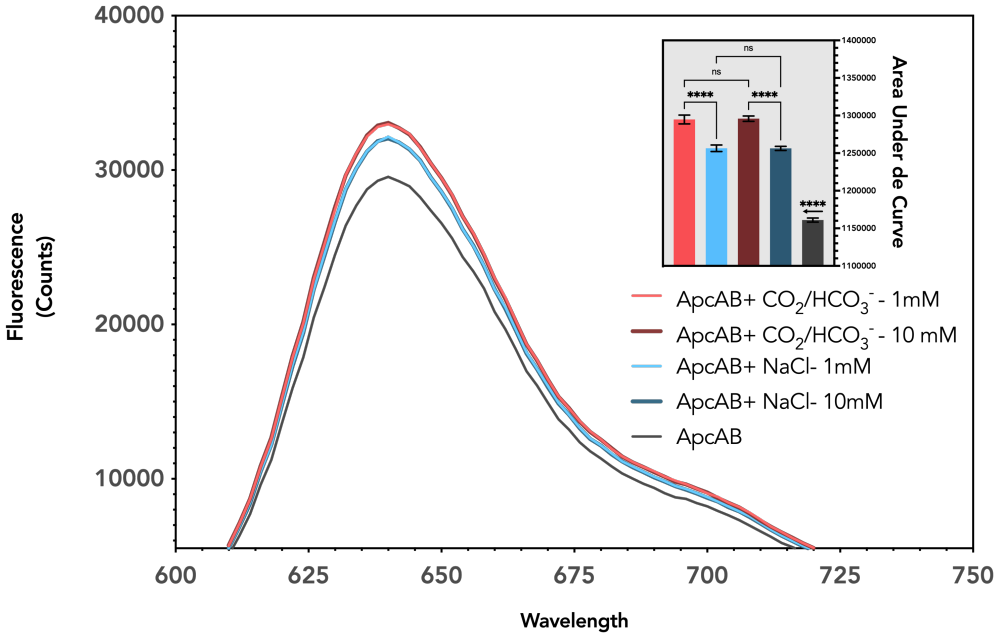

Fig. 4.5 ApcAB Fluorescence CO_2 effect. Inset graph represents area under the curve of fluorescence emission of different $NaHCO_3$/NaCl conditions (Ordinary two-way ANOVA, Šidák multiple comparison test, ****p<0.0001, n=12, mean with 95% CI.)

ApcAB ($\alpha\beta$) monomer fluorescence emissions were higher when adding CO_2/HCO_3^- compared to NaCl and pure protein (Fig. 4.5). However, there was no difference in emission intensity when incorporating higher concentrations of inorganic carbon nor NaCl. Interestingly, a response to Na cations was observed by an increased in intensity from pristine APC proteins with the addition of either NaCl or $NaHCO_3$. This effect has been previously described effect on *Spirulina* phycobiliproteins fluorescence with Na^+ stress [93]. For the purpose of this project, possible Na cation effect concerns were controlled by using NaCl as a control henceforth.

4.4.2 PBP comparison

Once we identified the CO_2 effect in ApcAB fluorescence, we aimed to compare CO_2 absolute quantum yields of ApcAB to a control PBP. Phycocyanin (CpcAB) is located at the top of the phycobilisome rod; they share a common structural theme with all PBPs and has a single absorption peak at $\approx$ 621 nm and an emission maximum at $\approx$ 642 nm. These features makes CpcAB a good candidate as a control protein.

For this experiment, QYs of the different PBP were measured (λex=610 nm; λabs=600-620 nm; λem=620-750 nm). Inorganic carbon (CO_2/HCO_3^-) enhanced the QY for recombinant ApcAB $(\alpha\beta)_3$ trimers and α subunits ($ApcA^{WT}$) by approximately 25% compared to NaCl (normalised to 1). However, Ci did not enhance recombinant protein corresponding to the phycocyanin heterodimer (CpcAB $(\alpha\beta)_3$ trimer) assessed as a control (Fig. 4.6).

CO_2/HCO_3^- therefore specifically enhances QY of ApcAB $(\alpha\beta)_3$ trimers compared to a control protein. We next asked whether carbamylation of ApcA K6 was responsible for the increase in QY in ApcAB $(\alpha\beta)_3$ trimers in response to CO_2/HCO_3^-.

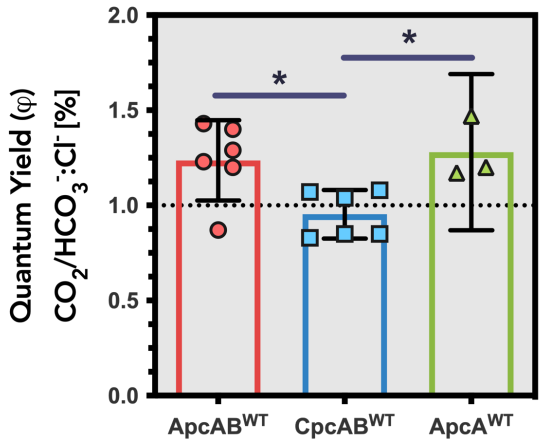

Fig. 4.6 Ratio of the measured quantum yield with 1 mM $NaHCO_3$ and NaCl for recombinant PBPs (*p = 0.01, ordinary one-way ANOVA, Tukey's multiple comparisons test, n=6 independent replicates for $ApcAB^{WT}$ and $CpcAB^{WT}$, n=3 independent replicates for $ApcA^{WT}$, ±95% C.I.)

4.5 Spectroscopic analysis of ApcA Lys 6 carbamylation

4.5.1 Spectral properties of mutant $ApcAB^{K6A}$

CO_2/HCO_3^- was shown to increase QYs of ApcAB $(\alpha\beta)_3$ trimers. CO_2 trapping results from NMR and LC-MS/MS (Chapter 3) suggested that the enhancement of QYs could be accountable to ApcA K6 carbamylation. Therefore, spectroscopic properties were tested to elucidate a definite response to CO_2.

For this purpose, a single site-directed mutation was performed in the ApcAB pET100 vector to express $ApcAB^{K6A}$ mutant protein. The substitution of Lys 6 to Ala 6 was confirmed by sequencing the final expression vector. The expression and purification of both $ApcAB^{WT}$ and $ApcAB^{K6A}$ proteins were performed correspondingly.

We first compared the excitation and emission spectra of ApcAB wild type and K6A (Fig. 4.7). Absorbance and fluorescence spectras were normalised to the maximum intensity for comparison purposes. The excitation and emission spectra were similar. Pooled fractions from the purification of proteins showed a mixture of monomers and trimers, identified from absorption peaks at 620 nm and a shoulder at 650 nm (Fig. 4.7A). Characteristic emission of ApcAB $(\alpha\beta)_3$ trimers prevailed on fluorescence spectra with a maximum emission at 658 nm for both $ApcAB^{WT}$ and $ApcAB^{K6A}$ (Fig. 4.7B). Nevertheless, we observed a different

intensity in the shoulder intensity at 650 nm between $ApcAB^{WT}$ and $ApcAB^{K6A}$ proteins. This difference in absorbance strength could be due to the incorporated Ala neutral charge, indicating a different exciton coupling behaviour between $ApcAB^{WT}$ and $ApcAB^{K6A}$. Higher fluorescence intensity can also be observed at 640 nm in $ApcAB^{K6A}$. Therefore, the neutral charge incorporated by Ala insertion affects exciton coupling.

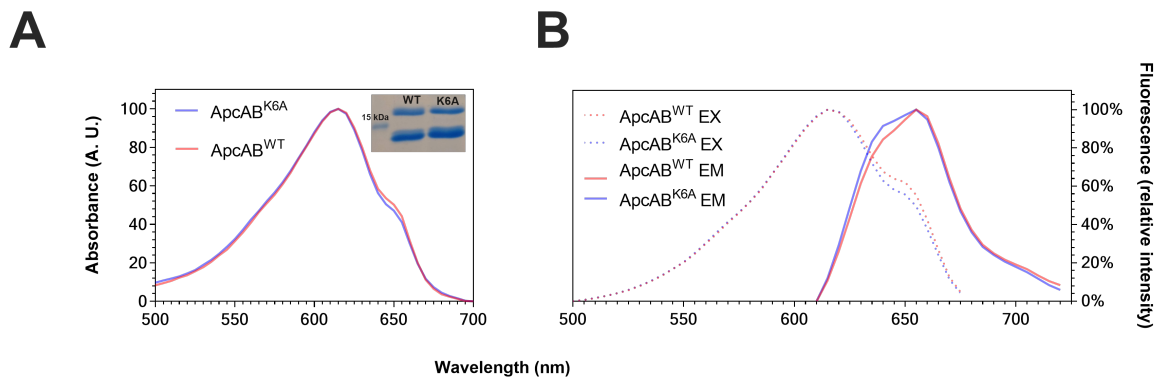

Fig. 4.7 Spectral properties of purified $ApcAB^{WT}$ and $ApcAB^{K6A}$. **A.** Absorbance and **B.** Fluorescence excitation (dotted lines) and emission (solid line) spectra of purified $ApcAB^{WT}$ and $ApcAB^{K6A}$.

4.5.2 ApcA K6A CO_2 response

After ensuring that spectral properties were not disturbed by K6A mutation, we investigated the response to CO_2 of the mutant protein. The purified $ApcAB^{WT}$ and $ApcAB^{K6A}$ proteins, containing trimers and monomers (650/620 ratio of 1.4), were set to an absorption maximum of 0.1. Fluorescence emissions were measured in a fluorimeter (Fluorolog 3) (λex=610 nm; λem=620-750 nm).

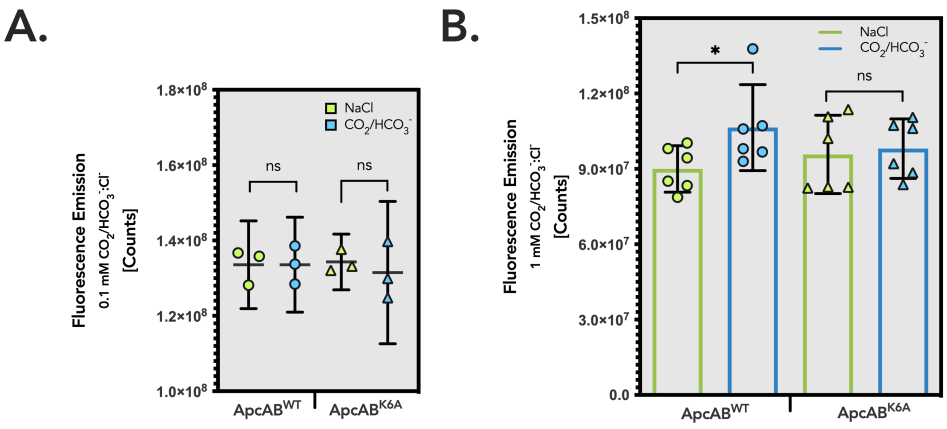

Fig. 4.8 Maximum fluorescence emission values of recombinant ApcAB^{WT} and ApcAB^{K6A} with **A.** 0.1 mM NaCl and $NaHCO_3$; and **B.** 1 mM NaCl and $NaHCO_3$. (*p=0.05, multiple unpaired t-test, n=6, df=10, Mean with 96% CI).

ApcAB^{WT} and ApcAB^{K6A} proteins showed similar fluorescence spectra with a maximum emission at 660 nm when excited at 610 nm. Low concentrations of inorganic carbon (0.1 mM $NaHCO_3$) did not affect the fluorescence intensity of ApcAB compared to 0.1 mM NaCl (Fig. 4.8**A**). However, an increase of almost 20% in fluorescence intensity was observed on ApcAB^{WT} in the presence of 1 mM of inorganic carbon compared to 1 mM NaCl. That increment was not detected in ApcAB^{K6A} (Fig. 4.8**B**), indicating that Lys 6 plays an important role in energy transfer when ApcA K6 is carbamylated.

ApcA K6A QYs response to CO_2

Fluorescence spectral measurements of $ApcAB^{WT}$ and $ApcAB^{K6A}$ proteins indicated that inorganic carbon played an important role in the energy transfer of allophycocyanin. We, therefore, measured QYs (λex=620, λabs=610-630, λem=630-750 nm) of recombinant $ApcAB^{WT}$ and $ApcAB^{K6A}$ $(\alpha\beta)_3$ trimers in the presence of CO_2/HCO_3^- or the corresponding NaCl concentration.

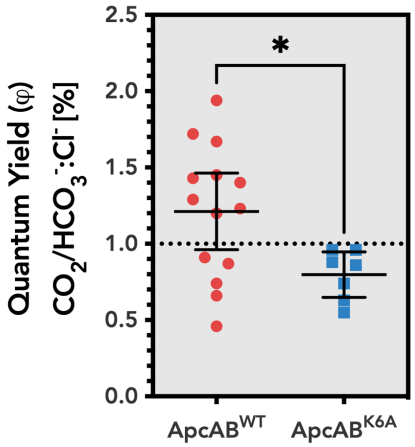

Fig. 4.9 Ratio of the measured quantum yield with 1 mM $NaHCO_3$ and NaCl for recombinant *Synechococcus* sp. PCC 7002 $ApcAB^{WT}$ and $ApcAB^{K6A}$ trimers (*p = 0.039, two-tailed non parametric test, n>7 independent replicates, mean ± 95% C.I.)

A QY enhancement with CO_2/HCO_3^- compared to NaCl for $ApcAB^{WT}$ $(\alpha\beta)_3$trimers was observed, similarly to fluorescence emission response previously seen (Fig. 4.9). This increase in fluorescence efficiency is clearly altered when lysine is mutated, and carbamate formation cannot occur. As a result, ApcAB EET is enhanced by CO_2/HCO_3^-, based on carbamylation at K6.

Fluorescence lifetimes

On the timescale of molecular events, as proton or electron transfer, the fluorescence lifetime of a molecule is a relatively long process. A high energy fluorophore can undergo a wide range of transformations during this period, ranging from electron redistribution and geometric alteration to a reorganization of the surrounding molecules and chemical reactions. We hypothesized that the K6 carbamylation effect in EET could be detected by measuring fluorescence decays.

Fluorescence lifetimes were measured in the presence of inorganic carbon (CO_2/HCO_3^-) or NaCl. For this experiment, we used a Time-Correlated Single Photon Counting (TCSPC) previously built in the lab. In TCSPC, one measures the time between sample excitation by a pulsed laser and the arrival of the emitted photon at the detector. Samples were excited with a laser beam at λex=485 nm, and emission was detected with a bandpass filter at 630 nm. We applied a non-linear two exponential fit routine to the measured fluorescence data and Instrumental Response Function (IRF) to obtain the fluorescence lifetimes from the measured data.

The fluorescence lifetimes for the purified ApcAB^{WT} and ApcAB^{K6A} were compared. We observed a predominant fluorescence lifetime for ApcAB^{WT} of 1.87±0.04 ns (96.8±2.8 % yield; S.D.) and ApcAB^{K6A} of 1.96±0.10 ns (97.0±3.3 % yield; S.D.). These results align with the QY variations and reflect the fluorescence lifetime from the APC antennae [54].

Table 4.1 Fluorescence lifetimes of ApcAB detected at 630 nm (Mean ± SD, n=6).

	NaCl				**CO_2/HCO_3^-**			
	$\tau_1(ns)$	**Yield (%)**	$\tau_2(ns)$	**Yield (%)**	$\tau_1(ns)$	**Yield (%)**	$\tau_2(ns)$	**Yield (%)**
ApcAB^{WT}	1.87 ± 0.04	96.8 ± 2.8	0.3 ± 0.1	3.2 ± 2.8	1.86 ± 0.17	98.9 ± 1	0.14 ± 0.1	1.07 ± 1
ApcAB^{K6A}	1.96 ± 0.1	97 ± 3.3	0.3 ± 0.2	3 ± 3.3	1.91 ± 0.11	95.56 ± 5.3	0.3 ± 0.34	4.43 ± 5.31

Based on the data presented in Table 4.1, CO_2 does not affect the fluorescence lifetimes of either ApcAB^{WT} or ApcAB^{K6A}. We, therefore, used a different approach to compare the lifetimes of a CO_2 depleted protein. ApcAB^{WT} and ApcAB^{K6A} proteins were incubated in an inert atmosphere glove box and sealed to avoid any $CO_{2(g)}$ diffusion from the atmosphere, and fluorescence lifetimes were immediately read. ApcAB^{WT} and ApcAB^{K6A} under an absent CO_2 environment showed similar fluorescence decays (Table 4.2).

Table 4.2 Fluorescence lifetimes detected at 630 nm of CO_2 depleted ApcAB (Mean ± SD, n=6).

	CO_2 free				**CO_2/HCO_3^-**			
	$\tau_1(ns)$	**Yield (%)**	$\tau_2(ns)$	**Yield (%)**	$\tau_1(ns)$	**Yield (%)**	$\tau_2(ns)$	**Yield (%)**
ApcAB^{WT}	1.97 ± 0.09	97.7 ± 1.5	0.5 ± 0.4	2.3 ± 1.5	1.87 ± 0.07	98.96 ± 1.4	0.65 ± 0.4	1.94 ± 1.4
ApcAB^{K6A}	1.96 ± 0.04	96.9 ± 1	0.4 ± 0.3	3.1 ± 1	1.97 ± 0.4	97.17 ± 0.82	0.34 ± 0.28	2.83 ± 0.82

We concluded that the basal fluorescence properties from ApcAB^{WT} and ApcAB^{K6A} proteins are not affected by K6 single-site mutation. We next hypothesised that mutation of K6 to glutamate would represent the local charge state of a carbamate at 100% occupancy.

4.5.3 ApcA K6E CO_2 response

The analysis of a K6A mutant allowed us to identify the role of carbamylated Lys 6 on allophycocyanin energy transfer. We then sought to substitute Lys 6 to Glu to test it as a potential positive control. It would resemble the acidic side chain of a carbamylated Lys representing a full carbamate occupancy.

Single site-directed mutagenesis was performed to substitute Lys to Glu (Section 2.3.16). $ApcAB^{WT}$, $ApcAB^{K6A}$ and $ApcAB^{K6E}$ were expressed in *E. coli* and purified by affinity chromatography and SEC. The secondary structure of recombinant proteins was compared by measuring the circular dichroism in the UV region. Recombinant proteins secondary structures were not changed significantly by single-site mutations of Lys 6, as shown in Fig. 4.10.

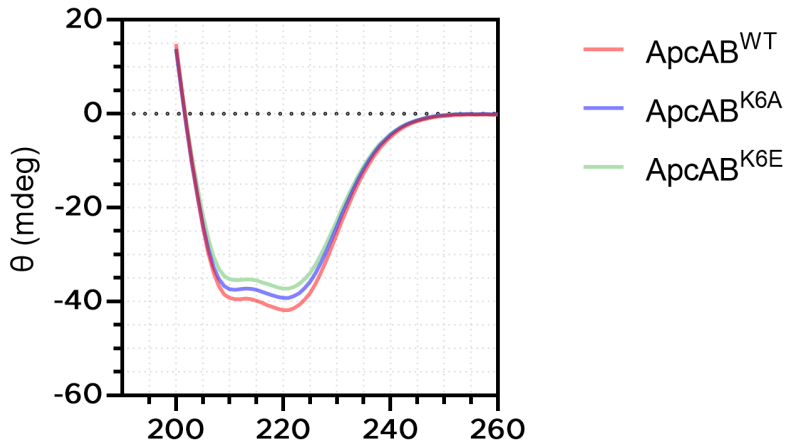

Fig. 4.10 CD-UV spectra of $ApcAB^{WT}$ (red), $ApcAB^{K6A}$ (purple) and $ApcAB^{K6E}$ (green) proteins reflecting identical secondary structure

For the initial analysis of $ApcAB^{K6E}$, proteins were set to the same protein concentration, and their spectral properties with 1 mM $NaHCO_3$ and 1 mM NaCl were investigated. We first measured the absorbance, fluorescence emission and excitation with a Synergy H4 plate reader. I sought to deplete all the $CO_{2(g)}$ that could be present from protein's expression and purification steps for this assay. In an inert atmosphere environment, N_2 was injected into WT and mutant ApcAB proteins. Samples were immediately treated either with NaCl or $NaHCO_3$ and scanned.

The spectroscopic properties of wild type and mutant proteins were comparable (Fig. 4.11). The three proteins showed a maximum emission at 658 nm with a shoulder at 635 nm. Residue mutation nor CO_2 shifted the maximum peaks to which ApcAB absorbs and emits. However, we observed an increase in fluorescence intensity by CO_2/HCO_3^- in $ApcAB^{WT}$ and $ApcAB^{K6E}$ (Fig. 4.11**A**), whilst this effect was not observed in $ApcAB^{K6A}$. Interestingly, the absorbance and the excitation of all proteins was lower with CO_2/HCO_3^- than with NaCl (Fig. 4.11**B-C**). If the fluorescence emission is normalised to the maximum absorbance of CO_2/HCO_3^- and NaCl, respectively, a larger difference in the $ApcAB^{WT}$ emission intensity would be found (data not shown). Experimental difficulties were encountered when comparing the proteins absorbance and fluorescence emission during this assay. Even though care was taken to compare the same concentrations of proteins, a small difference in protein concentration not sensitive to our methods could represent a false difference between fluorescence detection with or without CO_2 in the plate reader. In this assay, the same plate with prepared samples was read for absorption and excitation detection minutes after emission was detected. Considering that the plate reader was not fully sealed to avoid gas diffusion into the atmosphere, differences in $CO_{2(g)}$ in solution could have played a role in the differences observed in the assay during absorption and excitation detection with the plate reader. Therefore, the results observed during this assay could not be compared to previous QY measurements, and I proceeded to repeat this test in a sealed system in the integrating sphere where the possible differences in concentration of the samples do not affect our comparisons.

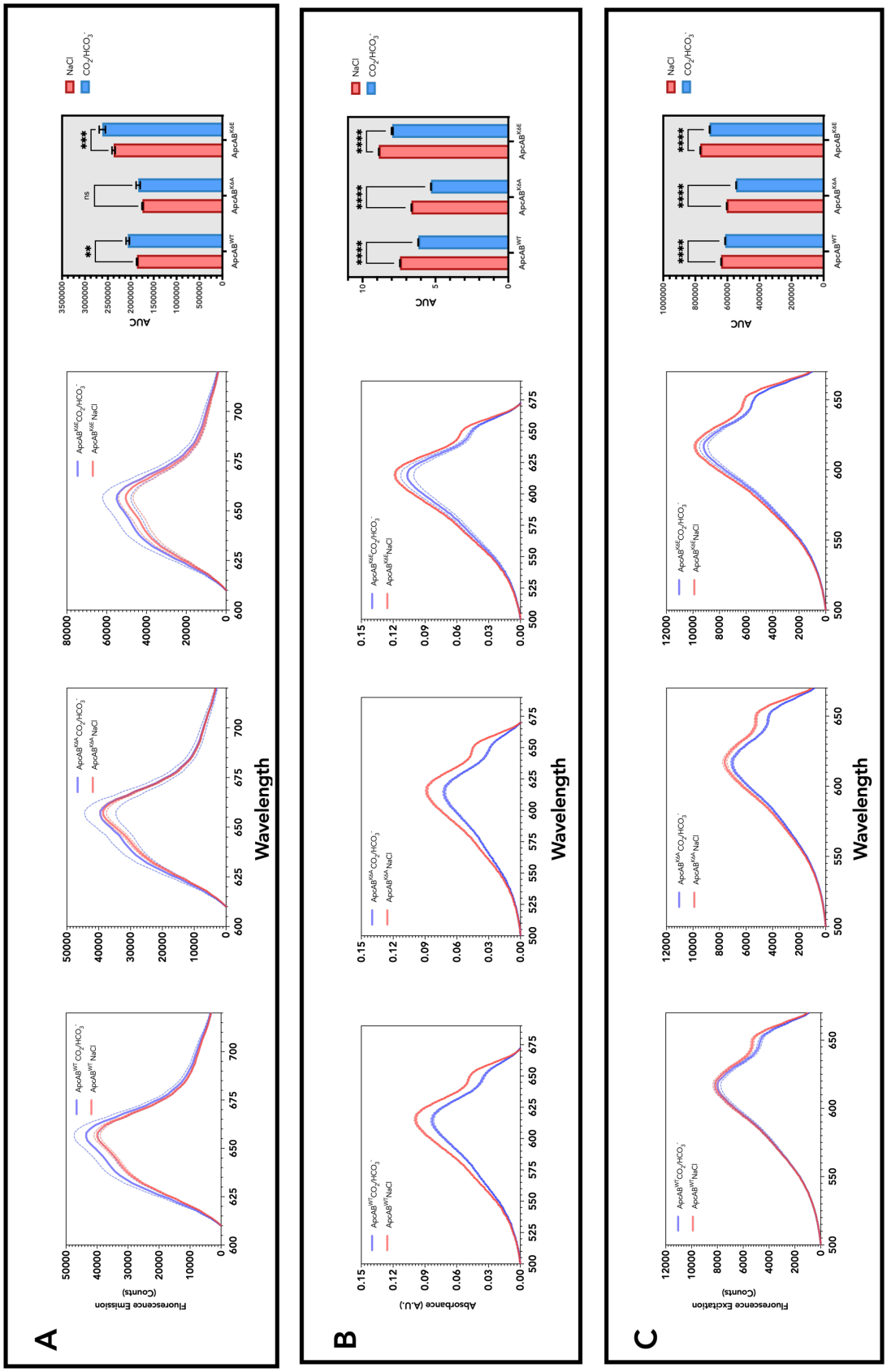

Fig. 4.11 Spectroscopic analysis of CO_2/HCO_3^- response in ApcAB^{WT}, ApcAB^{K6A} and ApcAB^{K6E}. **A.** Fluorescence Emission spectra. **B.** Absorbance spectra. **C.** Fluorescence Excitation Spectra. AUC: Area under the curve (Ordinary two-way ANOVA, Šidák multiple comparison test, **p<0.002, ***p<0.0001, ns=not significant, n=12, mean with 95% CI shown.)

ApcAB K6E QYs response

To assess ApcA K6E recombinant protein response to CO_2/HCO_3^- in ApcAB energy transfer efficiency, we compared QYs in the presence and absence of CO_2. Recombinant protein samples were prepared at the same concentration depleting $CO_{2(g)}$ present from previous steps in an inert atmosphere environment. QYs were measured before and after adding 1 mM NaCl or 1 mM $NaHCO_3(CO_2/HCO_3^-)$. A minor increase from free CO_2 samples with the addition of either NaCl or CO_2/HCO_3 was observed in $ApcAB^{WT}$ and $ApcAB^{K6A}$ and $ApcAB^{K6E}$ mutant proteins. Although the observed difference when adding NaCl was due to chance ($p>0.05$). A statistically significant difference between CO_2 depleted samples and the addition of CO_2/HCO_3^- was found only in $ApcAB^{WT}$. This difference was not found significant in K6A nor K6E proteins. The enhancement of $ApcAB^{WT}$ QYs with CO_2 was 50% higher (Fig. 4.12). The CO_2 effect was observed to be greater, almost 25% more in this assay, where CO_2 from the sample was depleted.

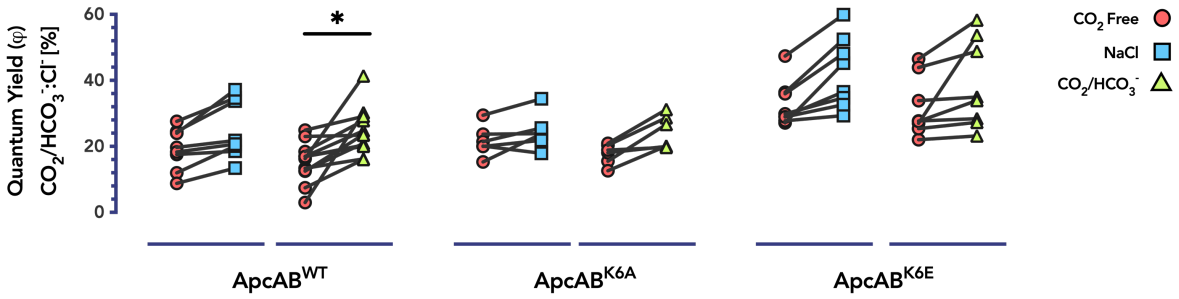

Fig. 4.12 Measured quantum yield with 1 mM $NaHCO_3$ and NaCl for recombinant $ApcAB^{WT}$, $ApcAB^{K6A}$ and $ApcAB^{K6E}$ trimers. Increase of QY from a CO_2 depleted protein (Red circles) to NaCl (Blue squares) or CO_2 addition (Green triangles) is shown (*p = 0.02, ordinary one-way ANOVA, Sidak multiple comparisons test, n>6 independent replicates, ±95% C.I.)

For comparison purposes, the CO_2 free QYs obtained from Fig. 4.12 were compared between proteins (Fig. 4.13). We observed QYs of $ApcAB^{K6E}$ ranging from 25-50%, whereas the range of $ApcAB^{WT}$ and $ApcAB^{K6A}$ QYs was 7-30% (Fig. 4.13). Fixed anionic charge of $ApcAB^{K6E}$ shows in general significantly higher QYs, which represents an established effect of K6 carbamylation. However, a difference $ApcAB^{K6E}$ QYs is not observed with the addition of $NaHCO_3$ due to unlikely interaction with CO_2. Contrarily, $ApcAB^{WT}$ and $ApcAB^{K6A}$ quantum

yield similarity represent the neutral state of an unmodified lysine. Therefore, CO_2 specifically modifies Lys 6, which significantly influences wild type allophycocyanin energy transfer.

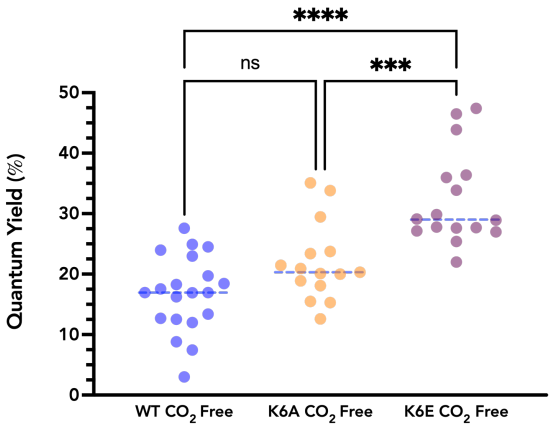

Fig. 4.13 Quantum yield of CO_2 depleted recombinant *Synechococcus* sp. PCC 7002 $ApcAB^{WT}$, $ApcAB^{K6A}$ and $ApcAB^{K6E}$ trimers (Ordinary one-way ANOVA, Tukey multiple comparison test, ***p<0.0001, ****p<0.0001, ns=not significant, n>15, mean with 95% CI shown.

4.6 Conclusions

This chapter demonstrated the effect of CO_2/HCO_3^- in photosynthetic protein properties *in vitro*. CO_2 has an apparent effect on allophycocyanin energy transfer. The enhancement of fluorescence emission and absolute quantum yields was observed at the different conformational states of the protein. QYs were enhanced by 25% only in $ApcAB^{WT}$ protein compared to a PBP control.

It was demonstrated that the enhancement in energy efficiency was due to the carbamylation of Lys 6. An increase in $ApcAB^{WT}$ QYs was observed with the addition of CO_2/HCO_3^-. This effect was not observed in the neutral analogue $ApcAB^{K6A}$ mutant. The evidence highlighted the involvement of a negative charge from the carbamylated lysine residue in the energetic performance. When the capacity to carbamylate at one site was removed (K6A), the enhancement of quantum efficiency in the presence of CO_2 was not observed. When the acidic residue was incorporated to imitate a 100% occupied carboxylated lysine (K6E), the response to CO_2 was not observed, but the overall percentage of QY was higher than wild type ApcAB.

In addition to energy efficiency evaluation, we measured fluorescence lifetimes to get an insight into the dynamics of energy transfer of ApcAB with CO_2. We did not observe a significant difference in fluorescence lifetimes measured with the presence or absence of CO_2. Comparable lifetimes were obtained for the K6A mutant indicating that the mutation did not affect chromophore fluorescence decays. The sensitivity of the settings used for lifetime measurements could have limited our investigation on a difference in EET of chromophores interaction in the presence of CO_2. We consider that additional lifetime measurements in a ps or fs scale are needed to unravel the mechanism underlying the increase in QY in ApcAB. This chapter demonstrated that CO_2/HCO_3^- enhances ApcAB EET dependent on carbamylation at K6.

Chapter 5

The Influence of ApcA carbamylation on *Synechocystis* sp PCC 6803 *in vivo*

5.1 Overview

The carbamylation of allophycocyanin Lys 6 enhances energy transfer efficiency *in vitro* (Fig. 4.6). However, the impact *in vivo* has not been elucidated. This chapter investigates the impact of CO_2 *in vivo*.

In this study, *Synechocystis* was used to investigate ApcA Lys 6 carbamylation. CRISPR-Cpf1 was employed to substitute ApcA Lys 6 for a neutral (K6A) and an anionic (K6E) residue *in vivo* to analyse the impact of carbamylation. Several analysis methods were developed using the mutants obtained to compare the energetic performance of wild-type *Synechocystis* and mutants in the presence of CO_2. However, demonstrating a clear dependence of ApcA energetic performance on CO_2 represented a challenge. Nevertheless, we observed an effect when we introduced a negative charge in place of Lys 6 to represent a fully carbamylated protein.

Wild-type *Synechocystis* demonstrated an increase in PBS fluorescence in the presence of CO_2 while the K6A mutant did not. A permanent negative charge (K6E) exhibited higher PBSs fluorescence emission compared to wild-type *Synechocystis*. The response of an anionic residue resembling a permanent carbamylated protein, was followed by slower fluorescence kinetics overall..

5.2 Site-directed mutagenesis of *Synechocystis*

CO_2-dependent carbamylation at ApcA K6 has been demonstrated to enhance the QY *in vitro* (Fig. . The ApcA protein and the light-harvesting complex, in general are essential for the activity of the downstream photosystem; we investigated the impact of CO_2-dependent carbamylation at ApcA K6 on downstream processes. We investigated these processes in wild-type organisms and organisms in which K6 carbamylation was either ablated (K6A) or mimicked (K6E).

5.2.1 CRISPR-Cpf1 plasmid design and cloning

Single site-directed mutagenesis was performed in *Synechocystis sp.* PCC 6803 (*Synechocystis*) to substitute Lys 6. Synechocystis was chosen for this study due to its versatility and practicality. Several techniques have been developed to genetically modify this organism for the study of photosynthesis [92]. CRISPR is a powerful technique to edit any genetic sequence. However, Cas9, a nuclease enzyme used to modify various organisms from mammals to plants to bacteria, is not often used to modify cyanobacteria genetically due to apparent toxicity in these organisms. Instead, Cpf1 is more effective for the engineering of markerless knock-ins, knockouts or specific point mutations in cyanobacteria [92]. Hence, we followed the Ungerer *et al.* CRISPR-Cpf1 methodology for K6A and K6E mutations.

The CRISPR-Cpf1 genomic editing plasmid consists of Cpf1 (or Cas12a) harbouring one RNA cleavage domain and a split RuvC motif (RuvC I, RuvC II, and RuvC III) for DNA cleavage [27]. Cpf1 possesses specific ribonuclease activity that cleaves the 36 bp repeat of the pre-crRNA four nucleotides upstream of a hairpin in a sequence, structure, and Mg^{2+} dependent manner. Next, the mature crRNA guides Cpf1 to its DNA target, where its nuclease activity induces a five bp staggered double-stranded break (DSB) 17 nucleotides downstream from the YTN PAM sequence [92]. The pSL2680-based vector (Addgene, plasmid 85581) has 1-kb homology domains that complement the target gene locus to be edited and express Cas12a and the protein-targeting crRNA. The inducible *lac* promoter and the constitutive J23119 promoter were used to regulate Cas12a and the protein crRNA, respectively. The crRNA-encoding array contains the *F. novicida* leader sequence followed by the direct repeat, spacer sequences, and the *F. novicida* terminator. Finally, after introducing the DSB, the homologous regions within

the donor DNA serve as templates for homology-directed repair, and cells are cured of the editing plasmid.

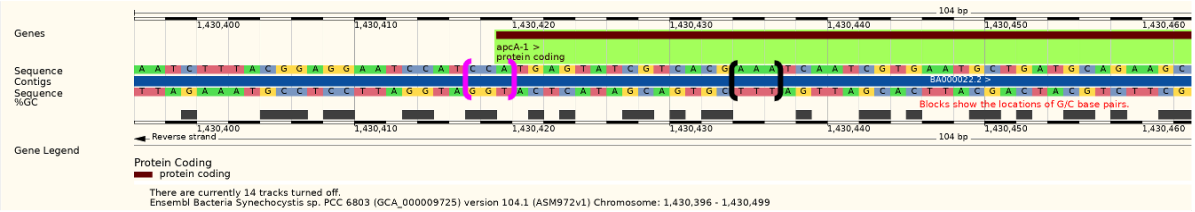

Fig. 5.1 Sequence of *Synechocystis* sp. 6803 *apcA*. Fuchsia brackets indicate PAM elected site. Black brackets indicate Lysine 6 sequence.

CRISPR-Cpf1 editing plasmids were designed following Ungerer *et al.*. The targeting RNA was chosen to precede a PAM sequence and cloned before the repair template (Fig. 5.1). The repair template contained the desired amino acid to be mutated. The homology template used was 1330 bp and cloned into the pSL2680gRNA vector by restriction digest and sticky ends ligation. The repair template, including K6A (or K6E) mutation, contained a PAM sequence after Lys 6. To eliminate the PAM, a second silent mutation was introduced to avoid Cpf1 plasmid cleavage. A final 13 518 bp vector was obtained and purified.

5.2.2 Transformation of a markerless K6A and K6E *Synechocystis* sp mutant

To achieve ApcA K6A (or K6E) mutation, circular pSL280_K6A (or pSL2680_K6E) were transformed to *Synechocystis* sp. by conjugal transfer. *E. coli* with cargo plasmid pSL2680 and *E. coli* with conjugal plasmid pRL443 were cultivated overnight in liquid BG11-1% LB media. Next, an *E. coli* and cyanobacteria mix was carefully introduced to Km BG11 media and incubated at 30°C until colonies appeared. Selected colonies were re-plated several times in Km-BG11 plates to segregate K6A (or K6E) mutations across *Synechocystis* chromosomes.

Fig. 5.2 Selective plates of an ApcA K6A *Synechocystis* mutant. Colonies 2 and 4 lost resistance to Km. Left: BG11 media, Right: BG11 media with the antibiotic.

Markerless mutations allow the addition or deletion of an unlimited number of genes while reducing concerns of growing antibiotic-resistant bacteria. We, therefore, cured *Synechocystis* K6A(6803^{K6A}) and K6E(6803^{K6E}) mutants from the antibiotic resistance (pSL2680 plasmid) by streaking cells multiple times in BG11 plates without antibiotics. Selection of a markerless *Synecho* mutant consisted in growing mutant colonies on BG11 agar plates parallel to BG11+Km agar plates. Colonies that would stop growing in Km-BG11 plates were selected (Fig. 5.2). Markerless mutants were next cultivated in BG11 liquid media to extract genomic DNA for mutagenesis validation. ApcA genomic DNA from (6803^{K6A}) and (6803^{K6E}) was amplified by PCR using primers MJC947 and MJC946 (Table 2.5). The resulting amplicons were analysed by sequencing, and point mutation was confirmed. Finally, cryo-stocks of Km resistant K6A (or K6E) mutants and markerless mutants were stored at -80°C until further use.

5.3 Study of an ApcA K6A *Synechocystis* mutant

5.3.1 Growth rate and fluorescence characterisation

To elucidate the *in vivo* effect of CO_2 on ApcA energy transfer, we first sought to compare growth rates and fluorescence profile of wild-type *Synechocystis* (6803^{WT}) against K6A ApcA mutant (6803^{K6A}). If carbamylation of ApcA Lys 6 enhances APC energy transfer efficiency, we reasoned that increased CO_2 fixation would favour the growth of WT *Synechocystis*. Therefore, we cultivated markerless mutants in BG11 liquid media as in 2.3.1 for consequent CO_2 response assays.

6803^{WT} and 6803^{K6A} growth curves were first compared. *Synechocystis* cell growth was analysed by reading the cell density at 730 nm. Under 30 µmol/m^2/s of cool white-light conditions and 80 rpm mixing, the growth rate of 6803^{K6A} mutant cells was identical to that of the 6803^{WT} (Fig. 5.3**A**); the doubling time during logarithmic growth in both strains was approximately 10 h. This suggests that the Lys 6 mutation does not affect the growth and viability of *Synechocystis* cells under these conditions.

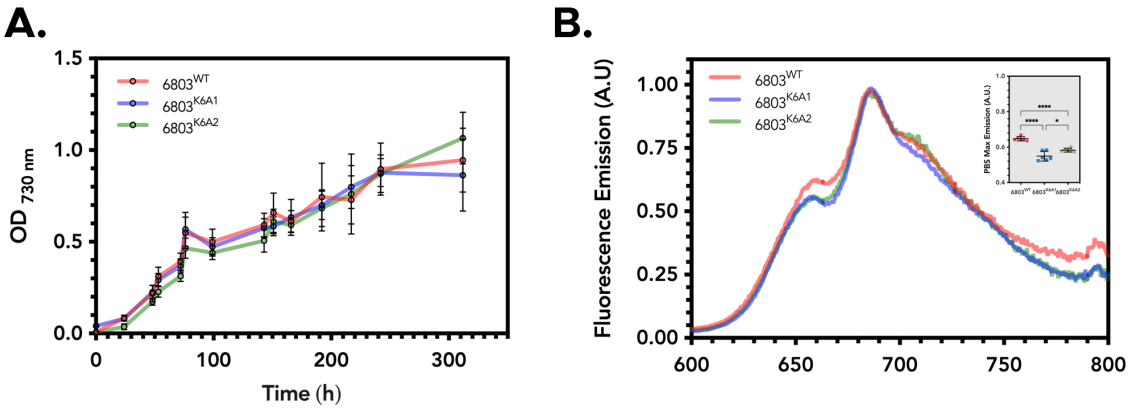

Fig. 5.3 Characterisation of *Synechcoystis* 6803^{K6A} mutant cells. **A.** 6803^{WT} and 6803^{K6A} growth in BG11 at pH 8.0. **B.** Fluorescence profile of 6803^{WT} and 6803^{K6A} cells obtained from the exponential growth phase.

Three growth phases were identified for both strains, the exponential phase, a linear phase and the stationary phase. These phases have been previously reported for *Synechocystis*, where a gradual shift was found in the energy transfer of light-harvesting phycobilisomes to photosystems, as well as a marked change in the redox state of the plastoquinone pool between different growth phases. However, the observed transition from exponential to linear growth is caused solely by light limitation, while a transition to the stationary phase is caused by nutrient limitation [82]. Moreover, according to Schuurmans *et al.*, growth phases are defined only by shape, and cell density at which the transitions occur varies depending on the path length of the light through the culture and incident illumination intensity.

To understand the effect of ApcA Lys 6 carbamylation on PBS energy transfer, we sought to compare allophycocyanin emission maxima at 660 nm. We asked whether CO_2/HCO_3- could enhance EET in the context of the whole organism. Therefore, we cultivated 6803^{WT} and 6803^{K6A} at 30°C under 30 µmol/m^2/s constant illumination. Cells for fluorescence measurements were obtained by taking samples directly from the culture at the exponential growth phase. The cells were incubated in the dark for 15 min at room temperature to eliminate the possible effects of state transition. Chla and PBS were excited at 485 nm, and fluorescence emission was detected from 600 to 800 nm with a Fluorolog3 fluorometer.

Two independent 6803^{K6A} mutants were compared to 6803^{WT} (Fig. 5.3**B**). PBS emission at 660 nm was normalised to Chla fluorescence emission at 688 nm, emission from the reaction centre P680. 6803^{WT} showed a relative PBS intensity of almost 20% higher than 6803^{K6A} when incubated with 50 mM total inorganic carbon. Thus, ApcA K6 carbamate formation has an apparent analogous impact on PBS energy transfer as previously detected *in vitro*. We next sought to investigate the role of Lys 6 carbamylation on absolute energy transfer efficiency in the cells.

5.3.2 *Synechocystis* fluorescence response to CO_2

PBS reaction to the absence of CO_2

The fluorescence response of Lys 6 carbamylation to CO_2 was demonstrated *in vitro* in Chapter 3. If CO_2 increases PBSs fluorescence *in vivo*, then CO_2 depletion would negatively affect PBSs energy transfer. Therefore, we measured QY of *Synechocystis* cells to investigate overall APC energetic activity *in vivo* without CO_2.

We, therefore, depleted 6803^{WT} and 6803^{K6A} cells of inorganic carbon under cool white light, and measured the absolute QY when exciting Chla and PBSs at 485 nm (Fig. 5.4). A Clark-type electrode was used to confirm the absence of CO_2 in culture samples.

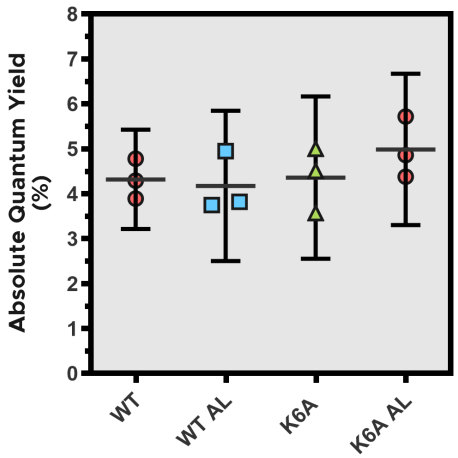

Fig. 5.4 Quantum yield of CO_2 depleted 6803^{WT} and 6803^{K6A} cells. AL: After carbon depletion with light. No statistical difference was found from an Ordinary one-way ANOVA, n=3, mean with 95% CI shown.

For this experiment, QY was first measured with a neutral-density filter like how isolated PBPs were analysed *in vitro*. The limitations of low signal detection due to the amount of fluorescence intensity detected from Chla and PBSs excess emission showed considerable variability in QY readings. We did not observe a difference in QYs after CO_2 depletion (AL)(Fig. 5.6). QY between 6803^{WT} and 6803^{K6A} were not different, oscillating between 4% and 5%.

In vivo QY measurements are typically an order of magnitude lower than for the isolated recombinant proteins. This is due to efficient EET from the PBS to PSII via the terminal pigment. Therefore, the observed QY *in vivo* reflects energy lost from the PBS that is not transmitted to PSII.

We subsequently examined the PBS fluorescence spectra in the absence of CO_2. 6803^{WT} and 6803^{K6A} cells were exposed to cool white light similarly to QY assays for CO_2 depletion. Cells were incubated in the dark for 15 minutes, and fluorescence emission was detected from 600 to 800 nm (λ_{ex}=485 nm). The obtained PBS emission at 660 nm was normalised to Chla emission at 690 nm to compare 6803^{WT} and 6803^{K6A} PBS response to CO_2 depletion. We observed a difference between cells directly taken from the culture (presumably with CO_2) and cells exposed to white light (without CO_2) in both strains (Fig. 5.5**A)**.

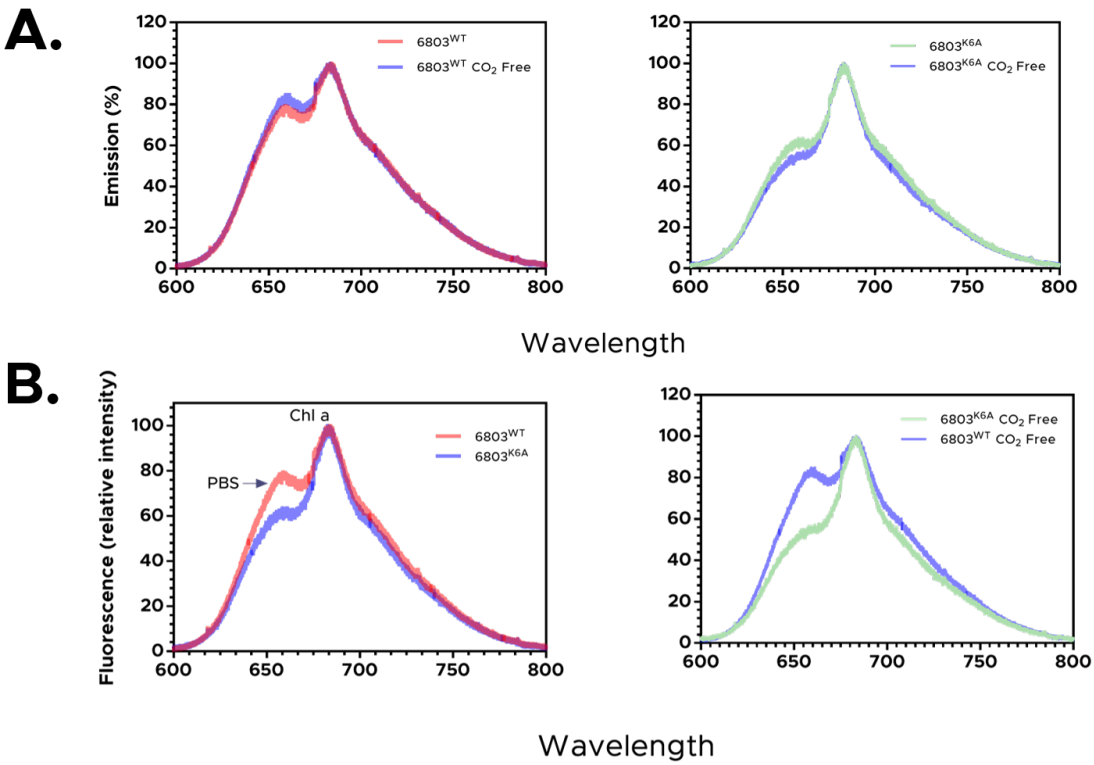

Fig. 5.5 Fluorescence emission of 6803^{WT} and 6803^{K6A} cells mainly exciting PBSs (λ_{ex}=485 nm). Cells were collected from the linear growht phase. **A.** Fluorescence comparison of PBS emission at 660 nm normalised to P680 (PSII chlorophyll pair) emission at 690 nm in the presence and absence of CO_2. Fluorescence comparison of 6803^{WT} cells is shown on the left and 6803^{K6A} cells fluorescence comparison on the right graph. **B.** Fluorescence comparison of 6803^{WT} and 6803^{K6A} with CO_2 (Left) and without CO_2 (Right).

For comparative purposes, 6803^{WT} and 6803^{K6A} were plotted in the same graph (Fig. 5.5**B**). The PBS fluorescence intensity normalised to Chla emission of 6803^{WT} showed to be 20% higher than 6803^{K6A} PBS relative emission (Left graph Fig. 5.5), similarly to the response previously reported from the fluorescence characterisation of 6803^{WT} and 6803^{K6A} cells from the exponential growth phase (Fig. 5.3**B**).
The relative emission of CO_2 depleted cells was evaluated (Right graph Fig. 5.5**B**). 6803^{WT} CO_2 free showed an increased emission of almost 30% higher than 6803^{K6A} under the same conditions.

Fluorescence spectra of 6803^{WT} suggested that PBS emission at 660 nm is affected by the absence of CO_2.

In vivo Absolute Quantum Yields

To address limitations on low detection of fluorescence intensity in QY measurements, a neutral-density filter with an OD of 1.8 was used to detect higher signals of *Synechocystis* cells fluorescence emission. This optical filter allowed the Fluorolog-3 detector to increase excitation power to achieve a sufficient signal-to-noise ratio when measuring 6803^{WT} and 6803^{K6A} cell QY using the HORIBA Fluorolog integrated sphere.

For this assay, cells were sampled at different growth stages: linear phase (4-9 days of growth) (Fig. 5.6**A**) and stationary phase (10 days of growth) (Fig. 5.6**B**). Cells were CO_2 depleted under cool white light and QY was measured after the addition of either NaCl or $NaHCO_3$. We observed a small significant enhancement of QY for 6803^{WT} cells, but not for 6803^{K6A} cells after the introduction of CO_2/HCO_3^- from samples taken at the stationary phase (Fig. 5.6). Similar changes in photophysiology have been observed in the transition of growth phases, and they appear to rely on the antennae adaptation to photosystem connectivity [82]. The ApcA response to CO_2 dependent on Lys 6 may indicate part of that adaptation.

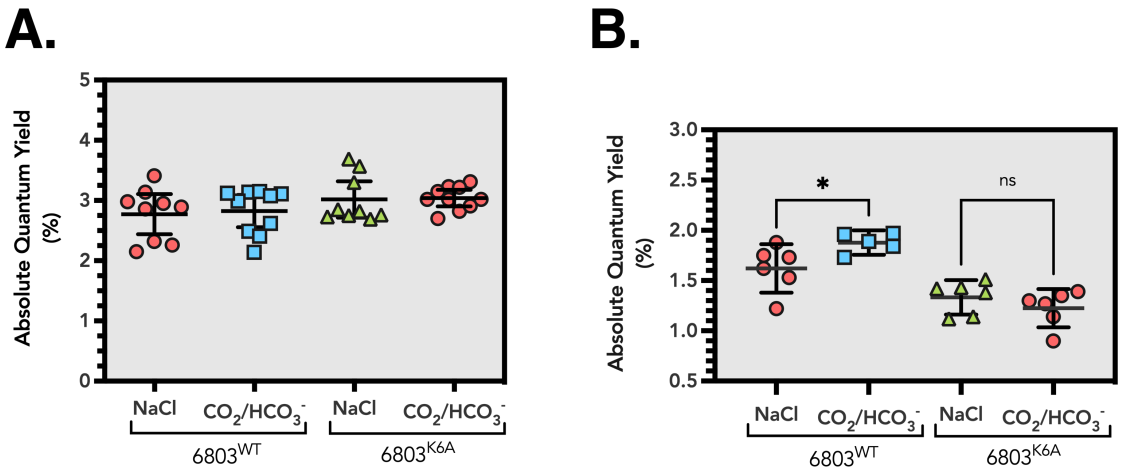

Fig. 5.6 ApcAB *in vivo* quantum yield. The measured quantum yield with 1 mM $NaHCO_3$ (CO_2/HCO_3^-) and NaCl for 6803^{WT} and 6803^{K6A} cells collected from the exponential phase (**A**) and late exponential/stationary phase (**B**) (*q = 0.0058, one-way ANOVA with post hoc two-stage linear set-up procedure of Benjamini, Krieger and Yekutieli, n = 5-6 independent replicates, t = 2.382, df = 19, nd = no discovery, ±95% C.I.)..

O_2 generation by phototrophic organisms is part of the light-dependent reactions of photosynthesis. In cyanobacteria and the chloroplasts of green algae and plants, the energy of light is used to split a water molecule through a reaction catalysed by a manganese-containing cofactor found in photosystem II. Water is split into its protons and electrons for photosynthesis, where O_2 is generated. Therefore, if the reported rise in QY is induced by ApcA carbamylation *in vivo*, would increased EET to PSII activity be evident in photosynthetic O_2 generation?

5.4 CO_2 carbamylation in photosynthetic O_2 evolution

O_2 evolution of 6803^{WT} and 6803^{K6A} cells was measured under different light conditions by exciting cells under cool white light. O_2 evolution was first tested under a low and a high range of light intensity. Cells were taken from the linear phase and washed to resuspend in fresh BG11 media without dissolved CO_2. Cells with a Chla concentration of 5 µg/ml were incubated in the dark for 15 min and then transferred to a Clark-type electrode at 25°C. A final concentration of 25 mM of $NaHCO_3$ was added, and the light was immediately turned on. O_2 rates were calculated as discussed in 2.4.6.

For the low light assay, 6803^{WT} and 6803^{K6A} cell O_2 evolution rates were tested from 0 to 25 µmol/m^2/s photon flux rates (Fig. 5.7**A**), and the range from 50 to 400 µmol/m^2/s was considered for high concentrations of light (Fig. 5.7**B**). No statistical difference was found between 6803^{WT} and 6803^{K6A} O_2 evolution rates (Ordinary one-way ANOVA, Šidák corrected multiple comparisons, p>0.05, n=6).

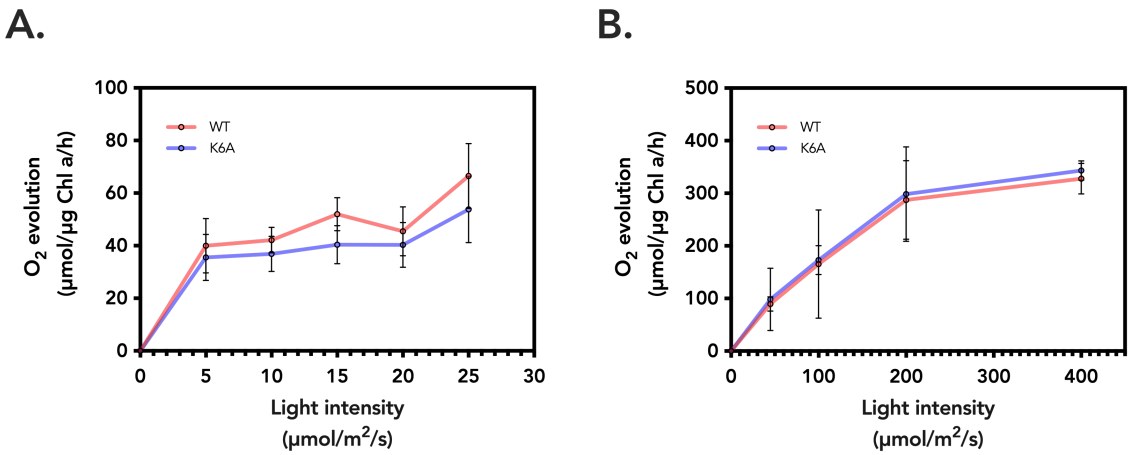

Fig. 5.7 Photosynthetic oxygen evolution of 6803^{WT} and 6803^{K6A} mutant under indicated light intensities. The culture samples collected from the linear phase were adjusted to a cell density containing 5µg chlorophyll mL^{-1} and tested in the presence of 50 mM $NaHCO_3$ in BG11 media. **A.** O_2 evolution rates under low range of light intensity. **B.** O_2 evolution rates under high range of light intensity.

The photosynthetic O_2 evolution assay was next repeated, comparing 6803^{WT} and two additional independently transformed 6803^{K6A} mutants. Cells were obtained from the linear

growth phase and prepared similarly to the description above. Both independently transformed mutants, 6803^{K6A1} and 6803^{K6A2}, showed identical growth rates to 6803^{WT} (Fig. 5.8**A**).

Photosynthetic O_2 evolution rates under low light (5 µmol/m^2/s) and 20 mM $NaHCO_3$ between 6803^{WT} and mutants were similar. However, under 35 and 50 µmol/m^2/s of light illumination 6803^{K6A} mutants showed slightly reduced respiration activity, as observed in Fig. 5.8**B-C**. Still, with white light excitation on all pigments occur at the same time, so the reaction centre could be excited directly instead of getting energy from the peripheral antenna systems. The apparent difference observed in this experiment must be due to something other than an impact on the EET. Repeated experiments with filtered light directing excitation to APC could assist this effect.

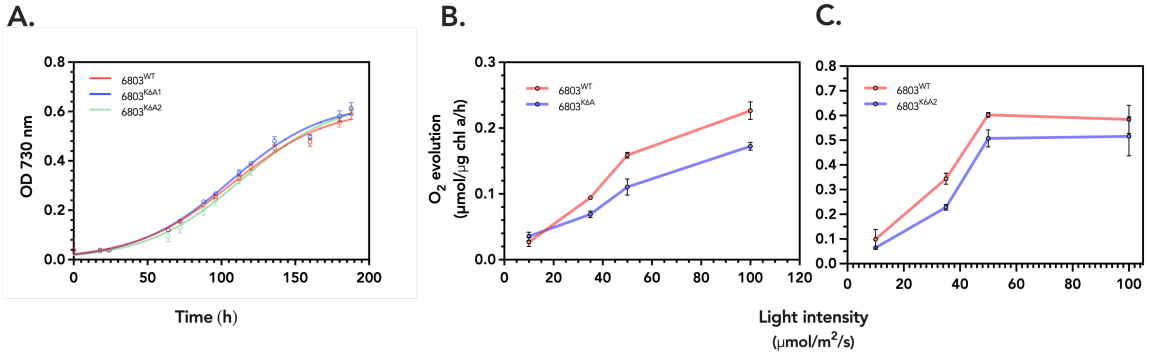

Fig. 5.8 Photosynthetic O_2 evolution of 6803^{WT} and two independent 6803^{K6A} mutants. The culture samples were collected from the linear growth phase. Cell density was adjusted to 5µg chlorophyll mL^{-1} and tested in the presence of 20 mM $NaHCO_3$ in BG11 media. **A.** Growth curves of 6803^{WT} and 6803^{K6A} demonstrating identical phases of independently transformed mutants. **B-C.** O_2-evolving activity of 6803^{WT} and two independent 6803^{K6A} mutants. 95% CI were estimated from three independent measurements. Ordinary one-way ANOVA with Šidák corrected multiple comparisons showed a significant difference between 6803^{WT} and 6803^{K6A} O_2 rates under 35 and 50 µmol/m^2/s of light intensity, n=3, $p<0.05$.

ApcA K6 carbamate effect could be altered by different CO_2 concentrations. Therefore, the photosynthetic behaviour with different concentrations of CO_2/HCO_3^- was tested. Cells were collected from the linear growth phase, resuspended in CO_2-free BG11 media and incubated in the dark for 15 minutes. Cells were transferred to a Clark-type electrode under 200 µmol/m^2/s of white light illumination and O_2 evolution was tested with different CO_2/HCO_3^- concentrations (Fig. 5.9). No difference was observed in O_2 evolution rates between 6803^{WT} and 6803^{K6A}

under any concentration of CO_2/HCO_3^-. However, due to time restrictions arising from the COVID-19 pandemic, the presented assay could not be replicated. Thus, it is suggested that further investigation is needed to confirm this preliminary results of CO_2 effect on 6803^{WT} and 6803^{K6A}.

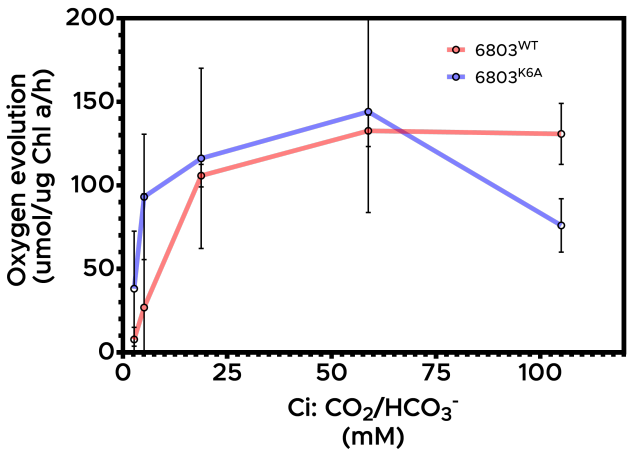

Fig. 5.9 Oxygen evolution of 6803^{WT} and 6803^{K6A} under different inorganic carbon concentrations (Ci:CO_2/HCO_3^-). 95% CI were estimated from three independent measurements. Ordinary one-way ANOVA with Šidák corrected multiple comparisons showed no statistical significant difference.

Our O_2 evolution experiments do not provide conclusive evidence for the extent of carbamylation involvement in oxygenic photosynthesis. Instrument limitations presented at this stage of the study did not allow us to replicate the experiment. Further investigation on PSII-derived physiological state of cells is suggested.

5.5 *Synechocystis* ApcA K6E mutant response to CO_2

We next examined a *Synechocystis* ApcA K6E mutant (6803^{K6E}) to elucidate the effect of an introduced negative charge at Lys 6 to mimic a carbamate at 100% occupancy albeit lacking one methyl group. Unfortunately, due to time constraints and pandemic limitations in the last year of this project, photosynthetic O_2 evolution could not be explored. However, fluorescence spectroscopy analysis was analysed.

5.5.1 Fluorescence characterisation

A K6E mutation was introduced into *Synechocystis* sp. PCC 6803 as discussed in section 5.2. Due to time constraints at this project stage, I first decided to evaluate the obtained 6803^{K6E} mutant containing the pSL2680 plasmid with Km resistance. This allowed performing experiments while curing of the 6803^{K6E} mutant from the plasmid was ongoing.

Therefore, 6803^{K6A} and 6803^{K6E} were grown in BG11 media with antibiotic (Km) under 30 µmol/m^2/s of cool white-light at 30°C. Cells were collected from the mid-linear phase, centrifuged and resuspended in degassed BG11 media. To evaluate fluorescence emission 6803^{K6E} response, a final concentration of 20 mM $NaHCO_3$ was added to cells, and fluorescence emission was detected from 600 to 800 nm (λ_{ex}=485 nm). PBS fluorescence spectra was normalised to the maximum emission of Chla at 690 nm to compare PBS maximum emission at 658 nm similar to previously compared with 6803^{K6A}.

Under these conditions, 6803^{K6E} mutant cells showed a significant 20% increase in PBSs peak emission detected at 658 nm compared to 6803^{WT} and 6803^{K6A} PBS emission (Fig. 5.10). However, a difference between 6803^{WT} and 6803^{K6A} was not observed (red and purple spectra at Fig. 5.10). This suggests that a permanent negative charge on the ApcA Lys 6 enhances fluorescence emission.

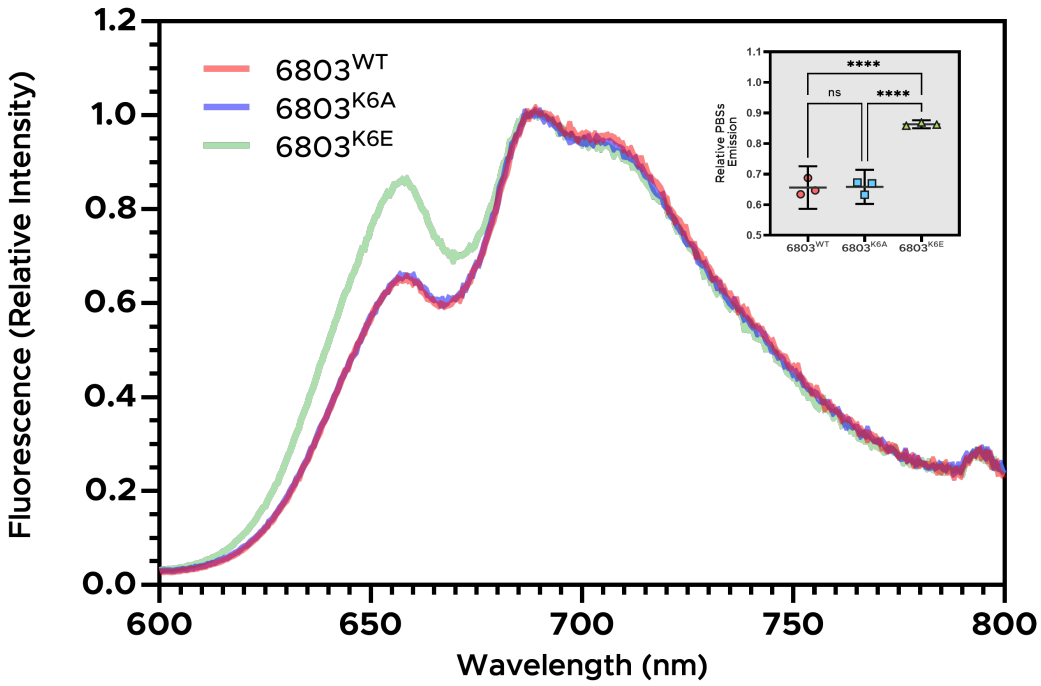

Fig. 5.10 Relative PBS fluorescence emission at 660 nm of 6803^{WT}, 6803^{K6A} and 6803^{K6E}. Inset graph show values of PBS relative emission at 658 nm (Ordinary one-way ANOVA, Šidák multiple comparison test, ****p<0.0001, ns=not significant, n=3, mean with 95% CI shown).

The fluorescence lifetime is a characteristic of fluorescent probes widely employed in research on biomolecules to study their microenvironment and molecular interactions. The average time refers to the amount of time a molecule spends in its excited state before returning to its ground state. A fluorophore can change conformation over its lifetime in the excited state and interact with other molecules, and rotate or diffuse through the local environment, which can lead to a quenching of the fluorescence. Therefore, it was hypothesized that the demonstrated effect of the anionic charge induced by ApcA carbamate formation would be detected on PBS fluorescence lifetimes *in vivo*.

5.5.2 *In vivo* fluorescence lifetimes CO_2 response

By this stage of the study, a markerless 6803^{K6E} mutant was obtained. To elucidate if the detected carbamylation effect in APC is involved in chromophores excited state, we, therefore, tested *in vivo* PBSs fluorescence lifetimes of 6803^{WT} and markerless mutants in the presence and absence of inorganic carbon. The use of the fluorescence lifetime is advantageous because it is not affected by the dilution of the probe volume or different cell density.

6803^{WT}, 6803^{K6A} and 6803^{K6E} markerless cells were collected from the linear growth phase and resuspended with BG11 media free of dissolved CO_2. Cells were incubated under cool white light to deplete CO_2 remaining in the cells and fluorescence decays were measured after the addition of either 1 mM NaCl or $NaHCO_3$. Fluorescence lifetimes were collected with a HORIBA Scientific Deltaflex TCSPC spectrometer exciting samples with a DD-635L laser (λ_{ex}=635 nm). The data was analysed using a reconvolution analysis using the DAS6 analysis software. From the analysis of the 10 000 counts acquired for 10 ns, the average lifetime was obtained. This was returned using a bi-exponential decay model, and an average lifetime was obtained. The average fluorescence lifetimes were compared since this would be a reflection of the fluorescence QYs. Representative fluorescence decays, from 6803^{WT}, 6803^{K6A} and 6803^{K6E}, showing short and longer average lifetimes are presented in Fig. 5.11.

Fluorescence lifetimes were detected at two different wavelengths: 660 and 690 nm. If CO_2 enhances PBS fluorescence emission, the outcome on lifetimes would be only detected at decays from PBS emission at 660 nm and not from Chla emission at 690 nm. Therefore, cells were excited at 635 nm, closer to APCs maximum absorption at 650 nm than the 620 nm shoulder peak; far from Chla excitation at 435 nm. *Synechocystis* fluorescence lifetimes with or without CO_2/HCO_3^- did not show a noticeable change in any of the strains detected at 660 nm(Table 5.1) nor at 690 nm detection (Table 5.2). This could be due to concentrations of inorganic carbon used for this *in vivo* assay. 1 mM of $NaHCO_3$ corresponds to 19 µM CO_2 in a pH 8 solution, and as fluorescence decays were measured within seconds, it is possible that carbamate formation had not occurred. The average lifetimes obtained matches the steady state spectra in Fig. 5.10 as the integrated fluorescence there for 6803^{K6E} is larger. Nevertheless, we observed a clear increase in the average decay time in 6803^{K6E} when compared to wild-type and 6803^{K6A}, which indicates the spectroscopic effect of a permanent negative charge on ApcA Lys 6.

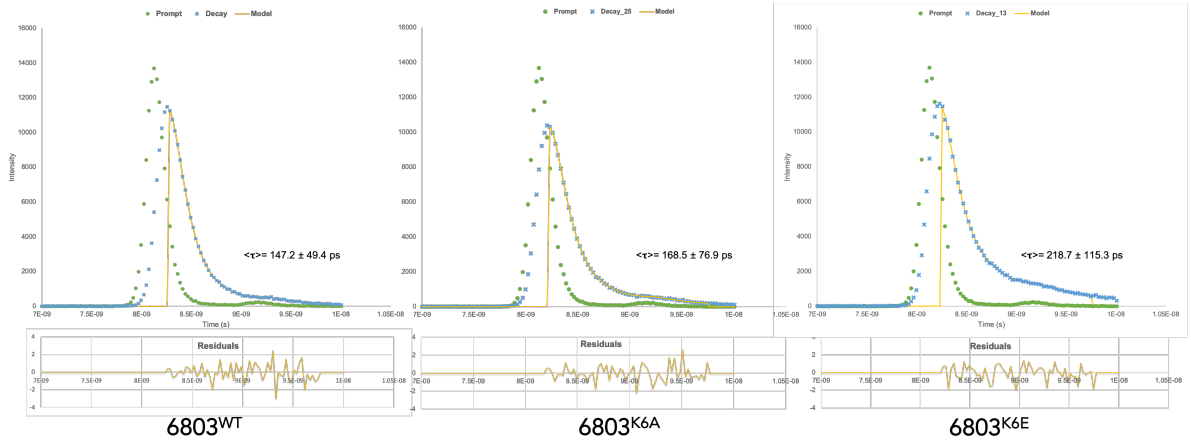

Fig. 5.11 Representative fluorescence decay of 6803^{WT}, 6803^{K6A} and 6803^{K6E}. Cells were excited with a 635 nm laser and decays detected at 660 nm. Green dots represent instrument response, blue dots represent cells decay detection, yellow line represent a bi-exponential model fitting for each decay. Residuals are shown at the bottom of each corresponding decay.

Table 5.1 Representative fluorescence lifetimes of 6803^{WT}, 6803^{K6A} and 6803^{K6E} detected at 660 nm. $\lambda_{\mathrm{ex}} = 635nm$. Mean $\pm$ SD of components obtained from a bi-exponential fit.

	$\tau_1(ps)$	Relative Amplitude (%)	$\tau_2(ps)$	Relative Amplitude (%)	$<\tau>(ps)$	Chi-squared
$6803^{\mathrm{WT+Na}}$	128 ± 21	69%	313 ± 33	31%	157 ± 39	1.12
$6803^{\mathrm{WT+Ci}}$	133 ± 20	70%	349 ± 38	30%	164 ± 43	1.12
$6803^{\mathrm{K6A+Na}}$	142 ± 20	60%	434 ± 39	40%	194 ± 44	1.00
$6803^{\mathrm{K6A+Ci}}$	150 ± 22	75%	479 ± 95	25%	181 ± 98	1.20
$6803^{\mathrm{K6E+Na}}$	154 ± 24	56%	606 ± 81	44%	230 ± 85	1.16
$6803^{\mathrm{K6E+Ci}}$	161 ± 36	52%	560 ± 83	48%	245 ± 90	1.17

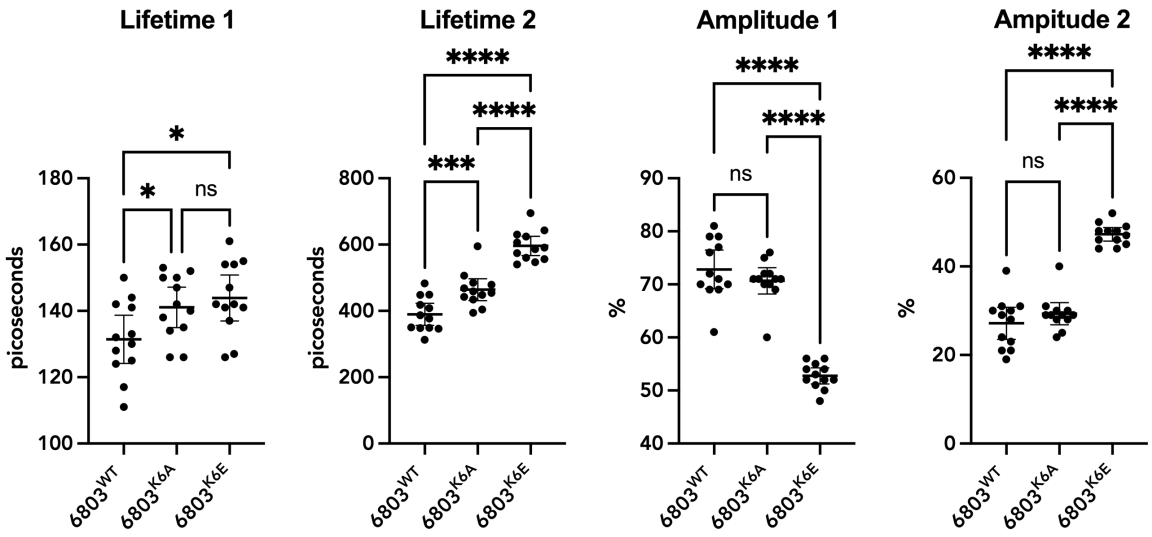

Fig. 5.12 Fluorescence lifetimes and corresponding amplitudes of 6803^{WT}, 6803^{K6A} and 6803^{K6E} cells detected at 660 nm. (One-way ANOVA with post hoc two-stage linear set-up procedure of Benjamini, Krieger and Yekutieli, n = 12 independent replicates, *= p<0.05, **= p<0.002, ***=p<0.0002, ****=p<0.0001, ns = no significant, ±95% CI.)

A significant difference in PBSs lifetimes and their respective amplitudes measured at 660 nm were observed between 6803^{WT} and 6803 mutants (Fig. 5.12). We observed no difference in the shorter lifetime (τ_1) between 6803^{K6A} and 6803^{K6E} with 141.1 and 143.9 ps lifetime values, respectively. However, both mutant τ_1 lifetimes were different to 6803^{WT} of 131.4 ps. Regarding the longer lifetimes (τ_2), a greater difference was observed between the three strains; 389.7 ps for 6803^{WT}, 464 ps for 6803^{K6A} and 596 ps for 6803^{K6E}. Interestingly, amplitudes detected at 660 nm changed drastically on 6803^{K6E} compared to 6803^{WT}. 6803^{K6A} showed similar amplitudes to 6803^{WT}, being 70% and 30% for the shorter and longer lifetimes. In contrast, 6803^{K6E} showed distinct from the 6803^{WT} and 6803^{K6A} with a 50% and 50% distribution of lifetimes. Average lifetimes were different between the three strains; 6803^{K6E} showed a higher average lifetime of 230 ps, almost double of 165 ps from 6803^{WT} (Fig. 5.11).

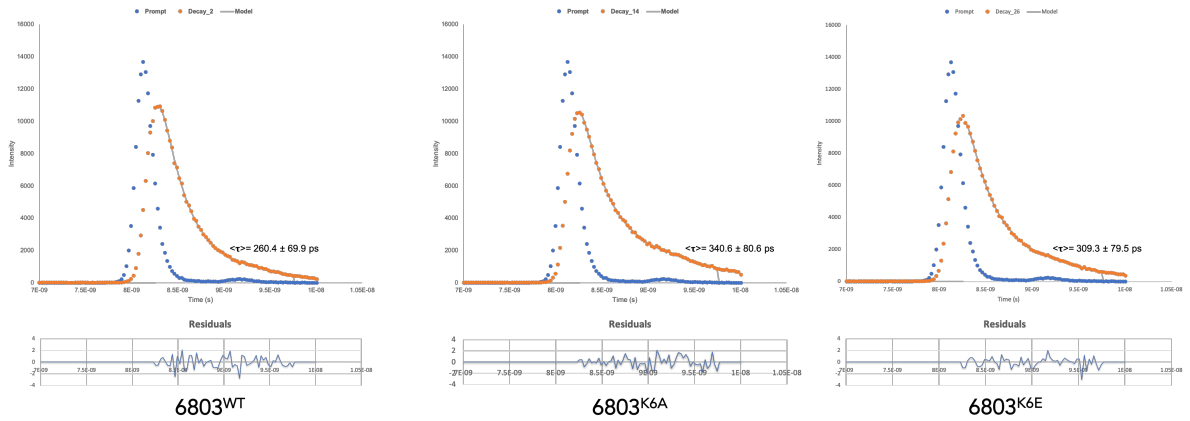

Fig. 5.13 Representative fluorescence decays of 6803^{WT}, 6803^{K6A} and 6803^{K6E} cells detected at 690 nm. Cells were excited with a 635 nm laser. Blue dots represent instrument response, orange dots represent cells decay detection, gray line represent a bi-exponential model fitting for each decay. Residuals are shown at the bottom of each corresponding decay.

Table 5.2 Representative fluorescence lifetimes of 6803^{WT}, 6803^{K6A} and 6803^{K6E} detected at 690 nm. $\lambda_{ex} = 635nm$. Mean ± SD of components obtained from a bi-exponential fit.

	$\tau_1(ps)$	Relative Amplitude (%)	$\tau_2(ps)$	Relative Amplitude (%)	$<\tau>(ps)$	Chi-squared
6803^{WT+Na}	189 ± 45	55%	477 ± 59	45%	259 ± 74	0.92
6803^{WT+Ci}	190 ± 57	52%	437 ± 54	48%	261 ± 79	1.17
6803^{K6A+Na}	163 ± 52	39%	468 ± 41	61%	271 ± 66	1.12
6803^{K6A+Ci}	196 ± 58	40%	574 ± 66	60%	326 ± 88	1.09
6803^{K6E+Na}	165 ± 44	36%	527 ± 46	64%	295 ± 64	1.07
6803^{K6E+Ci}	191 ± 72	26%	608 ± 62	74%	387 ± 95	1.04

For fluorescence lifetimes detection at 690 nm, parameters mainly from Chla emission were obtained from a bi-exponential fit (Table 5.2). The presence of CO_2/HCO_3^- did not affect on fluorescence lifetimes or their respective amplitudes detected at 690 nm in any of the strains. However, average lifetimes showed to be significantly different between 6803^{WT}, 6803^{K6A} and 6803^{K6E}, exhibiting average lifetimes of 277, 310 and 343 ps, respectively (Fig. 5.13) (Ordinary one-way ANOVA, Šidák corrected multiple comparisons, n=6, p<0.05). No statistical difference was found between 6803^{WT} τ_1 and mutants τ_1, presenting an averaged τ_1 ≈170 ps. A comparable lifetime of 245 ps has been previously assigned to APC_{680}-PBS terminal pigments and CP47 in PSII, which are spectrally all very close and both emitting at ≈685 nm

[18]. In contrast, 6803^{WT} τ_2 of 477 ps was different from both mutants, 546 ps from 6803^{K6A} and 595 ps from 6803^{K6E}. Furthermore, amplitudes of τ_1 and τ_2 were found to be different only between 6803^{WT} and 6803^{K6E}. 6803^{WT} showed a 41%-59% distribution of amplitudes whereas 6803^{K6E} showed 28% and 78% (Table 5.2). Lifetimes obtained from 690 nm detection ($\approx$170 and $\approx$500 ps) can be attributable to Chla-binding PS core complexes, which have been previously identified from *Synechocystis* decays associated spectra (DAS) [77].

On the whole, 6803^{K6E} mutation demonstrated an effect not only on PBS excitation states but also in PSII. The influence of the negatively charged modification on ApcA may promote an efficient EET from PBS-Chla to PSII as previously observed in 6803^{K6E} cells steady-state fluorescence spectra.

5.6 Conclusions

This Chapter demonstrated the effect of CO_2 in *Synechocystis* sp PCC 6803 PBS energy transfer. The carbamate formation at ApcA K6 suggests having an effect on EET in whole cells. CO_2 enhances QY of 6803^{WT} cells from the late exponential phase, which PBS mediates. This effect is consistent with differences in *Synechocystis* photosynthetic O_2 evolution rates between 6803^{WT} and a 6803^{K6A} mutant. However, more tests are needed to relate this effect to Lys 6 carbamylation.

The reproduction of full carbamylated occupancy of APC (6803^{K6E}) demonstrated the role of CO_2 PTM *in vivo*. It was demonstrated that *Synechocystis* fluorescence lifetimes are affected by Lys 6 single-site mutation. K6E mutation introduced an increase of $\approx$100 ps in the longer lifetime associated with APC emission. The impact of full carbamate occupancy is also reflected with an even distribution of relative amplitudes of APC lifetimes, different to wild-type *Synechocystis* and K6A mutant cells. Based on the detection of fluorescence lifetimes at 690, it was demonstrated that the anionic charge of a modified lysine alters Chla lifetimes and the relative amplitudes. This effect suggests that the APC Lys charge has an important role in energetic interactions involving Chla and PSII, promoted by the anionic state of APC K6 carbamylation. The results demonstrated in this chapter further encourages the investigation of molecular dynamics of carbamate formation in APC energy transfer. It has been shown that CO_2 PTM has an important role in cyanobacteria photophysiology.

Chapter 6

Discussion

6.1 Introduction

CO_2 is a gas of significant concern as it has a significantly greater warming effect than all other gases in the Earth's atmosphere combined. As atmospheric CO_2 concentrations continue to rise, carbon capture and utilization methods to reduce CO_2 emissions and fossil fuel usage are being developed. The use of cyanobacteria as bio-refineries has been proposed for recycling CO_2 directly into fuels or chemicals using photosynthesis. Towards this goal, it is well known how cyanobacteria sense and store inorganic carbon. Nevertheless, protein-CO_2 interactions remain unexplored.

CO_2 interacts with the NH_2 group of dissociated amines, forming a carbamate bond. This can occur at either lysine side chains or the N-terminus of a protein. Until recently [48], the identification of carbamate sites was challenging due to the reversible nature of carbamate formation; incorporating a chemical labelling system and LC-MS/MS technology allowed Linthwaite *et al.* (2018) to develop a method to address those challenges. The TEO trapping method allows the ion-mediated trapping of carbamates on proteins by transferring an ethyl group to the anionic carbamate derived from CO_2 and protein primary amine. This thesis demonstrated the identification of a previously unknown photosynthetic carbamate site in *Synechocystis* and the physiological implications of the CO_2-mediated PTM. This chapter summarises the discovery of APC carbamylation and discusses the findings with currently available literature. From this study, questions arise regarding mechanisms by which CO_2

regulates ApcA energy transfer; suggestions to address this topic will be presented in this chapter.

6.2 Discovery of a cyanobacterial carbamylation site

This thesis followed Linthwaite *et al.* work on *A. thaliana* [48] carbamate trapping. Here, we demonstrated that TEO usage enables the identification of exchangeable CO_2-binding sites on *Synechocystis* protein lysate. ^{14}C radioactive labelling was a valuable technique to identify the presence and abundance of CO_2 bound protein from total protein lysate in *Synechocystis*. Protein carbamates in photosynthetic organisms have been previously observed in air-grown *Euglena gracilis* [96]. Nearly half of intracellular CO_2/HCO_3^- was found as protein carbamate in *Euglena* protein lysate using ^{14}C radioactive labelling. The identification of *Euglena* cell protein ^{13}C-carbamate was also demonstrated using $^{13}CO_2$ NMR. Radioactive techniques allow the identification of carbamate protein complexes present in an organism proteome as shown for the analysis of Hb [66]], class D β -lactamases [29][53] and RubisCO [55]. However, the limitations of these techniques lie in their inability to identify carbamate sites under relevant physiological conditions. Thus, the carbamate trapping mechanism used in this project reveals the advantages of carbamate site detection with TEO-trapping. MS/MS technology also allows spectra matching to an organism's proteome, identifying ethylated carbamates under relevant physiological conditions.

Chapter 3 details the identification of exchangeable CO_2-binding sites on *Synechocystis* ApcA by TEO-trapping and LC-MSMS analysis. Under physiologically relevant conditions, we first identified the Lys 6 carboxyethyl modification from a *Synechocystis* protein lysate screen. The natural occurrence of ApcA carbamylation was confirmed by the identification of carbamate formation on PBS isolated from *Synechocystis* and recombinant ApcA. CO_2 trapping of recombinant ApcA protein allowed an improvement in protein coverage and peptide MSMS spectra compared to native PBS trapping. The trapping of ApcAB with $^{13}CO_2$ labelling showed that carbamylation is caused by CO_2 being formed in solution under the experimental conditions. The specificity of Lys 6 as a CO_2 binding site was validated by ^{13}C NMR. ^{13}C NMR has been widely used to monitor the behaviour of Lys carbamates as a catalytically important residue [53]. A second carbamate site was identified in CpcA Lys 2. Nevertheless, further research is required to confirm CpcA carbamylation by ^{13}C-NMR detection.

The identification of carbamylation sites in cyanobacteria light-harvesting antennae indicates a unique role of CO_2/HCO_3^- in photosynthesis. HCO_3^- has been previously reported to facilitate proton transfer in PSII [87]. In oxygenic photosynthesis, bicarbonate acts as a ligand to the quinone–iron complex, where it stabilizes the QA–NHI–QB structure of the PSII RC, and thus allows efficient electron transport and protonation of QB. The importance of lysine carbamylation, in general, is becoming more widely recognized, and the number of proteins known to contain this post-translational modification is increasing. Carbamate identification is likely to lead to the elucidation of the essential role of CO_2/HCO_3^- in oxygenic photosynthetic organisms.

6.3 *In vitro* APC CO_2 response

This study demonstrated that the carbamylation of Lys 6 plays an important role within APC energy transfer. A Lys 6 privileged environment formed by the ApcA and ApcB subunit pockets in the monomeric and trimeric form suggests optimal conditions for carbamate formation as observed from the APC crystal structure For example, in APC trimers, Lys 6 is located at 2.8 nm from chromophore α-84 and chromophore β-84 in each monomer. A similar distance has been reported as the closest distance between chromophore pairs of adjacent monomers, α-84 and β-84. The short distance of 2.1 nm of this coupled pair allows the interaction across the monomer-monomer interfaces to produce the 650 nm absorption maximum and the 660 nm emission maximum of APC [57]. Therefore, a modification of the environment by CO_2 carbamylation at a similar distance between Lys 6 and chromophore pairs α-84 and β-84 can be expected to cause the increased energy transfer efficiency of APC observed in this project (Fig. 6.1).

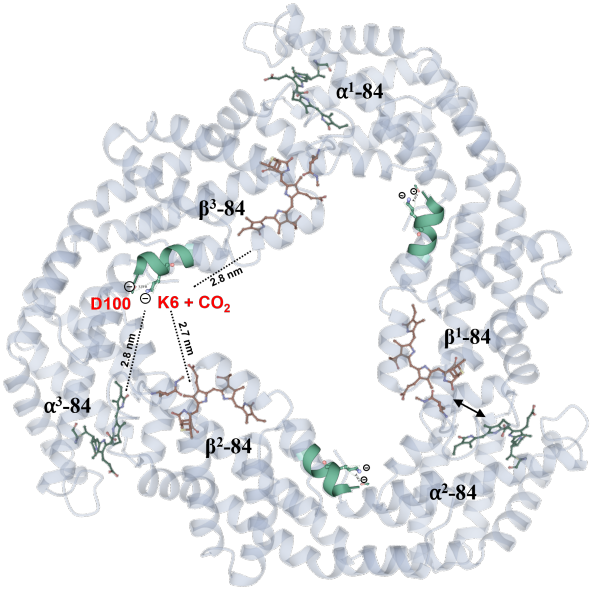

Fig. 6.1 Structure of the *Spirulina platensis* ApcAB $(\alpha\beta)_3$ trimer (PDB: 1ALL). Representative Lys 6 carbamate short-range interaction to each chromophore.

ApcAB EET enhanced by CO_2/HCO_3^- is based on carbamylation at K6. An analogous increase of ApcAB QYs was also observed in the ApcA subunit protein, although the increase was smaller. Different CO_2 responses between monomeric and trimeric states can be expected as the local environment of carbamate formation differs. Thus, the negative charge of a carbamate formed would have a different resonance with chromophore interactions depending on the APC conformation state. For example, in the case of the ApcA subunit, the carbamate would be interacting only with chromophore β-84. For monomers, Lys 6 carbamate would interact with β-84 and chromophore pair α84-β84. Most importantly in the native trimeric state, carbamate would interact with the three chromophore pairs ($\alpha^1$84-$\beta^3$84, $\alpha^3$84-$\beta^2$84, and $\alpha^2$84-$\beta^1$84) and individually with the three β84. The anionic charge of Lys 6 would change the local environment in APC which could also impact dipole-dipole interactions. Therefore, heterogeneity found in CO_2 response in this project at the different APC conformation states can be expected.

The ApcA K6A mutation does not alter trimeric APC fluorescence lifetimes. *In vitro* steady-state fluorescence lifetimes of APC were indistinguishable. The long lifetime of 1.9 ns is broadly similar to the previously reported 1.7 ns [75] attributed to APC monomer fluorescence

emission. On the other hand, the obtained shorter lifetime presented a relatively long decay of 300 ps compared to 95 ps reported by Ranjbar *et al*. Femtosecond experiments have identified even shorter ultrafast APC lifetimes of 430 fs [84]. In addition, *in vitro* studies of Ying *et al*. reported 1.51 ns and 0.63 ns lifetimes of a cross-linked APC. Therefore, the fluorescence decays of recombinant proteins obtained in this study could be attributed to conformational changes from a His-tagged APC trimer. The predominant amplitude of 96% of the long decay detected at 660 nm in this study indicates the detection of fluorescence emission from the APC monomer with an individual fluorescence at 650 nm [54]. However, the dynamic equilibrium between the monomeric and trimeric forms may also lead to the observed heterogeneity in APC solutions.

ApcA Lys 6 is surrounded by hydrophilic amino acids such as Asp 99 and Thr 101, indicating that it is located in a highly hydrophilic microenvironment favouring short-range interactions (Fig. 6.1). The negative charge imposed by CO_2 in APC trimers is likely to be involved in the short-range interactions of the closest chromophores. Based on our results, in a CO_2 depleted system, QYs of $ApcAB^{K6E}$ are higher than $ApcAB^{K6A}$ and $ApcAB^{WT}$. The negative charge provided by the K6E mutation demonstrates the effect of enhanced energy transfer by a permanent negative charge induced by carbamylation in APC.

Modifications in electronic coupling induced by the negative charge of an aspartate residue near PCBs have been previously reported in computational studies [78]. In the presence of the aspartate residue in the $PCBH^{+}$, the electronic couplings exhibited almost two-fold decrease, especially for the α^2-84 $\rightarrow$ β^1-84 and α^1-84 $\rightarrow$ β^3-84 EET pathways. Likewise, single-molecule experiments have shown that the broad distribution of APC lifetimes can be attributed to the formation of transitory and long-lived radical cation traps [95]. For example, if a β-84 forms a radical cation trap, it can quench the emission from adjacent pairs more efficiently than an α-84 trap because of β-84's vicinity to the pair. Therefore, the magnitudes of transition dipole moments and electronic coupling could be influenced by both short and long-range interactions between chromophores and the environmental protein moieties.

Here we propose that carbamylation of Lys 6 is stabilized and conserved in the APC monomer interface. The short-range interactions of the predominant negative charge of the carbamylated lysine, based on $ApcAB^{K6E}$ mutant response to CO_2, causes conformational changes in the protein to make energy transfer more efficient *in vitro*. Further experiments are required to evaluate the possibility of CO_2 involvement in chromophore interactions.

6.4 The Influence of ApcA carbamylation on *Synechocystis* sp PCC 6803 *in vivo*

Evidence demonstrating the effect of ApcA Lys 6 carbamylation on energy transfer was obtained *in vitro* (Chapter 4) and *in vivo* (Chapter 5). We generated markerless mutants ApcA K6A and K6E via CRISPR-cpf1. Obtaining mutants with the pSL2680 CRISPR-based system provided a practical and accurate directed method. Nevertheless, compared to *E. coli* or yeast, the growth rates of this commonly used cyanobacterial model strain were significantly slower, requiring extended time frames (weeks to months) to accomplish genome editing. Since *Synechocystis* contain multiple chromosome copies per cell, segregation of point mutation required several rounds of segregation to guarantee complete chromosome mutations and additional weeks for curing plasmid without antibiotics. This study demonstrated that the CRISPR-based pSL2680 system could create markerless knockouts with advantages over conventional strategies.

Synechocystis single-site mutation editing did not perturb growth rates. As carbamylation of Lys 6 is demonstrated to affect PBSs energy efficiency (Chapter 4), we initially expected to identify an escalated effect on growth in the wild type strain, which was not detected in this study. Under the same culture conditions of growth, 6803^{WT} and 6803^{K6A} cell growth rates were identical. However, 6803^{WT} relative ratio of PBS and Chla fluorescence intensities ($\lambda_{ex} = 485nm$) was higher than 6803^{K6A}. The Chla fluorescence peak was always higher than PBS in *Synechocystis* cells, which indicates an efficient energy transfer from phycobilisomes to Chla. Hence, PBSs are likely to be fully coupled to PSII, and the increased PBS emission observed in 6803^{WT} is induced by ApcA Lys 6 carbamylation. The last was demonstrated by the enhancement in 6803^{WT} QY only when CO_2 is present.

6803^{WT} QY response to CO_2 was only observed from cells obtained from the stationary phase. This is not the first time when photophysiology differences between growth phases have been reported. Schuurmans *et al.* identified that despite the ratio between PC and APC fluorescence remaining stable (PC/APC ratio) across the different growth phases, energy transfer from the PBS to the two photosystems in the linear and stationary growth phases are higher. They analysed *Synechocystis* sp PCC 6803 77K fluorescence emission and observed increased energy transfer from these antennae to the two photosystems as cell density increased [82]. Therefore, a particular ApcA CO_2 response at the stationary phase could imply an approach to the adaptation of the antennae to photosystem connectivity. However, more investigations

evaluating this hypothesis on different growth conditions would be required to attribute APC CO_2 QY to a specific growth phase response.

From O_2 evolution rates tested in this study, an apparent EET effect on PSII activity was only observed in wild-type *Synechocystis*. However, we cannot provide conclusive evidence from our experiments. Further investigation testing specific APC excitation with filtered light could relate to Lys 6 carbamylation effect on oxygenic photosynthesis. Short-range interactions of a negative charge from a carbamylated lysine could be fixing conformational changes to make PBS EET to Chl a more efficient process. Nevertheless, further repeats are necessary to be able to draw significant conclusions.

A permanent carbamylated Lys 6 was mimicked by *in vivo* substitution of this residue by glutamine. The anionic charge induced in APC trimers showed an increase in relative PBS emission, 20% higher than wild-type with CO_2/HCO_3^-. The observed Chla and PSII emission at 688 nm and 710 nm indicate a stable PSII activity between the strains. The increased PBS emission promoted by the anionic charge can be attributed to a stabilised ApcA carbamate, an energy that is, in fact, not reaching Chla. The PBS emission observed in our experiments may be limited by the redox state of the reaction centre when the measurements were performed, and therefore not be efficiently transferred to PSII. We can only speculate on the mechanisms and structures that can explain our findings. Further experiments measuring K6E PBS emission at the different plastoquinone redox states could help to elucidate this process.

In biological systems, the lifetime distribution of chromophores can either be static or dynamic [95][25]. In particular, conformational changes of the protein can vary the environment of a chromophore and thus fluorescence lifetimes. The wavelengths used for fluorescence decay detection of 6803^{WT} and 6803 mutants were assigned due to the APC fluorescence band previously seen (660 nm) and the band detected of Chla fluorescence (690 nm) that would also include fluorescence from the reaction centre P680. The excitation light used for these measurements (635 nm) is absorbed predominantly by APC. Consequently, the major part of the decay-associated spectra under these conditions represent fluorescence mainly from the APC core. Judging from the decay curve of fluorescence monitored at 660 nm, the amplitude of the 130-150 ps components in 6803^{WT} cells is higher than that of similar components from 6803^{K6E} mutant cells. Similar fluorescence lifetimes have been reported for intact *Synechocystis* sp. PCC 6803 cells [10], attributed to APC emission with lifetimes of 160-220 ps. The second component of 400 ps was detected in 6803^{WT} and 6803^{K6A}, with amplitude significantly smaller than 6803^{K6E} mutant. This lifetime can be attributed to APC B and pigments associated

with the anchor peptide, which has been previously described to be in the range of 370-550 ps [69]. In this study, commonly long-lived components (1.2-1.8 ns) observed in measurements performed under closed RC conditions were not found, indicating that PBSs are fully coupled to PSII [43]. The impact of short-range interactions from a negatively charged residue in ApcA was demonstrated. The increase of 100 ps of the average time is of great interest. This suggests that a permanent CO_2 PTM causes longer APC average lifetimes and significantly different energy transfer distributions: from 70%-30% relative amplitudes in wild type to 50%-50% in 6803^{K6E}.

From the 690 nm detection, ≈170 ps and ≈500 ps components have been attributed to Chla-binding PS core complexes. The different amplitudes of lifetimes between 6803^{WT} and 6803^{K6E} may indicate the adaptation of EET to PSII to a permanent anionic charge in Lys 6. Therefore, Glu 6 appears to exert a negligible effect on the energy transfer process in APC.

Light-harvesting processes are strictly related to inorganic carbon assimilation and detection. Carbamate formation has been demonstrated in the past to depend upon light energy and Ci accumulation in algal cells [96]. It is known that cyanobacteria respond to light and inorganic carbon limitation by the optimisation of protein expression and by keeping protein reserves in anticipation of varying environmental conditions [37][83]. Additionally, carbon is required as the terminal electron acceptor to synthesise carbohydrates and regulate photosynthetic electron transport in PSII by binding with HCO_3^- [12][87]. In this investigation, we demonstrated photophysiological responses to CO_2 in *Synechocystis*. CO_2 carbamylation PTM might have a role in photosynthesis as a regulator and enhancer of energy transfer efficiency. Mechanisms and structures of which are yet to be unravelled. This knowledge will bring valuable knowledge into new ways to improve greener methods of carbon capture with cyanobacteria.

6.5 Conclusions

This thesis demonstrated the role of CO_2 in EET of ApcA in *Synechocystis* sp. PCC 6803. The previously unknown carbamate on ApcA Lys 6 was validated under physiological conditions.

The ability to identify protein carbamates significantly advances our understanding of cellular CO_2 interactions. Cyanobacteria light-harvesting proteins interact with CO_2 via carbamylation at the K6 of the allophycocyanin alpha subunit, suggesting an important role of CO_2 in photosynthetic energy transfer. Further investigation on CO_2 PTM occurring in photosynthetic organisms could provide answers to the uncertainty on how phototrophs will adapt to Earth's rising CO_2 concentrations.

6.6 Further work

Significant findings have been made during this research. However, several questions were raised from the results obtained; with that in mind, the following future work is proposed to elucidate if (and how) CO_2 alters chromophore interactions.

Further *in vitro* analysis

- Crystallography of different carbamylated proteins has elucidated important knowledge on carbamate bonds interactions. Crystallography of APC trimers with high concentrations of CO_2 could elucidate the molecular state of the K6 carbamate.
- Circular dichroism of the recombinant proteins could be tested with the addition of CO_2/HCO_3^-.
- As changes to APC lifetimes in K6E mutant cells *in vivo* were detected, measurements of fluorescence decays of $ApcAB^{K6E}$ recombinant trimers could elucidate more information on short-range interactions of K6 carbamate with chromophore coupling.
- The fluorescence emission spectra of photosynthetic microorganisms at liquid nitrogen temperature (77 K) reveals details about the structure of photosynthetic machinery that are not detectable at room temperature. Measuring the emission of APC trimers at 77K at varying CO_2 could be used to identify promotion and inhibition concentrations of carbon interactions.

In vivo carbamate response

- A specific response to CO_2 on APC fluorescence decays detected at 660 nm in cells was not detected in this study. However, the concentrations of CO_2/HCO_3^- used in this particular assay was 1 mM. Such concentrations would correspond to approximately 19 µM of CO_2, which may mean that not enough CO_2 reached thylakoid membranes and thus PBSs, making any CO_2 response too small to detect. Increasing tested concentrations of CO_2/HCO_3^- could address this issue.

- PSII-derived fluorescence can be recorded with non-invasive PAM fluorimetry technique. The PSII-derived fluorescence can be used to indicate the physiological response to CO_2 of the WT and mutant cells.
- Decay Associated Spectra (DAS) and lifetimes of the excited state relaxation kinetics in whole cells of *Synechocystis sp. PCC 6803* would reveal the distinct components of a heterogeneous mixture from the global analysis of time-resolved spectroscopy data.
- The reproducibility of O_2 evolution tests could be addressed by direct excitation to phycobilisomes/APC using 630 nm filtered light.
- Low-temperature fluorescence measurements suggested for *in vivo* analysis could also be performed on WT and mutant cells.

Finally, further carbamate identification in *Synechocystis* by optimizing the CO_2 trapping methodology used in this study would bring valuable knowledge on cyanobacterial interactions with CO_2. *Synechocystis* carbamylation could depend on CO_2 cellular concentrations; carbamate trapping under different CO_2 conditions could mark a difference in the number of proteins identified with LC-MSMS. The increased number of cyanobacterial proteins identified could be obtained by the fractionation of samples post-digest. This technique will considerably minimize the complexity of the peptide mixture preceding LC-MSMS. With the identification of new carbamylated sites, CRISPR-based systems could be used similarly to this study to elucidate the biological role of cyanobacterial carbamate formation.

References

[1] Sherwin J. Abraham, Tomoyoshi Kobayashi, R. John Solaro, and Vadim Gaponenko. Differences in lysine pKa values may be used to improve NMR signal dispersion in reductively methylated proteins. *Journal of Biomolecular NMR*, 43(4):239–246, 2009. ISSN 09252738. doi: 10.1007/s10858-009-9306-2. URL /pmc/articles/PMC2736131/.

[2] Juan A. Aguilar and Simon J. Kenwright. Robust NMR water signal suppression for demanding analytical applications. *Analyst*, 141(1):236–242, 1 2016. ISSN 13645528. doi: 10.1039/c5an02121a. URL https://pubs.rsc.org/en/content/articlehtml/2016/an/c5an02121a.

[3] T. J. Andrews, M. R. Badger, and G. H. Lorimer. Factors affecting interconversion between kinetic forms of ribulose diphosphate carboxylase-oxygenase from spinach. *Archives of Biochemistry and Biophysics*, 171(1):93–103, 1975. ISSN 10960384. doi: 10.1016/0003-9861(75)90011-9.

[4] Leen Assil-Companioni, Hanna C. Büchsenschütz, Dániel Solymosi, Nina G Dyczmons-Nowaczyk, Kristin K F Bauer, Silvia Wallner, Peter Macheroux, Yagut Allahverdiyeva, Marc M Nowaczyk, and Robert Kourist. Engineering of NADPH Supply Boosts Photosynthesis-Driven Biotransformations. *ACS Catalysis*, 10(20):11864–11877, 10 2020. ISSN 2155-5435. doi: 10.1021/acscatal.0c02601. URL https://dx.doi.org/10.1021/acscatal.0c02601https://pubs.acs.org/doi/10.1021/acscatal.0c02601.

[5] Murray R. Badger and G. Dean Price. CO_2-concentrating mechanisms in cyanobacteria: Molecular components, their diversity and evolution. *Journal of Experimental Botany*, 54 (383):609–622, 2003. ISSN 00220957. doi: 10.1093/jxb/erg076.

[6] Murray R. Badger, G. Dean Price, Ben M. Long, and Fiona J. Woodger. The environmental plasticity and ecological genomics of the cyanobacterial CO_2 concentrating mechanism.

Journal of Experimental Botany, 57(2 SPEC. ISS.):249–265, 2006. ISSN 00220957. doi: 10.1093/jxb/eri286.

[7] Sean A. Beausoleil, Judit Villén, Scott A. Gerber, John Rush, and Steven P. Gygi. A probability-based approach for high-throughput protein phosphorylation analysis and site localization. *Nature Biotechnology*, 24(10):1285–1292, 2006. ISSN 10870156. doi: 10.1038/nbt1240.

[8] Matthew M. Benning, Jane M. Kuo, Frank M. Raushel, and Hazel M. Holden. Three-dimensional structure of the binuclear metal center of phosphotriesterase. *Biochemistry*, 34(25):7973–7978, 1995. ISSN 15204995. doi: 10.1021/bi00025a002. URL https://pubs.acs.org/doi/abs/10.1021/bi00025a002.

[9] Avijit Biswas, Yasmin M. Vasquez, Tierna M. Dragomani, Monica L. Kronfel, Shervonda R. Williams, Richard M. Alvey, Donald A. Bryant, and Wendy M. Schluchter. Biosynthesis of cyanobacterial phycobiliproteins in *Escherichia coli*: Chromophorylation efficiency and specificity of all bilin lyases from *Synechococcus* sp. strain PCC 7002. *Applied and Environmental Microbiology*, 76(9):2729–2739, 2010. ISSN 00992240. doi: 10.1128/AEM.03100-09.

[10] Edith Bittersmann and Wim Vermaas. Fluorescence lifetime studies of cyanobacterial photosystem II mutants. *BBA - Bioenergetics*, 1098(1):105–116, 12 1991. ISSN 00052728. doi: 10.1016/0005-2728(91)90014-F.

[11] Katjuša Brejc, Ralf Ficner, Robert Huber, and Stefan Steinbacher. Isolation, crystallization, crystal structure analysis and refinement of allophycocyanin from the cyanobacterium *Spirulina platensis* at 2.3 Å resolution. *Journal of Molecular Biology*, 249(2):424–440, 1995. ISSN 0022-2836. doi: https://doi.org/10.1006/jmbi.1995.0307. URL http://www.sciencedirect.com/science/article/pii/S0022283685703075.

[12] Katharina Brinkert, Sven De Causmaecker, Anja Krieger-Liszkay, Andrea Fantuzzi, and A. William Rutherford. Bicarbonate-induced redox tuning in Photosystem II for regulation and protection. *Proceedings of the National Academy of Sciences of the United States of America*, 113(43):12144–12149, 10 2016. ISSN 10916490. doi: 10.1073/pnas.1608862113. URL https://www.pnas.org/content/113/43/12144https://www.pnas.org/content/113/43/12144.abstract.

[13] D A Bryant. *The molecular biology of cyanobacteria*. Advances in Photosynthesis, Vol 1. Springer, 1995. ISBN 9780792332732. doi: 10.1007/bf00032589. URL https://books.google.co.uk/books?id=gZelQWTwxyQC.

[14] Donald A. Bryant, Gérard Guglielmi, Nicole Tandeau de Marsac, Anne Marie Castets, and Germaine Cohen-Bazire. The structure of cyanobacterial phycobilisomes: a model. *Archives of Microbiology*, 123(2):113–127, 11 1979. ISSN 03028933. doi: 10.1007/BF00446810. URL https://link.springer.com/article/10.1007/BF00446810.

[15] Roger Buick. The antiquity of oxygenic photosynthesis: Evidence from stromatolites in sulphate-deficient Archaean lakes. *Science*, 255(5040):74–77, 1992. ISSN 00368075. doi: 10.1126/science.11536492.

[16] Center for environmental visualization. Ocean acidification chemistry, 2014. URL http://www.cev.washington.edu/file/Ocean_Acidification_Chemistry.html. [Online; accessed April 27, 2021].

[17] Leifu Chang, Xianwei Liu, Yanbing Li, Cui Cui Liu, Fan Yang, Jindong Zhao, and Sen Fang Sui. Structural organization of an intact phycobilisome and its association with photosystem II. *Cell Research*, 25(6):726–737, 2015. ISSN 17487838. doi: 10.1038/cr.2015.59. URL http://dx.doi.org/10.1038/cr.2015.59.

[18] Volha Chukhutsina, Luca Bersanini, Eva-Mari Mari Aro, and Herbert van Amerongen. Cyanobacterial Light-Harvesting Phycobilisomes Uncouple From Photosystem I During Dark-To-Light Transitions. *Scientific Reports*, 5(1):14193, 11 2015. ISSN 2045-2322. doi: 10.1038/srep14193. URL http://www.nature.com/articles/srep14193.

[19] J.J. Cole and Y.T. Prairie. Dissolved CO_2 in Freshwater Systems. In *Reference Module in Earth Systems and Environmental Sciences*. Elsevier, 1 2014. doi: 10.1016/b978-0-12-409548-9.09399-4.

[20] Jason W. Cooley, Crispin A. Howitt, and Wim F.J. J Vermaas. Succinate:quinol oxidoreductases in the cyanobacterium Synechocystis sp. strain PCC 6803: Presence and function in metabolism and electron transport. *Journal of Bacteriology*, 182(3):714–722, 2 2000. ISSN 00219193. doi: 10.1128/JB.182.3.714-722.2000. URL /pmc/articles/PMC94334/?report=abstracthttps://www.ncbi.nlm.nih.gov/pmc/articles/PMC94334/.

[21] Thomas R. Cundari, Angela K. Wilson, Michael L. Drummond, Hector Emanuel Gonzalez, Kameron R. Jorgensen, Stacy Payne, Jordan Braunfeld, Margarita De Jesus, and

Vanessa M. Johnson. CO_2-formatics: How do proteins bind carbon dioxide? *Journal of Chemical Information and Modeling*, 49(9):2111–2115, 2009. ISSN 15499596. doi: 10.1021/ci9002377.

[22] Catherine F Demoulin, Yannick J Lara, Luc Cornet, Camille François, Denis Baurain, Annick Wilmotte, and Emmanuelle J Javaux. Cyanobacteria evolution: insight from the fossil record. *Free Radical Biology and Medicine*, 140:206–223, 2019. ISSN 0891-5849. doi: https://doi.org/10.1016/j.freeradbiomed.2019.05.007. URL http://www.sciencedirect.com/science/article/pii/S0891584918324845.

[23] Axel Ducret, Walter Sidler, Ernst Wehrli, Gerhard Frank, and Herbert Zuber. Isolation, characterization and electron microscopy analysis of a hemidiscoidal phycobilisome type from the cyanobacterium *Anabaena* sp. PCC 7120. *European Journal of Biochemistry*, 236(3):1010–1024, 3 1996. ISSN 0014-2956. doi: 10.1111/j.1432-1033.1996.01010.x. URL http://doi.wiley.com/10.1111/j.1432-1033.1996.01010.x.

[24] Axel Ducret, Shirley A. Müller, Kenneth N. Goldie, Andreas Hefti, Walter A. Sidler, Herbert Zuber, and Andreas Engel. Reconstitution, characterisation and mass analysis of the pentacylindrical allophycocyanin core complex from the cyanobacterium *Anabaena* sp. PCC 7120. *Journal of Molecular Biology*, 278(2):369–388, 5 1998. ISSN 00222836. doi: 10.1006/jmbi.1998.1678. URL https://linkinghub.elsevier.com/retrieve/pii/S0022283698916783.

[25] Lars Edman, U. Mets, and Rudolf Rigler. Conformational transitions monitored for single molecules in solution. *Proceedings of the National Academy of Sciences*, 93 (13):6710–6715, 6 1996. ISSN 0027-8424. doi: 10.1073/pnas.93.13.6710. URL http://www.pnas.org/cgi/doi/10.1073/pnas.93.13.6710.

[26] Ido Eisenberg, Felipe Caycedo-Soler, Dvir Harris, Shira Yochelis, Susana F. Huelga, Martin B. Plenio, Noam Adir, Nir Keren, and Yossi Paltiel. Regulating the Energy Flow in a Cyanobacterial Light-Harvesting Antenna Complex. *Journal of Physical Chemistry B*, 121(6):1240–1247, 2017. ISSN 15205207. doi: 10.1021/acs.jpcb.6b10590.

[27] Ines Fonfara, Hagen Richter, Majda Bratovia, Anais Le Rhun, and Emmanuelle Charpentier. The CRISPR-associated DNA-cleaving enzyme Cpf1 also processes precursor CRISPR RNA. *Nature*, 532(7600):517–521, 4 2016. ISSN 14764687. doi: 10.1038/nature17945. URL https://www.nature.com/articles/nature17945.

[28] Theodor Forster. *Delocalized excitation and excitation transfer*. Florida State University, Tallahassee, Flor, 1965.

[29] Dasantila Golemi, Laurent Maveyraud, Sergei Vakulenko, Jean Pierre Samama, and Shahriar Mobashery. Critical involvement of a carbamylated lysine in catalytic function of class D β-lactamases. *Proceedings of the National Academy of Sciences of the United States of America*, 98(25):14280–14285, 12 2001. ISSN 00278424. doi: 10.1073/pnas.241442898. URL www.rcsb.org.

[30] E. I. (Eric Ian) Goodwin, T. W. (Trevor Walworth) Mercer. *Introduction to plant biochemistry*. Oxford : Pergamon, 1983. ISBN 0080249213 9780080249216.

[31] Jozef Grabowski and Elisabeth Gantt. Photophysical Properties of Phycobiliproteins From Phycobilisomes: Fluorescence Lifetimes, Quantum Yields, and Polarization Spectra. *Photochemistry and Photobiology*, 28(1):39–45, 1978. ISSN 17511097. doi: 10.1111/j.1751-1097.1978.tb06927.x.

[32] Gerolf Gros and Christian Bauer. High pK value of the N-terminal amino group of the γ-chain causes low CO_2 binding of human fetal hemoglobin. *Biochemical and Biophysical Research Communications*, 80(1):56–62, 1 1978. ISSN 10902104. doi: 10.1016/0006-291X(78)91103-8.

[33] Pamela R Hall, Run Zheng, Lizamma Antony, Marianne Pusztai-Carey, Paul R Carey, and Vivien C Yee. Transcarboxylase 5S structures: assembly and catalytic mechanism of a multienzyme complex subunit. *The EMBO Journal*, 23(18):3621–3631, 9 2004. ISSN 0261-4189. doi: 10.1038/sj.emboj.7600373. URL http://emboj.embopress.org/cgi/doi/10.1038/sj.emboj.7600373.

[34] Xi Han, Lin He, Lei Xin, Baozhen Shan, and Bin Ma. PeaksPTM: Mass spectrometry-based identification of peptides with unspecified modifications. *Journal of Proteome Research*, 10(7):2930–2936, 7 2011. ISSN 15353893. doi: 10.1021/pr200153k. URL https://pubmed.ncbi.nlm.nih.gov/21609001/.

[35] H J Hofmann. Precambrian Microflora, Belcher Islands, Canada: Significance and Systematics. *Journal of Paleontology*, 50(6):1040–1073, 5 1976. ISSN 00223360, 19372337. URL http://www.jstor.org/stable/1303547.

[36] Jerry D. Holman, David L. Tabb, and Parag Mallick. Employing ProteoWizard to convert raw mass spectrometry data. *Current Protocols in Bioinformatics*, 46(SUPPL.46), 2014.

ISSN 1934340X. doi: 10.1002/0471250953.bi1324s46. URL https://pubmed.ncbi.nlm.nih.gov/24939128/.

[37] Michael Jahn, Vital Vialas, Jan Karlsen, Gianluca Maddalo, Fredrik Edfors, Björn Forsström, Mathias Uhlén, Lukas Käll, and Elton P. Hudson. Growth of cyanobacteria is constrained by the abundance of light and carbon assimilation proteins. *Cell Reports*, 25(2):478–486, 2018. ISSN 22111247. doi: 10.1016/j.celrep.2018.09.040.

[38] David Jimenez-Morales, Larisa Adamian, Dashuang Shi, and Jie Liang. Lysine carboxylation: Unveiling a spontaneous post-translational modification. *Acta Crystallographica Section D: Biological Crystallography*, 70(1):48–57, 2014. ISSN 09074449. doi: 10.1107/S139900471302364X.

[39] Takakazu Kaneko, Shusei Sato, Hirokazu Kotani, Ayako Tanaka, Erika Asamizu, Yasukazu Nakamura, Nobuyuki Miyajima, Makoto Hirosawa, Masahiro Sugiura, Shigemi Sasamoto, Takaharu Kimura, Tsutomu Hosouchi, Ai Matsuno, Akiko Muraki, Naomi Nakazaki, Kaoru Naruo, Satomi Okumura, Sayaka Shimpo, Chie Takeuchi, Tsuyuko Wada, Akiko Watanabe, Manabu Yamada, Miho Yasuda, and Satoshi Tabata. Sequence analysis of the genome of the unicellular cyanobacterium *Synechocystis* sp. strain PCC 6803. II. Sequence determination of the entire genome and assignment of potential protein-coding regions. *DNA Research*, 3(3):109–136, 1996. ISSN 13402838. doi: 10.1093/dnares/3.3.109.

[40] Aaron Kaplan and Leonora Reinhold. CO_2 Concentrating Mechanisms in Microorganisms. *Transport*, 50:539–570, 1999. ISSN 0008-4026. doi: 10.1139/b05-907. URL http://www.ncbi.nlm.nih.gov/pubmed/15012219.

[41] Gordon J. King, Carlo Gazzola, Robert L. Blakeley, and Burt Zerner. Triethyloxonium Tetrafluoroborate as an ethylating agent in aqueous solution. *Inorganic Chemistry*, 25(8):1078, 1986. ISSN 1520510X. doi: 10.1021/ic00228a003. URL https://pubs.acs.org/doi/abs/10.1021/ic00228a003.

[42] Diana Kirilovsky. Modulating energy arriving at photochemical reaction centers: Orange carotenoid protein-related photoprotection and state transitions. *Photosynthesis Research*, 126(1):3–17, 10 2015. ISSN 01668595. doi: 10.1007/s11120-014-0031-7. URL http://link.springer.com/10.1007/s11120-014-0031-7.

[43] S. B. Krumova, S. P. Laptenok, J. W. Borst, B. Ughy, Z. Gombos, G. Ajlani, and H. Van Amerongen. Monitoring photosynthesis in individual cells of *Synechocystis*

sp. PCC 6803 on a picosecond timescale. *Biophysical Journal*, 99(6):2006–2015, 2010. ISSN 15420086. doi: 10.1016/j.bpj.2010.07.015. URL http://dx.doi.org/10.1016/j.bpj.2010.07.015.

[44] Jay Kumar, Divya Singh, Madhu B. Tyagi, and Ashok Kumar. *Cyanobacteria: Applications in Biotechnology*, volume 7421. Elsevier Inc., 2018. ISBN 9780128146682. doi: 10.1016/B978-0-12-814667-5.00016-7. URL https://doi.org/10.1016/B978-0-12-814667-5.00016-7.

[45] David J. Lea-Smith, Paolo Bombelli, Ravendran Vasudevan, and Christopher J. Howe. Photosynthetic, respiratory and extracellular electron transport pathways in cyanobacteria. *Biochimica et Biophysica Acta - Bioenergetics*, 1857(3):247–255, 2016. ISSN 18792650. doi: 10.1016/j.bbabio.2015.10.007. URL http://dx.doi.org/10.1016/j.bbabio.2015.10.007.

[46] Wenjun Li, Yang Pu, Na Gao, Zhihong Tang, Lufei Song, and Song Qin. Efficient purification protocol for bioengineering allophycocyanin trimer with N-terminus Histag. *Saudi Journal of Biological Sciences*, 24(3):451–458, 2017. ISSN 1319562X. doi: 10.1016/j.sjbs.2017.01.011. URL http://dx.doi.org/10.1016/j.sjbs.2017.01.011.

[47] Victoria Linthwaite. *Development of a technology for the discovery of protein carbamates*. PhD thesis, Durham University, 2016.

[48] Victoria L. Linthwaite, Joanna M. Janus, Adrian P. Brown, David Wong-Pascua, AnnMarie Marie C. O'Donoghue, Andrew Porter, Achim Treumann, David R.W. W Hodgson, and Martin J. Cann. The identification of carbon dioxide mediated protein post-translational modifications. *Nature Communications*, 9(1):1–11, 2018. ISSN 20411723. doi: 10.1038/s41467-018-05475-z. URL https://doi.org/10.1038/s41467-018-05475-z.

[49] Huanting Liu and James H. Naismith. An efficient one-step site-directed deletion, insertion, single and multiple-site plasmid mutagenesis protocol. *BMC Biotechnology*, 8:91, 2008. ISSN 14726750. doi: 10.1186/1472-6750-8-91.

[50] J Y Liu, T Jiang, J P Zhang, and D C Liang. Crystal structure of allophycocyanin from red algae *Porphyra yezoensis* at 2.2-A resolution. *The Journal of Biological Chemistry*, 274(24):16945–52, 6 1999. ISSN 0021-9258. doi: 10.1074/jbc.274.24.16945. URL http://www.ncbi.nlm.nih.gov/pubmed/10358042.

[51] Lu Ning Liu. Distribution and dynamics of electron transport complexes in cyanobacterial thylakoid membranes. *Biochimica et Biophysica Acta - Bioenergetics*, 1857(3):256–265, 3 2016. ISSN 18792650. doi: 10.1016/j.bbabio.2015.11.010.

[52] Shaofang Liu, Yingjie Chen, Yandu Lu, Huaxin Chen, Fuchao Li, and Song Qin. Biosynthesis of fluorescent cyanobacterial allophycocyanin trimer in *Escherichia coli*. *Photosynthesis Research*, 105(2):135–142, 2010. ISSN 01668595. doi: 10.1007/s11120-010-9574-4.

[53] Christopher T. Lohans, David Y. Wang, Christian Jorgensen, Samuel T. Cahill, Ian J. Clifton, Michael A. McDonough, Henry P. Oswin, James Spencer, Carmen Domene, Timothy D.W. W Claridge, Jürgen Brem, and Christopher J. Schofield. ^{13}C-Carbamylation as a mechanistic probe for the inhibition of class D β-lactamases by avibactam and halide ions. *Organic and Biomolecular Chemistry*, 15(28):6024–6032, 2017. ISSN 14770520. doi: 10.1039/c7ob01514c.

[54] Davey Loos, Mircea Cotlet, Frans De Schryver, Satoshi Habuchi, and Johan Hofkens. Single-molecule spectroscopy selectively probes donor and acceptor chromophores in the phycobiliprotein allophycocyanin. *Biophysical Journal*, 87(4):2598–2608, 10 2004. ISSN 15420086. doi: 10.1529/biophysj.104.046219.

[55] George H. Lorimer. Carbon dioxide and carbamate formation: the makings of a biochemical control system. *Trends in Biochemical Sciences*, 8(2):65–68, 1983. ISSN 09680004. doi: 10.1016/0968-0004(83)90393-6.

[56] George H. Lorimer and Henry M. Miziorko. Carbamate formation on the ε-amino group of a lysyl residue as the basis for the activation of ribulosebisphosphate carboxylase by carbon dioxide and magnesium $^{2+}$. *Biochemistry*, 19(23):5321–5328, 1980. ISSN 15204995. doi: 10.1021/bi00564a027.

[57] Robert MacColl. Allophycocyanin and energy transfer. *Biochimica et Biophysica Acta - Bioenergetics*, 1657(2-3):73–81, 2004. ISSN 00052728. doi: 10.1016/j.bbabio.2004.04.005.

[58] Robert MacColl, Donald S. Berns, Eveline Traeger, and Károly Csatorday. Chromophore Interactions in Allophycocyanin. *Biochemistry*, 19(12):2817–2820, 1980. ISSN 15204995. doi: 10.1021/bi00553a043.

[59] C. Magnabosco, K. R. Moore, J. M. Wolfe, and G. P. Fournier. Dating phototrophic microbial lineages with reticulate gene histories. *Geobiology*, 16(2):179–189, 3 2018. ISSN 14724677. doi: 10.1111/gbi.12273. URL http://doi.wiley.com/10.1111/gbi.12273.

[60] Niall M. Mangan, Avi Flamholz, Rachel D. Hood, Ron Milo, and David F. Savage. PH determines the energetic efficiency of the cyanobacterial CO_2 concentrating mechanism. *Proceedings of the National Academy of Sciences of the United States of America*, 113 (36):E5354–E5362, 2016. ISSN 10916490. doi: 10.1073/pnas.1525145113.

[61] Ailie Marx and Noam Adir. Allophycocyanin and phycocyanin crystal structures reveal facets of phycobilisome assembly. *Biochimica et Biophysica Acta - Bioenergetics*, 1827 (3):311–318, 2013. ISSN 00052728. doi: 10.1016/j.bbabio.2012.11.006. URL http://dx.doi.org/10.1016/j.bbabio.2012.11.006.

[62] Kanika Mehta, Damini Jaiswal, Monalisha Nayak, Charulata B. Prasannan, Pramod P. Wangikar, and Sanjeeva Srivastava. Elevated carbon dioxide levels lead to proteome-wide alterations for optimal growth of a fast-growing cyanobacterium, *Synechococcus elongatus* PCC 11801. *Scientific Reports*, 9(1):1–14, 2019. ISSN 20452322. doi: 10.1038/s41598-019-42576-1. URL http://dx.doi.org/10.1038/s41598-019-42576-1.

[63] Jack J. Middelburg. Biogeochemical processes and inorganic carbon dynamics. In *Marine Carbon Biogeochemistry*, pages 77–105. Springer, Cham, 2019. doi: 10.1007/978-3-030-10822-9{\{}{\textbackslash}{_}{\}}5. URL https://doi.org/10.1007/978-3-030-10822-9_5.

[64] Anthony A. Morollo, Gregory A. Petsko, and Dagmar Ringe. Structure of a Michaelis complex analogue: Propionate binds in the substrate carboxylate site of alanine racemase. *Biochemistry*, 38(11):3293–3301, 3 1999. ISSN 00062960. doi: 10.1021/bi9822729. URL https://pubs.acs.org/doi/abs/10.1021/bi9822729.

[65] J. S. Morrow, P. Keim, R. B. Visscher, R. C. Marshall, and F. R. Gurd. Interaction of $^{13}CO_2$ and bicarbonate with human hemoglobin preparations. *Proceedings of the National Academy of Sciences of the United States of America*, 70(5):1414–1418, 1973. ISSN 00278424. doi: 10.1073/pnas.70.5.1414. URL https://pubmed.ncbi.nlm.nih.gov/4514311/.

[66] J. S. Morrow, J. B. Matthew, R. J. Wittebort, and F. R.N. N Gurd. Carbon 13 resonances of $^{13}CO_2$ carbamino adducts of α and β chains in human adult hemoglobin.

Journal of Biological Chemistry, 251(2):477–487, 1976. ISSN 00219258. doi: 10.1016/s0021-9258(17)33904-2.

[67] Conrad W. Mullineaux. Co-existence of photosynthetic and respiratory activities in cyanobacterial thylakoid membranes. *Biochimica et Biophysica Acta - Bioenergetics*, 1837(4):503–511, 2014. ISSN 00052728. doi: 10.1016/j.bbabio.2013.11.017. URL http://dx.doi.org/10.1016/j.bbabio.2013.11.017.

[68] Conrad W Mullineaux and John F Allen. State 1 - State 2 transitions in the cyanobacterium *Synechococcus* 6301 are controlled by the redox state of electron carriers between Photosystems I and II. *Photosynthesis Research*, 23(3):297–311, 1990. ISSN 1573-5079. doi: 10.1007/BF00034860. URL https://doi.org/10.1007/BF00034860.

[69] Conrad W. Mullineaux and Alfred R. Holzwarth. Kinetics of excitation energy transfer in the cyanobacterial phycobilisome-Photosystem II complex. *BBA - Bioenergetics*, 1098 (1):68–78, 12 1991. ISSN 00052728. doi: 10.1016/0005-2728(91)90010-L.

[70] Akio Murakami, Mamoru Mimuro, Kaori Ohki, and Yoshihiko Fujita. Absorption spectrum of allophycocyanin isolated from *Anabaena* cylindrica: Variation of the absorption spectrum induced by changes of the physico-chemical environment. *Journal of Biochemistry*, 89(1):79–86, 1981. ISSN 0021924X. doi: 10.1093/oxfordjournals.jbchem.a133205.

[71] Marion H. O'Leary, Robert J. Jaworski, and Fred C. Hartman. ^{13}C nuclear magnetic resonance study of the CO_2 activation of ribulosebisphosphate carboxylase from *Rhodospirillum rubrum*. *Proceedings of the National Academy of Sciences*, 76(2): 673–675, 2 1979. ISSN 0027-8424. doi: 10.1073/PNAS.76.2.673. URL https://www.pnas.org/content/76/2/673.

[72] Joseph P. O'Shea, Michael F. Chou, Saad A. Quader, James K. Ryan, George M. Church, and Daniel Schwartz. PLogo: A probabilistic approach to visualizing sequence motifs. *Nature Methods*, 10(12):1211–1212, 12 2013. ISSN 15487091. doi: 10.1038/nmeth.2646. URL https://pubmed.ncbi.nlm.nih.gov/24097270/.

[73] G. Dean Price. Inorganic carbon transporters of the cyanobacterial CO_2-concentrating mechanism. *Photosynthesis Research*, 109(1-3):47–57, 2011. ISSN 01668595. doi: 10.1007/s11120-010-9608-y.

[74] G. Dean Price, Murray R. Badger, Fiona J. Woodger, and Ben M. Long. Advances in understanding the cyanobacterial CO_2-concentrating- mechanism (CCM): Functional

components, Ci transporters, diversity, genetic regulation and prospects for engineering into plants. *Journal of Experimental Botany*, 59(7):1441–1461, 2008. ISSN 00220957. doi: 10.1093/jxb/erm112. URL https://academic.oup.com/jxb/article-abstract/59/7/1441/636484.

[75] Reza Ranjbar Choubeh, Ravi R. Sonani, Datta Madamwar, Paul C. Struik, Arjen N. Bader, Bruno Robert, and Herbert van Amerongen. Picosecond excitation energy transfer of allophycocyanin studied in solution and in crystals. *Photosynthesis Research*, 135(1-3): 79–86, 2018. ISSN 15735079. doi: 10.1007/s11120-017-0417-4.

[76] Raimond B.G. G Ravelli and Sean M. McSweeney. The 'fingerprint' that X-rays can leave on structures. *Structure*, 8(3):315–328, 2000. ISSN 09692126. doi: 10.1016/S0969-2126(00)00109-X.

[77] William Remelli and Stefano Santabarbara. Excitation and emission wavelength dependence of fluorescence spectra in whole cells of the cyanobacterium *Synechocystis* sp. PPC 6803: Influence on the estimation of Photosystem II maximal quantum efficiency. *Biochimica et Biophysica Acta - Bioenergetics*, 1859(11):1207–1222, 11 2018. ISSN 18792650. doi: 10.1016/j.bbabio.2018.09.366.

[78] Yanliang Ren, Osama Melhem, Yongjian Li, Bo Chi, Xinya Han, Hao Zhu, Lingling Feng, Jian Wan, and Xin Xu. Clarifying and illustrating the electronic energy transfer pathways in trimeric and hexameric aggregation state of cyanobacteria allophycocyanin within the framework of Förster theory. *Journal of Computational Chemistry*, 36(3):137–145, 1 2015. ISSN 01928651. doi: 10.1002/jcc.23770. URL http://doi.wiley.com/10.1002/jcc.23770.

[79] L. Rossi-Bernardi and F. J. W. Roughton. The specific influence of carbon dioxide and carbamate compounds on the buffer power and Bohr effects in human haemoglobin solutions. *The Journal of Physiology*, 189(1):1–29, 3 1967. ISSN 00223751. doi: 10.1113/jphysiol.1967.sp008152. URL http://doi.wiley.com/10.1113/jphysiol.1967.sp008152.

[80] F J W Roughton. Some recent work on the interactions of oxygen, carbon dioxide and haemoglobin. The seventh Hopkins memorial lecture. Technical report, Meeting of the Biochemical Society at the University of Liverpool, 1970.

[81] Bettina E. Schirrmeister, Jurriaan M. de Vos, Alexandre Antonelli, and Homayoun C. Bagheri. Evolution of multicellularity coincided with increased diversification of cyanobacteria and the Great Oxidation Event. *Proceedings of the National Academy of*

Sciences, 110(5):1791–1796, 1 2013. ISSN 0027-8424. doi: 10.1073/PNAS.1209927110. URL https://www.pnas.org/content/110/5/1791.

[82] R. M. Schuurmans, J. C. P. Matthijs, and K. J. Hellingwerf. Transition from exponential to linear photoautotrophic growth changes the physiology of *Synechocystis* sp. PCC 6803. *Photosynthesis Research*, 132(1):69–82, 4 2017. ISSN 0166-8595. doi: 10.1007/s11120-016-0329-8. URL http://link.springer.com/10.1007/s11120-016-0329-8.

[83] Doreen Schwarz, Anke Nodop, Jan Hüge, Stephanie Purfürst, Karl Forchhammer, Klaus-Peter Michel, Hermann Bauwe, Joachim Kopka, and Martin Hagemann. Metabolic and transcriptomic phenotyping of inorganic carbon acclimation in the cyanobacterium *Synechococcus elongatus* PCC 7942. *Plant Physiology*, 155(4):1640–1655, 3 2011. ISSN 1532-2548. doi: 10.1104/pp.110.170225. URL www.plantphysiol.org/cgi/doi/10.1104/pp.110.170225https://academic.oup.com/plphys/article/155/4/1640/6108718.

[84] A.V. Sharkov, I.V. Kryukov, E.V. Khoroshilov, P.G. Kryukov, R. Fischer, H. Scheer, and T. Gillbro. Femtosecond energy transfer between chromophores in allophycocyanin trimers. *Chemical Physics Letters*, 191(6):633–638, 4 1992. ISSN 00092614. doi: 10.1016/0009-2614(92)85601-6. URL https://linkinghub.elsevier.com/retrieve/pii/0009261492856016.

[85] Gaozhong Shen, Wendy M. Schluchter, and Donald A. Bryant. Biogenesis of phycobiliproteins: I. cpcS-I and cpcU mutants of the cyanobacterium *Synechococcus* sp. PCC 7002 define a heterodimeric phyococyanobilin lyase specific for β-phycocyanin and allophycocyanin subunits. *Journal of Biological Chemistry*, 283(12):7503–7512, 3 2008. ISSN 00219258. doi: 10.1074/jbc.M708164200. URL http://dx.doi.org/10.1074/jbc.M708164200.

[86] Dmitriy Shevela. Adventures with cyanobacteria: a personal perspective. *Frontiers in Plant Science*, 2(July):1–17, 2011. ISSN 1664462X. doi: 10.3389/fpls.2011.00028. URL http://journal.frontiersin.org/article/10.3389/fpls.2011.00028/abstract.

[87] Dmitriy Shevela, Julian J. Eaton-Rye, and Jian-Ren Shen. Photosystem II and the unique role of bicarbonate: A historical perspective. *Biochimica et Biophysica Acta (BBA) - Bioenergetics*, 1817(8):1134–1151, 8 2012. ISSN 00052728. doi: 10.1016/j.bbabio.2012.04.003. URL https://linkinghub.elsevier.com/retrieve/pii/S0005272812001259.

[88] Walter A Sidler. *Phycobilisome and phycobiliprotein structures*, volume II. Springer, Dordrecht, 1995. ISBN 978-94-011-0227-8. doi: https://doi.org/10.1007/978-94-011-0227-8. URL http://link.springer.com/10.1007/978-94-011-0227-8.

[89] William C. Stadie and Helen O'Brien. The carbamate equilibrium. *Journal of Biological Chemistry*, 112(2):723–758, 1 1936. ISSN 00219258. doi: 10.1016/S0021-9258(18)74954-5. URL https://linkinghub.elsevier.com/retrieve/pii/S0021925818749545.

[90] Ngoc Hieu Tran, Rui Qiao, Lei Xin, Xin Chen, Chuyi Liu, Xianglilan Zhang, Baozhen Shan, Ali Ghodsi, and Ming Li. Deep learning enables de novo peptide sequencing from data-independent-acquisition mass spectrometry. *Nature Methods*, 16(1):63–66, 1 2019. ISSN 15487105. doi: 10.1038/s41592-018-0260-3. URL https://pubmed.ncbi.nlm.nih.gov/30573815/.

[91] Yasufumi Umena, Keisuke Kawakami, Jian Ren Shen, and Nobuo Kamiya. Crystal structure of oxygen-evolving photosystem II at a resolution of 1.9Å. *Nature*, 473(7345):55–60, 5 2011. ISSN 14764687. doi: 10.1038/nature09913. URL https://pubmed.ncbi.nlm.nih.gov/21499260/.

[92] Justin Ungerer and Himadri B. Pakrasi. Cpf1 is a versatile tool for CRISPR genome editing across diverse species of cyanobacteria. *Scientific Reports*, 6(November):1–9, 2016. ISSN 20452322. doi: 10.1038/srep39681. URL http://dx.doi.org/10.1038/srep39681.

[93] Kavita Verma and Prasanna Mohanty. Changes of the photosynthetic apparatus in *Spirulina* cyanobacterium by sodium stress. *Zeitschrift fur Naturforschung - Section C Journal of Biosciences*, 55(1-2):16–22, 2 2000. ISSN 09395075. doi: 10.1515/znc-2000-1-205. URL www.znaturforsch.com.

[94] Kazuya Yamaguchi and Robert P. Hausinger. Substitution of the urease active site carbamate by dithiocarbamate and vanadate. *Biochemistry*, 36(49):15118–15122, 12 1997. ISSN 00062960. doi: 10.1021/bi971767f. URL https://pubmed.ncbi.nlm.nih.gov/9398239/.

[95] Liming Ying and X. Sunny Sunney. Xie. Fluorescence spectroscopy, exciton dynamics, and photochemistry of single allophycocyanin trimers. *Journal of Physical Chemistry B*, 102(50):10399–10409, 1998. ISSN 1520-6106. doi: 10.1021/jp983227d.

[96] Akiho Yokota, Hiroshi Komura, and Shozaburo Kitaoka. Intracellular inorganic carbon exists as protein carbamate in photosynthesizing *Euglena gracilis Z*. *Biochemical and*

Biophysical Research Communications, 111(2):544–550, 3 1983. ISSN 0006291X. doi: 10.1016/0006-291X(83)90341-8. URL https://linkinghub.elsevier.com/retrieve/pii/0006291X83903418.

[97] Dmitry V. Zlenko, Irina V. Elanskaya, Evgeny P. Lukashev, Yulia V. Bolychevtseva, Natalia E. Suzina, Elena S. Pojidaeva, Irena A. Kononova, Aleksey V. Loktyushkin, and Igor N. Stadnichuk. Role of the PB-loop in ApcE and phycobilisome core function in cyanobacterium *Synechocystis* sp. PCC 6803. *Biochimica et Biophysica Acta - Bioenergetics*, 1860(2):155–166, 2019. ISSN 18792650. doi: 10.1016/j.bbabio.2018.10.004. URL https://doi.org/10.1016/j.bbabio.2018.10.004.

[98] Alexandre Zougman, Peter J. Selby, and Rosamonde E. Banks. Suspension trapping (STrap) sample preparation method for bottom-up proteomics analysis. *Proteomics*, 14 (9):1000–1006, 2014. ISSN 16159861. doi: 10.1002/pmic.201300553.